USING IN SITU COSMOGENIC ^{10}BE AS A SEDIMENT SOURCE TRACER IN GREENLAND'S PARAGLACIAL ENVIRONMENT

A Thesis Presented

by

Alice H. Nelson

to

The Faculty of the Graduate College

of

The University of Vermont

In Partial Fulfillment of the Requirements
for the Degree of Master of Science
Specializing in Geology

October, 2013

Accepted by the Faculty of the Graduate College, The University of Vermont, in partial fulfillment of the requirements for the degree of Master of Science, specializing in Geology

Thesis Examination Committee:

_____ Advisor
Paul R. Bierman, Ph.D

_____
Andrea Lini, Ph.D

_____ Chairperson
Jason Stockwell, Ph.D

_____ Dean, Graduate College
Domenico Grasso, Ph.D

ABSTRACT

Paraglacial environments are landscapes that have been exposed by retreating glaciers, where geomorphic change and sediment redistribution is thought to occur rapidly. In my Master's Thesis, I use the concentration of *in situ* ^{10}Be, which is a cosmogenically produced isotope, to trace the relative contribution of different sediment sources to Greenland's paraglacial sediment budget. Over the course of two field seasons, we visited three different paraglacial landscapes along the Greenland Ice Sheet margin near Kangerlussuaq, Narsarsuaq, and Tasiilaq. In total, we collected 62 sediment samples from glacial (n=19) and ice-free terrain (n=10), from channels where sediment is sourced from a mixture of glacial and ice-free terrain (n=28), from Holocene fluvial terraces (n=4), and from one aeolian sand dune.

The concentration of *in situ* ^{10}Be in sediment ranges from 1,600 to 34,000 atoms g^{-1}, and we are able to use *in situ* ^{10}Be concentration as a sediment source tracer because the ^{10}Be concentration in sediment sourced from glacial terrain is characteristically different from that sourced from ice-free terrain. The ^{10}Be concentration in sediment from ice-free terrain is significantly higher than the ^{10}Be concentration in sediment from glacial and mixed sources and is also higher than the concentration in terrace sediment deposited earlier during the Holocene.

In Kangerlussuaq and Tasiilaq, we constrained the exposure age of the ice-free landscape from previously published cosmogenic and radiogenic dating work, and in Narsarsuaq, we augmented previous research with exposure ages calculated from the *in situ* ^{10}Be concentration in bedrock (n=5) and boulder (n=6) samples. Ice-free portions of our field areas have had ~7 to 11 thousand years of recent subaerial exposure to cosmic radiation and thus, ^{10}Be concentration in sediment sourced from ice-free terrain is significantly higher than in glacial sediment, which is sourced from a landscape that has been shielded from cosmic rays for much of the last 3.5 million years. We calculated that the low concentrations of ^{10}Be measured in glacial sediment must have accumulated at depth, and have been inherited from a prolonged period of exposure that pre-dates the Greenland Ice Sheet.

The similarity in ^{10}Be concentration in sediment from glacial and mixed fluvial sources indicates that the Greenland Ice Sheet is the dominant source of sediment moving through the paraglacial landscape and into the fjords. The similarity in concentration between glacial sediment and terrace sediment indicates that glacially-sourced sediment also dominated the fluvial system earlier during the Holocene. Our findings imply that the ^{10}Be concentration in marine sediment sourced from Greenland will be controlled by the efficacy and timing of ice sheet erosion rather than the extent of paraglacial landscape exposure. These findings will help inform a larger research project in which ^{10}Be concentration in ocean core sediment will be used to create a 5 to 6 million year record of Greenland glaciation.

CITATION

Material from this thesis has been submitted for publication to Earth Surface Processes and Landforms on Month, day, 2013 in the following form:

Nelson, A., Bierman, P., Shakun, J., Rood, D.. Using *in situ* cosmogenic ^{10}Be as a sediment source tracer in Greenland's paraglacial environment: Earth Surface Processes and Landforms.

ACKNOWLEDGEMENTS

This research would not have been possible without the support of my advisor Paul Bierman. Thank you for giving me the opportunity to travel to Greenland and to be a part of this exciting research project; you have pushed my writing and research to be the very best that it could be, and while the process has been challenging, I appreciate and value the critical thinking, research, and writing skills that you have taught me.

From sample collection to data analysis, this research has been a team effort, and I am grateful to have worked on this project with our collaborators Dylan Rood and Jeremy Shakun. Thank you for all of your help in the steps that happen in between sand and data, for your insight into my analysis, for your feedback during the writing process, and most of all, for you encouragement along the way. University of Vermont's science reporter Joshua Brown was a fun addition to our field team, and Josh, you managed to document our trip and our research in a way that is humorous, scientifically accurate, and accessible. I am indebted to you for your amazing photographs; I have used them extensively in this thesis and also in posters and presentations. Funding for this project has been provided by the National Science Foundation award number ARC-1023191 to Bierman and the University of Vermont.

Thank you to my committee members Andrea Lini and Jason Stockwell. Andrea, I appreciate that your door is always open and that you are always willing to help and to listen, and Jason, thank you for serving as committee chair, your questions and perspective have made my research better. A big thank you to the rest of the faculty and staff in the UVM Geology Department, I appreciate your curiosity and engagement in my work, and I thank you for your encouragement and support. I am also thankful for the

support of my fellow graduate students; in particular, I thank Veronica Sosa-Gonzalez and Ben DeJong for your help in the cosmogenic lab, and I thank Thomas Neilson and Michael Ingram for your help with ArcGIS.

I would not be at UVM earning a Master's degree in geology if it were not for the support and guidance of the geosciences department at Williams College. Thank you for filling my freshman year of college with fieldtrips and for making me curious about glaciers and mountains. I appreciate that you encouraged me to continue my geosciences education beyond Williams, and I thank you for providing me with the skills necessary to be a successful student, scientist, and writer.

Finally, my biggest thank you is to my family. My parents Deb and Dan Nelson raised my brother Jack and me to be readers, writers, and critical thinkers. You are not scientists, but you have eagerly listened to me talk about isotopes and have supported me every step of the way. It means the world to me that you are proud of me and of what I have accomplished.

TABLE OF CONTENTS

LIST OF TABLES

LIST OF FIGURES

CHAPTER 2

CHAPTER 5

CHAPTER 1. INTRODUCTION

1. Introduction, Motivation, and Overview

The landmass of Greenland is 78% glaciated and is home to the largest ice sheet in North America (Escher and Watt, 1976; Thomas and Investigators, 2001). While Greenland is currently almost entirely covered by ice, glacial extent has fluctuated over time, perhaps greatly, with changes in Earth's climate (Alley et al., 2010). On Greenland, climate-driven fluctuations in ice sheet extent have an important role in the sediment system because glaciers erode the underlying landscape (Hallet, 1979), act as storage reservoirs for sediment (Drewry, 1986), and facilitate sediment transportation by entrainment within ice and suspension in outwash (Weertman, 1961). When glaciers retreat, they continue to influence sedimentary processes because they expose a landscape that is unstable and thus susceptible to rapid geomorphic change and sediment redistribution (Ballantyne, 2002b).

For my master's research, I am using the concentration of *in situ* ^{10}Be in fluvial sediment to understand sediment exposure, erosion, transportation, and storage processes during the current interglacial period. The research presented in this thesis is a component of a larger project that will use knowledge of sediment routing dynamics to infer past ice extent from the concentration of *in situ* ^{10}Be in a five million year (My) sediment core record.

2. Thesis Outline

The chapter that follows (Chapter 2) is a comprehensive literature review that includes a description of the geologic setting and relevant background information. Chapter 3 describes the methods used for sample collection, mineral separation, cosmogenic ^{10}Be isolation, and Accelerator Mass Spectrometry (AMS) data collection and reduction. In the methodology chapter, I also describe the mathematical equations that I use to interpret isotope concentration in sediment. The fourth chapter is a manuscript prepared for a special issue of Earth Surface Processes and Landforms that focuses on geomorphologic and proglacial processes in proglacial areas under conditions of rapid deglaciation. The manuscript, which will be submitted for publication, includes results, data analysis, and conclusions. The concluding chapter of my thesis describes my findings within the context of the larger research project, which will interpret long-term ice sheet history from the variable concentration of ^{10}Be in a marine sediment core.

CHAPTER 2. COMPREHENSIVE LITERATURE REVIEW

1. Introduction

The following literature review provides background information about Greenland and the Greenland Ice Sheet, including detailed geologic setting descriptions of the three field sites where we collected sediment samples. I am measuring the concentration of *in situ* ^{10}Be in the sediment samples to study sediment erosion, exposure, storage, and transportation along margins of the Greenland Ice Sheet during the present interglacial, and in this chapter I describe how ^{10}Be is produced by cosmic rays. A section on climate provides an overview of Greenland Ice Sheet history and glacial-interglacial cycles. I am using the concept of sediment budgeting as a framework for studying sediment routing dynamics, and I have included a description of the sediment budget, which will be relevant to my thesis research, and also a description of the long-term sediment budget, which will be relevant to the reconstruction of long-term ice sheet history.

2. Geologic Setting

2.1. Greenland and the Greenland Ice Sheet

Greenland is the largest island in the world with a surface area of 2.2×10^6 km^2 (Escher and Watt, 1976). The landmass is situated between 60º and 84º North and is bordered by the Arctic Ocean to the north, by Baffin Bay and the Davis Straight to the west, and by the Greenland Sea and the Denmark Straight to the east (Figure 1). The bedrock geology of Greenland is predominantly crystalline rocks of the Precambrian

shield that formed during a series of orogenic events during the Achaean and stabilized as the Laurentian shield during the Palaeoproterozoic (Henriksen et al., 2009). Greenland rifted from North America during the Cretacious, which is associated with basaltic dyke intrusion (Henriksen et al., 2009).

Today, the geology of Greenland is dominated by the Greenland Ice Sheet, which has a total ice area of ~1.7 x 10^6 km^2 (Alley et al., 2010) and maximum surface elevations of 3,200 m at the northern dome and 2,850 m at the southern dome (Thomas and Investigators, 2001). Ice-free margins of Greenland are predominantly uplands that reach maximum elevations of >2,000 m above sea level (asl) in the southeast and the exposed landscape is dissected by fjords and glacially overdeepened valleys (Weidick et al., 2004). Study areas relevant to this project are Kangerlussuaq on the west coast, Narsarsuaq along the southern margin, and Tasiilaq on the east coast (Figure 1).

Figure 1: Map of Greenland showing study area locations. Samples were collected in Kangerlussuaq on the west coast, Narsarsuaq at the southern margin, and Tasiilaq on the east coast. Also shown is ice sheet thickness and relevant ice core locations. The base map was modified from worldofmaps.net. Site 918 is an Ocean Drilling Program core location.

2.2. Study Area: Kangerlussuaq

Kangerlussuaq is a settlement on the west coast of Greenland that is located at ~67°N, inland of the coast, at the head of the 190 km Søndre Strømfjord (Figure 2). The Russell Glacier lobe of the ice sheet is ~25 km east of the fjord mouth. The fjord is fed by two major drainages of the ice sheet, the Watson River and the Qinnguata Kuussua River, both of which sit in wide, low-elevation valleys (Figures 2B and 2D). The region is bordered to the north and to the south by uplands that reach maximum elevations of ~800 m asl. Bedrock outcrops in the region are Achaean grandioritic gneiss (Escher and Pulvertaft, 1995).

Kangerlussuaq is within a zone of continuous permafrost (Weidick, 1968). The climate is characterized as low Arctic continental with low precipitation rates (<150 mm a^{-1}) and a mean annual temperature of -6°C and (Anderson et al., 2001). Vegetation, when present, is dwarf-shrub tundra and is concentrated in the low elevations and near streams, rivers, and lakes; rock outrcrops, thin soil cover, and sparse vegetation dominate the slopes and uplands (Anderson et al., 2001) (Figure 2D). Close to the ice margin, the landscape is blanketed by till and eratics and is not vegetated.

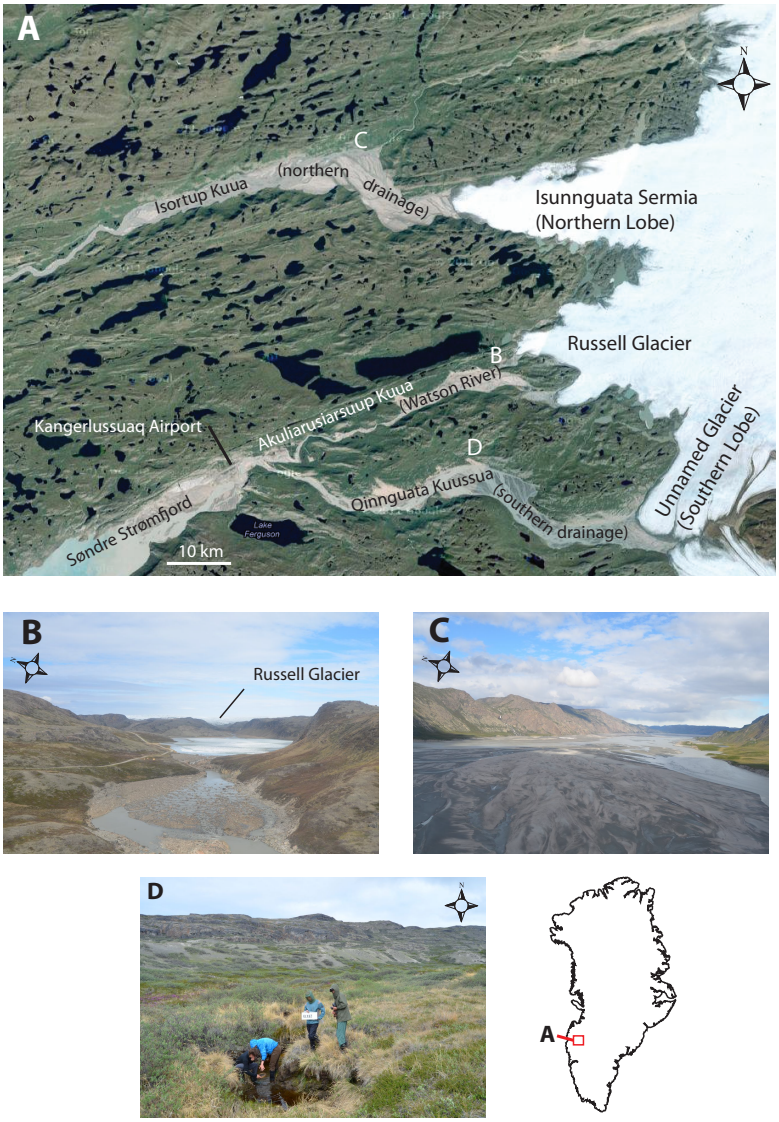

Figure 2: **A**: Google Earth image of the Kangerlussuaq field area on the west coast. We sampled at three ice margins (Northern Lobe, Russell Glacier, and Southern Lobe) and along the three drainages (Northern Drainage, Watson River, and Southern Drainage). We also sampled in small tributary drainages, in an early-Holocene terrace, and at the fjord mouth. The drainages sampled in this area are all in wide valleys. **B** is an oblique aerial photograph looking upstream towards the Russell Glacier margin. The low elevations are sparsely vegetated and the slopes are predominantly rock outcrop. **C** is an upstream view of the wide, braided Northern Drainage. **D** is an ice-free tributary stream that flows into the Southern Drainage. Photos by Paul Bierman.

2.3. Study Area: Narsarsuaq

Narsarsuaq is located at ~61°N, close to the southern tip of Greenland, near the head of the Tunulliarfik Fjord (Figure 3). The fjord is fed by rivers, which drain land-based tongues of the ice sheet and also by the Qooqqup Sermia tongue of the ice sheet, which has a marine-based calving margin. To the north and east of Narsarsuaq are uplands where peaks reach maximum elevations of ~2,000 m asl (Figure 3B). The regional geology consists of proterozoic gneisses and granite intrusions (Escher and Pulvertaft, 1995). Narsarsuaq is in a zone of discontinuous permafrost (Weidick, 1968), mean annual average temperature in Narsarsuaq is -3°C and average precipitation is ~600 mm a^{-1}. Vegetation in the region is dwarf-shrubs, mosses, and lichens (Sparrenbom et al., 2006), and is limited to the low elevations (Figure 3D); the higher elevations and slopes are predominantly bare rock with limited, thin soil cover (Figure 3).

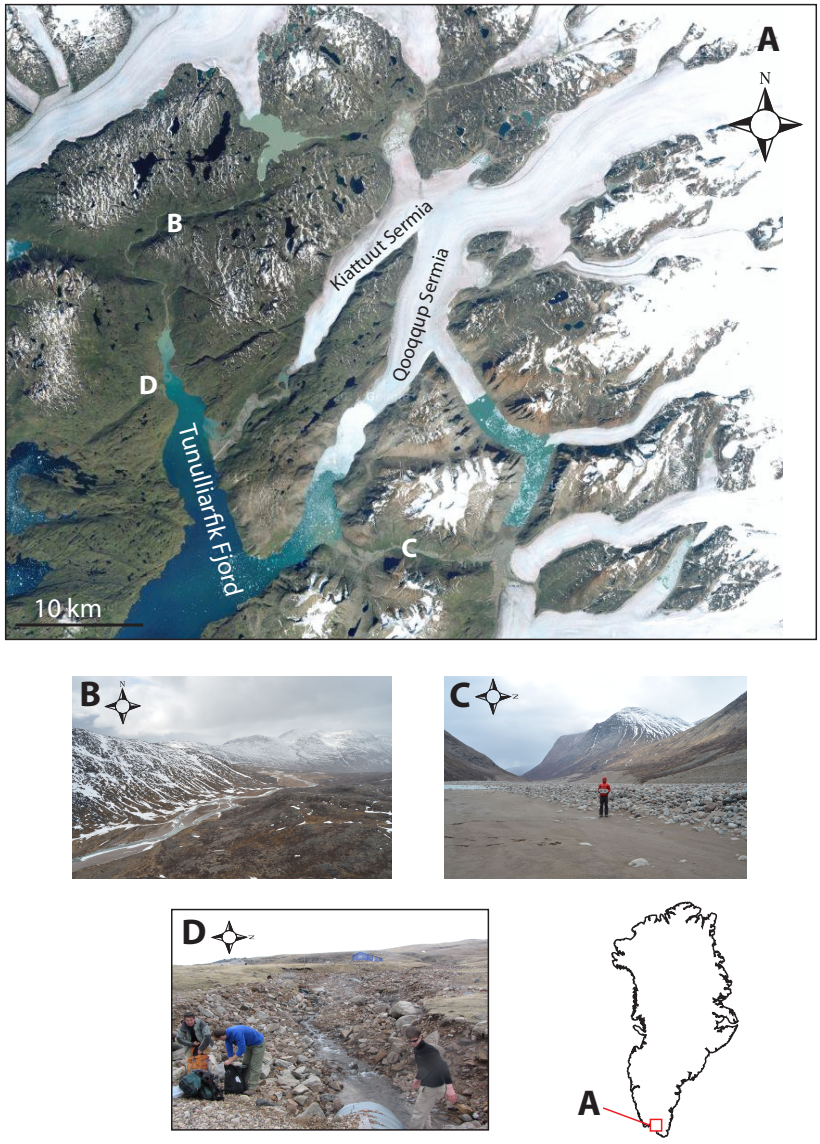

Figure 3: **A:** Google Earth image of the Narsarsuaq field area on the southern coast of Greenland. The northern portion of the field area is at a high elevation. Photo **B** is from an ice-free drainage basin because sediment sourced subglacially to the north is trapped in the upstream lake. The view in this photo is upstream, towards the highlands. The landscape here is mostly rocky with minimal vegetation and surficial cover. Photo **C** is from a glacial outwash channel that drains a low-elevation tongue of the ice sheet. The channel is in a steeply walled valley where there is minimal vegetation. The view is towards the fjord. Photo **D** is from a small ice-free drainage on the eastern side of Tunulliarfik Fjord. The stream flows through gently sloping terrain that is vegetated with shrubs and grasses. The view is up stream, to the southwest. Photos by Paul Bierman.

2.4. Study Area: Tasiillaq

Tasiilaq is on an island off the east coast of Greenland at ~65°N (Figure 4). The island separates the larger Sermilik Fjord to the west from the smaller Angmagssalik Fjord to the east (Figure 4B). Bedrock geology in the region is primarily granite and amphibolite facies and granulite facies gneiss (Escher and Pulvertaft, 1995). Southeast Greenland is mountainous and the study area is located at the southern end of the South Greenland Mountain Chain, where elevations exceed ~2,000 m asl. Three outlets of the main ice sheet feed Sermilik Fjord, including the marine terminating Helheim Glacier (Hughes et al., 2012). In the region there are also numerous local glaciers and ice caps, which are not connected to the main ice sheet (Hughes et al., 2012). Local climate is low arctic maritime and the region is within a zone of discontinuous permafrost. The average annual temperature is -2°C, average precipitation is ~980 mm a^{-1}, and the primary vegetation is dwarf-shrub heaths (Mernild et al., 2008).

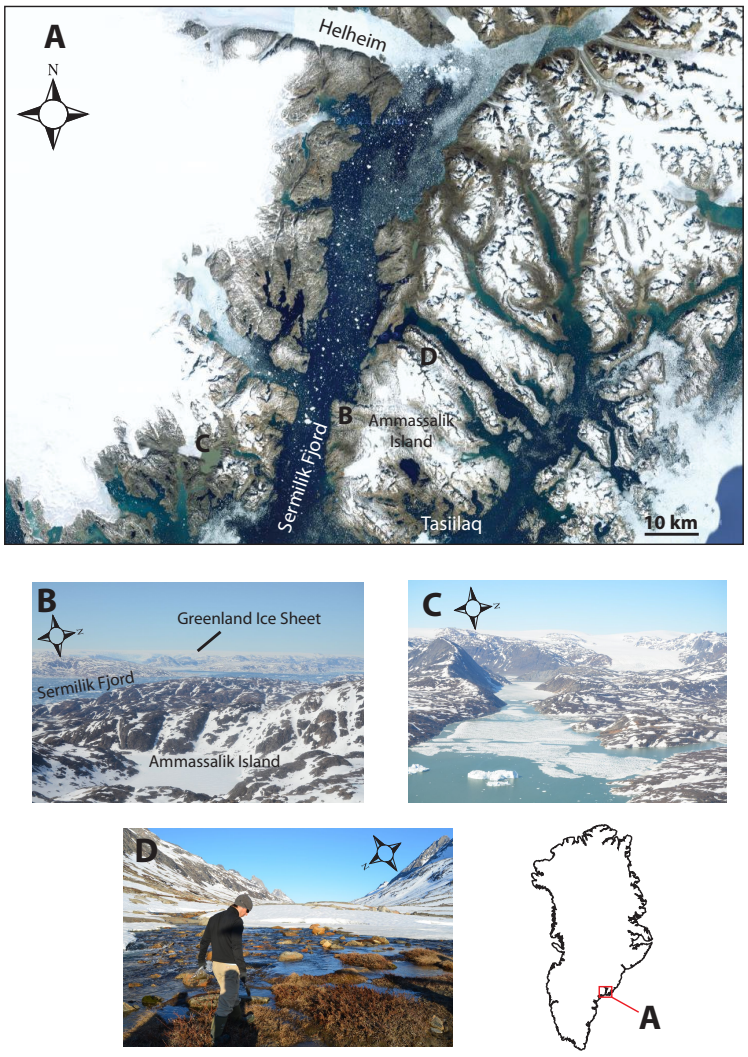

Figure 4: **A:** Google Earth image of the Tasiilaq field area. Photo **B** is an oblique areal photo looking to the west. The background of the photo is mainland Greenland and the Greenland Ice Sheet on the western side of Sermilik Fjord. The foreground of the photo is Ammassalik Island, which is partially glaciated by small ice caps and valley glaciers that are not connected to the main Greenland Ice Sheet. Photo **C** is an oblique aerial photo showing a tongue of the Greenland Ice Sheet. On the western side of the fjord, the land-based margins of the ice sheet terminate close to the fjord and so it was not possible to sample in downstream channel transects. Photo **D** is from an ice-free drainage on the eastern side of the fjord. The drainage has snow cover, but is not glaciated. The view is upstream, to the southeast. Photos by Paul Bierman.

3. Cosmogenic ^{10}Be

3.1. In Situ Production

The tool I am using to decipher ice sheet changes and sediment routing dynamics is the cosmogenic isotope ^{10}Be, which is produced *in situ* in near-surface rocks and sediment by cosmic rays. Primary cosmic rays are high-speed particles, mostly protons that originate from super novas in the Milky Way (Friedlander, 1990). These fast moving particles bombard the Earth where they change matter isotopically (Lal and Peters, 1967). Primary cosmic rays approach the Earth uniformly from all directions, and as they travel, they collide with one another, creating a cascading shower of secondary cosmic ray particles, mostly neutrons (Friedlander, 1990).

Primary cosmic ray particles are deflected by Earth's geomagnetic field and are more easily able to penetrate the atmosphere at the poles than at the equator (Lal and Peters, 1967). Secondary cosmic ray particles –protons, neutrons, or muons– are attenuated in Earth's atmosphere and so cosmic ray flux decreases with increasing atmospheric depth (Lal and Peters, 1967). As such, production of cosmogenic isotopes on Earth, such as *in situ* ^{10}Be, is strongly dependent on both latitude (geomagnetic effect) and altitude (atmospheric thickness) (Lal, 1991).

3.2. Application

In the 1980s, the advent of Accelerator Mass Spectrometry (AMS) enabled scientists to accurately measure very low isotope ratios and since then, cosmogenic isotopes have been used for a variety of geologic applications, such as terrestrial exposure dating (Gosse and Phillips, 2001). To use cosmogenic nuclides for research, isotope

concentrations must be accurately interpreted, which requires knowing the production rate of the given isotope at the specific sample location. Production rates of cosmogenic isotopes vary over space with depth, altitude and latitude, due to attenuation and geomagnetic deflection, and through time, due to modulation of cosmic-ray flux by the geomagnetic and heliomagnetic fields (Lal, 1988).

Spallation-produced cosmogenic isotopes are particularly useful for studying glacial processes because reactions that produce the isotope decrease exponentially with depth such that production is negligible 2 to 3 m below the surface (Lal and Peters, 1967). When a glacier advances, it will often erode enough surficial material to remove the upper portion of the rock where the highest concentration of cosmogenic isotopes has accumulated. The age of the exposed surface can then be calculated from the concentration of the isotope that has accumulated on the land surface since glacial retreat (Phillips et al., 1990). ^{10}Be can also be produced by muons – through negative muon capture and fast muon reactions (Lal and Peters, 1967). At the Earth's surface, ^{10}Be production by muons is very low, only about 1–3% of the production by spallation; but muons are able to penetrate deeply, and below ~4 m, production by muons exceeds production by spallation (Heisinger et al., 2002a; Heisinger et al., 2002b). Thus, over long periods of exposure and at great depths, muogenic production of ^{10}Be is significant (Braucher et al., 2003).

For this project, I am measuring the concentration of ^{10}Be in quartz because of its simple chemistry, relative abundance, resistance to weathering, and relatively long half-life (Kohl and Nishiizumi, 1992). The ^{10}Be production rate for Greenland, at sea level, is 3.98 ± 0.24 atoms g a^{-1}, and spatial changes in the production rate can be scaled using

CRONUS-Earth (Balco et al., 2008) according to the specific latitude, longitude, and elevation of a sample site (Briner et al., 2012). Temporal changes in production are less important because production rate changes are generally averaged out over the period of exposure (Gosse and Phillips, 2001). ^{10}Be has a relatively long half-life,1.39 My (Chmeleff et al., 2009; Korschinek et al., 2009), which means that isotope concentrations accumulated during the Holocene do not need to be corrected for decay. Additionally, the long half-life allows some of the isotopes to be preserved in marine sediments for millions of years.

4. Climate and Ice Sheet Overview

4.1. Climate Overview

Sediment processes on Greenland are directly related to climate because glaciers, which erode and condition the landscape (Church and Ryder, 1972), advance and retreat in response to changing climate. Greenland is a particularly useful setting to study the relationship between glaciers and sediment processes because the polar regions are more sensitive than the mid-latitudes to warming and cooling (Serreze et al., 2000). Climate is reconstructed from deep-sea sediment records, such as LR04 (Figure 5) (Lisiecki and Raymo, 2005) and SPECMAP (Imbrie et al., 1982), which use δ^{18}O values from benthic foraminifera as a proxy for ocean temperature and continental ice volume. The last five million years of climate change are of particular importance to this research because Greenland Ice Sheet inception likely occurred during the Pliocene, ~5–2.5 million years ago (Ma) and since inception, ice sheet extent has fluctuated with cyclical changes in

climate during the Pleistocene (~2.5 Ma–12 ka). The most recent period of warming and sediment exposure has occurred during the Holocene (12 ka–present).

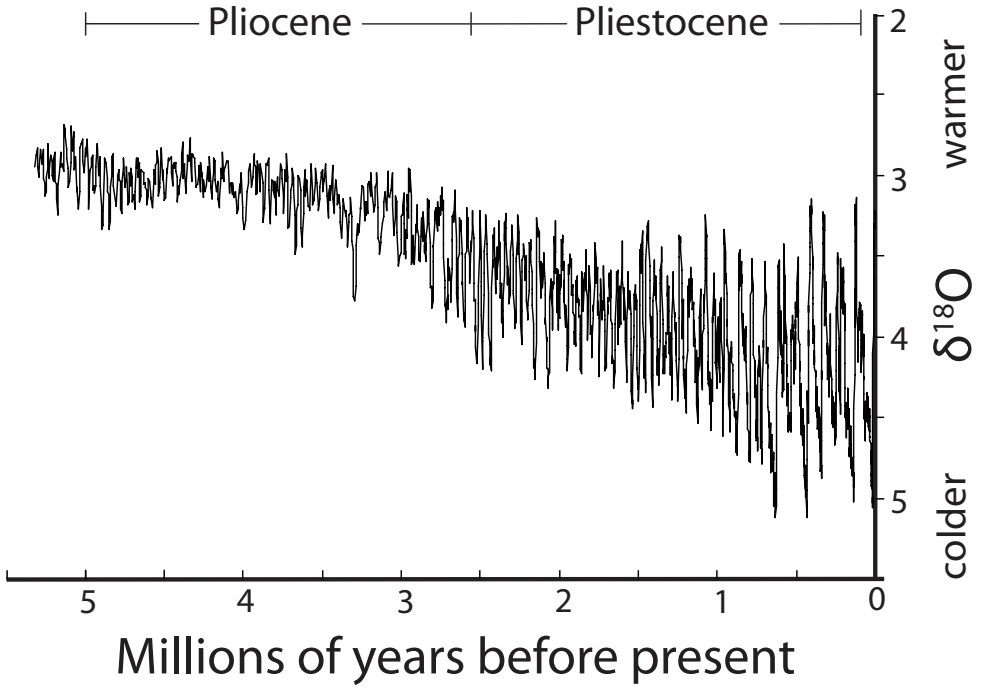

Figure 5: Pliocene-Pleistocene climate inferred from $\delta^{18}O$ data from (Lisiecki and Raymo, 2005). The graph shows climate cycles and an overall cooling trend.

4.2. Glacial cycles in the Pliocene and Pleistocene

The Pliocene was warmer and wetter than today (Salzmann et al., 2011) and ocean-atmosphere models, driven by sea surface temperature proxy records, indicate mid-Pliocene surface temperatures ~ 2 to 3ºC higher than present (Haywood et al., 2000; Lunt et al., 2010). The end of the Pliocene is coincident with major northern hemisphere glaciation, including inception of the Greenland Ice Sheet, and thus the epoch is characterized by relatively abrupt cooling as Earth transitioned from the warmer Miocene to the colder Pleistocene with cooling likely driven by plate motion (Cane and Molnar,

2001; Haug and Tiedemann, 1998; Keigwin, 1982) and declining greenhouse gas concentrations (Lunt et al., 2008). Throughout Pliocene and Pleistocene cooling (Figure 5) are Milankovitch cycles, which are fluctuations between warmer and colder states associated with changes in orbital precession, obliquity, and eccentricity (Imbrie et al., 1982). As a result of these cycles, the Earth swings between glacial and interglacial states and each shift is associated with major changes in glacial mass balance (Raymo et al., 2006).

For the last million years, changes in Earth's climate have been dominated by glacial-interglacial cycles that occur every 100 thousand years (ky) (Lisiecki and Raymo, 2007). Cycles are numbered according to their Marine Isotope Stage (MIS), with even numbers corresponding to glacial periods and odd numbers to interglacial periods (Figure 6) (Imbrie et al., 1982). The Pleistocene ends at the termination of the last glacial period (MIS 2) and is followed by Holocene (12 ka–present), during which temperatures warmed, and the Earth transitioned into its current interglacial state (MIS 1).

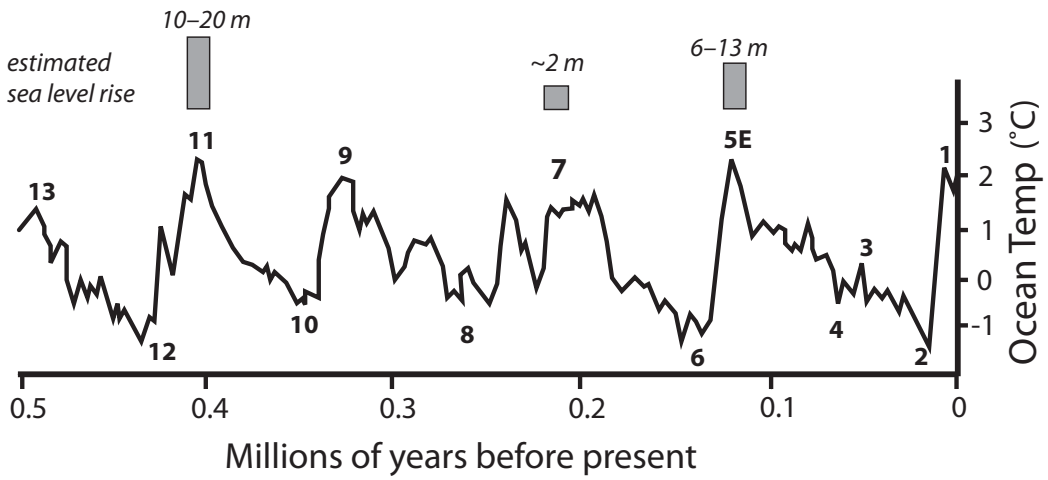

Figure 6: Temperature changes over the last half a million years (Imbrie et al., 1982). Climate cycles occur roughly every 100 ky and Marine Isotope Stages are numbered sequentially with odd numbers corresponding to interglacial periods and even numbers with glacial periods. Estimates are given for sea-level rise during MIS stages 5 (Kopp et al., 2009), 7 (Muhs, 2002), and 11 (Berger and Loutre, 1991; Hearty et al., 1999; Poore and Dowsett, 2001; Raymo et al., 2011; Roberts et al., 2012).

5. Glacial History of Greenland

5.1. Ice Sheet Inception

Records of long-term Greenland Ice Sheet history are derived primarily from ice rafted debris (IRD), which is the presence of coarse-grained sediment or drop stones in an otherwise fine-grained marine sediment matrix (Andrews, 2000; Gilbert, 1990; Ovenshine, 1970; Ruddiman, 1977). Coarse material reaches coring sites in the ocean when it is carried there by ice, and so the presence of IRD indicates glacial caving or ice shelf growth (Ovenshine, 1970). From the timing and distribution of IRD, it is possible to infer approximately when and where glaciers were reaching the marine realm; however,

other types of glacial reconstructions are needed to determine glacier or ice sheet size (St John and Krissek, 2002).

IRD records from the Arctic and North Atlantic Oceans suggest intermittent glaciation on Greenland since the Late Miocene (Alley et al., 2010). Ocean Drilling Program core 918 (Figure 1), has a pulse of IRD at ~7.3 Ma, followed by two fluxes at ~3.5 Ma and ~2.7 Ma (St John and Krissek, 2002). The mid Pliocene pulse at ~3.5 Ma is in other Arctic records, which show major increases in IRD between 3.5 and 2.4 Ma (Kleiven et al., 2002; Moran et al., 2006; Shackleton et al., 1984). Major Northern Hemisphere glaciation began ~2.75 Ma (Cane and Molnar, 2001; Lisiecki and Raymo, 2007), and so it is likely that expansion of the Greenland Ice Sheet at ~3.5 Ma preceded major ice sheet growth over Northern Europe and North America (St John and Krissek, 2002).

According to the timing of IRD pulses, the Greenland Ice Sheet likely began as a number of isolated alpine glaciers, which then grew and coalesced into one large ice sheet (DeConto et al., 2008). It is probable that southeast Greenland, which is mountainous and has high precipitation rates, was the nucleation site for large-scale ice sheet growth (Larsen et al., 1994; St John and Krissek, 2002). Expansion of the Greenland Ice Sheet would have changed the ^{10}Be concentration on the landscape. Prior to ice sheet growth, bedrock and surficial material would have accumulated significant amounts of ^{10}Be due to prolonged cosmic ray exposure. As the ice sheet grew, it would have shielded the landscape from cosmic rays, while eroding much of the underlying material containing high concentrations of ^{10}Be accumulated during the pre-ice period of exposure.

5.2. Ice Sheet Extent

Ice sheet size cannot be directly detected from IRD records, so Greenland Ice Sheet extent is often inferred from changes in eustatic sea level and from the stable isotope composition of seawater, with the caveat that these quantities reflect the total volume of ice on the planet rather than any particular ice sheet (Alley et al., 2010; Clark and Huybers, 2009; Cuffey and Marshall, 2000; Kopp et al., 2009). If sea level were significantly higher during a particular warm period, then the increased volume of water in the ocean had to come from a combination of thermal expansion and melting of ice sheets in the Arctic or the Antarctic. The two most likely sources of past sea-level rise are the Greenland Ice Sheet, which contains ~7 m sea level equivalent (Bamber et al., 2001), and the West Antarctic Ice Sheet, which contains ~3 m sea level equivalent (Bamber et al., 2009). Past sea-level rise is attributed to these two ice sheets because they are losing mass during the current period of warming (IPCC, 2007).

Since inception, the Greenland Ice Sheet has grown during glacial periods and has retreated during interglacial periods. Climate cycle amplitude has been linked to ice sheet mass balance (Alley et al., 2010) and marine isotope stages of particular interest are interglacial periods 5 and 11, when extent of the ice sheet was reduced, perhaps greatly, and glacial periods 6 and 2, when the ice sheet was at a maximum (Alley et al., 2010; Lisiecki and Raymo, 2005). These four stages are important to my sediment research because changes in ice sheet extent determine cosmic ray dosing of the landscape. Additionally, glaciation influences sediment processes in two ways. First, erosion is thought to be greater in glaciated landscapes than non glaciated landscapes (Cowton et

al., 2012; Gurnell et al., 1996; Hallet et al., 1996; Montgomery, 2002), however some studies have questioned this assumption (Hicks et al., 1990) and it is not yet fully understood how erosion rates for a given area might differ when ice covered versus when ice free. Second, perhaps most important to sediment mobility is the glacial history of a landscape and the timing of interglacial transitions. If a landscape is conditioned by glaciation, then there will be enhanced sediment movement in the paraglacial landscape that is exposed following glacier retreat (Ballantyne, 2002b; Church and Ryder, 1972; de Winter et al., 2012).

The four marine isotope stages mentioned above are also important to the larger research project because we expect the resultant changes in sediment ^{10}Be concentration to be visible in the core record. If the Greenland Ice Sheet were significantly smaller than it is today, there would be more land area exposed to cosmic rays and so the ^{10}Be concentration in sediment would be higher. In contrast, if the ice sheet extended past the continental shelf, there would be no ^{10}Be accumulation in sediment because the landscape would be entirely shielded from cosmic rays by ice.

5.3. MIS 11 (~425–375 ka)

MIS 11 was the longest, and possibly the warmest, of recent interglacials (Lisiecki and Raymo, 2005; Loutre, 2003; Roberts et al., 2012). Terrestrial and marine evidence suggest Greenland Ice Sheet extent was significantly, if not entirely reduced, likely due to the prolonged duration of warming. Sea levels were 10–20 m higher than today, indicating absence or significant reduction of the Greenland Ice Sheet (Alley et al., 2010; Berger and Loutre, 1991; Hearty et al., 1999; Poore and Dowsett, 2001; Raymo et

al., 2011; Roberts et al., 2012). Uncertain cosmogenic burial ages from beneath the GISP2 ice core site are consistent with a short duration of bedrock exposure (Figure 1), which supports complete loss of the ice sheet during MIS 11 (Nishiizumi et al., 1996). Pollen assemblages in marine sediment cores indicate boreal coniferous forest over much of southern Greenland and suggest that ice sheet reduction was significant enough for forest colonization (de Vernal and Hillaire-Marcel, 2008; Steig and Wolfe, 2008). If the ice sheet melted enough to expose bedrock at GISP2, and if it were reduced long enough for forest growth, then ^{10}Be would have accumulated on and below the land surface.

5.4. MIS 6 (188–130 ka)

The Greenland Ice Sheet was at a maximum during MIS 6, with ice extending over areas of southeast and northeast Greenland not glaciated today (Funder et al., 1998; Hakansson et al., 2011). Iceberg plow marks and evidence of ice sheet grounding suggest thick ice over the continental shelf and extending north over Ellesmere Island and the Canadian Arctic Archipelago (Jakobsson et al., 2010). During MIS 6 there was no ^{10}Be accumulation on the land surface, however ice sheet growth over the continental shelf would have rapidly delivered sediment to the ocean.

5.5. MIS 5E (130–115 ka)

The Greenland Ice Sheet was also smaller during MIS 5E (The Last Interglacial) when sea levels were at least 6.6 m higher than today (Kopp et al., 2009), though Greenland may have contributed only ~2 m to this high stand (Colville et al., 2011).

Pollen concentrations in ocean sediment cores spanning MIS 5E are much higher than during the Holocene and indicate shrub growth and fern vegetation on Greenland (de Vernal and Hillaire-Marcel, 2008). MIS 5E basal ice is absent at the Dye-3, Camp Century, and Renland ice coring locations (south, northwest, and east Greenland respectively), but is present at the GISP2, GRIP, and NGRIP core sites (central and north central Greenland), which suggests that margins of the ice sheet were considerably reduced (Alley et al., 2010). Modeling by Otto-Bliesner et al. (2006) produced an ice sheet of reduced extent in agreement with ice core data. In the model, simulated ice retreat contributes 2.2 to 3.4 m of sea-level rise (Otto-Bliesner et al., 2006). Similar to my expectations from MIS 11, the concentration of ^{10}Be in sediment exposed terrestrially during MIS 5E would be higher than during a glacial period and concentration would be related to the aerial extent of the exposed land surface and the duration of cosmic ray exposure.

5.6. MIS 2 (~26–20 ka)

MIS 2, commonly referred to as the Last Glacial Maximum (LGM), ends the Pleistocene and was the most recent time Earth was in a glacial state. Ice on Greenland covered most land margins and also extended out onto the continental shelf (Weidick et al., 2004). Previous cosmogenic research in Greenland has used ^{10}Be dating to constrain ice sheet thickness during the LGM because some glacially polished, high elevation peaks and plateaus contain high concentrations of ^{10}Be, indicating these regions were ice-free during MIS 2 and have been accumulating ^{10}Be since the end of MIS 6 (Figure 7) (Hakansson et al., 2007a; Hakansson et al., 2011; Rinterknecht et al., 2009; Roberts et al.,

2009). Aside from exposure in the ice-free high elevations, there was little *in situ* ^{10}Be accumulation on the landscape during MIS 2 because of extensive ice sheet growth. Erosion rates inferred from ^{10}Be depth profiles (Goehring et al., 2010) and paired bedrock and boulder ^{10}Be concentrations (Corbett et al., 2011) suggest the landscape has eroded differentially during the last glacial cycle with at least 2 m of erosion at some locations (Corbett et al., 2011; Goehring et al., 2010), but only limited erosion at others (Hakansson et al., 2011).

Previous studies have used cosmogenic isotope concentrations to show that subglacial erosion can be differential (Briner et al., 2006; Colgan et al., 2002; Davis et al., 2006) because glacial erosion is dependent on bedrock properties, tectonic activity, and the subglacial thermal regime (de Winter et al., 2012; Hallet et al., 1996; Harbor, 1993; Sugden, 1977). On Greenland, differences in subglacial erosion are most likely due to differences in basal temperature because Greenland is tectonically inactive and bedrock properties are relatively uniform across the island (Escher and Pulvertaft, 1995). Basal ice temperature is determined by a number of factors including, surface temperature, accumulation rate, surface warming, geothermal heat, and frictional heat (Sugden, 1977). More erosion occurs under areas of warm-based ice, versus cold-based ice that is frozen to its bed, because of greater sliding and mechanisms that promote evacuation of debris from beneath the ice (Hallet et al., 1996; Sugden, 1978).

Generally, the Greenland Ice Sheet is warm-based and more erosive along the margins, particularly in areas of low elevation, where the ice sheet thickness is great and subglacial melt water promotes basal sliding (Cowton et al., 2012; Sugden, 1977, 1978). Where sub-ice erosion is sufficiently deep to have removed most cosmogenic isotopes

accumulated during preceding interglacials, it is possible to date Holocene retreat from the concentration of cosmogenic ^{10}Be that has since accumulated on the land surface. However, in some areas of high elevation, bedrock and boulder surfaces contain inherited nuclide concentrations because the overlying ice sheet was thin and frozen to its bed, and subglacial erosion was not great enough to remove all of the cosmogenic isotopes accumulated during prior exposure (Corbett, 2011; Hakansson et al., 2011).

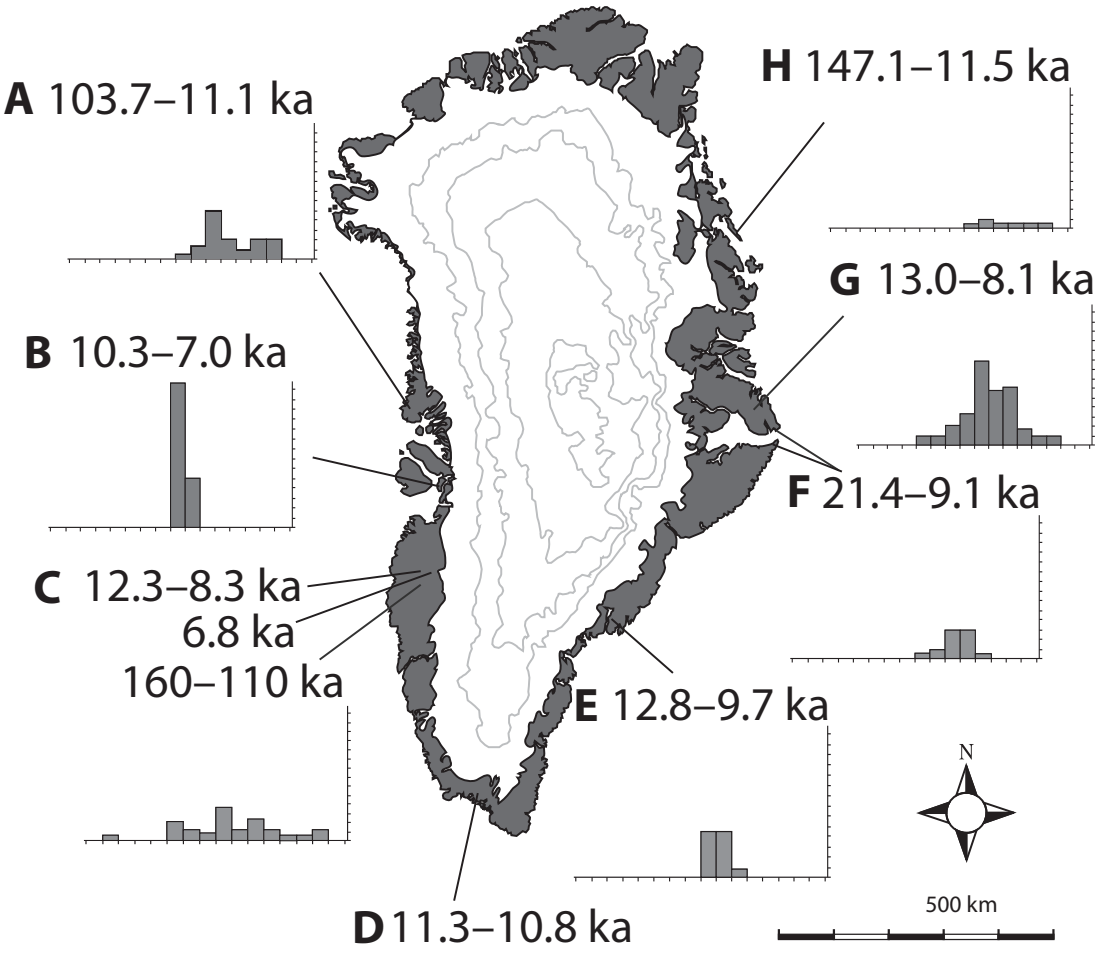

Figure 7: Map of Greenland showing single nuclide exposure age ranges from previously published cosmogenic ^{10}Be data (n=242). Ages and concentrations are as reported in papers. Histograms show the log-scale distribution of ^{10}Be concentration for each region. The count scale on the y-axis goes to 35 and the log-scale of concentration on the x-axis ranges from 2.5–6.5. Data is from **A** (Corbett, 2011), **B** (Corbett et al., 2011; Young et al., 2011), **C** (Levy et al., 2012; Rinterknecht et al., 2009; Roberts et al., 2009), **D** (Carlson et al., 2012), **E** (Roberts et al., 2008), **F** (Hakansson et al., 2007a; Hakansson et al., 2011; Hughes et al., 2012), **G** (Goehring et al., 2010; Kelly et al., 2008), **H** (Hakansson et al., 2007b).

5.7. Holocene (~12 ka–present)

The Holocene is particularly important to this research because timing of ice retreat is well constrained and sediment produced during deglaciation is currently sitting on the land surface, moving down stream networks, and accumulating ^{10}Be. We measured the concentration of ^{10}Be in modern fluvial sediment and in sediment from old deltas/terraces deposited when the ice sheet was outboard of its current extent, and related concentration to the exposure history of the sediment source area. The relationship that exists in the modern, between landscape exposure and sediment ^{10}Be concentration, is an analogue that will be used in the future to interpret the down core sediment record.

Ice extent during MIS 2, and subsequent Holocene retreat, is well constrained because moraine systems and exposed surfaces have not yet been overrun by a period of extensive glacial regrowth – making it possible to date retreat using lichenometry, radiocarbon, and cosmogenic ^{10}Be. A series of radiocarbon-dated moraines in western Greenland, first recorded and named by Ten Brink (1975), indicate terminal ice position during periods of Holocene stabilization or readvance. The oldest "Hellefisk" moraines, associated with the Last Glacial Maximum, sit on the continental shelf ~100 km off shore of Sisimiut (Kelly, 1985). The "Taserqat" moraine system indicates ice position at the present day land margin ~10 ka (van Tatenhove et al., 1996). Throughout the early Holocene, ice retreated to the position of the "Ørkendalen" moraine system, which lies 1 to 2 km from the present ice margin and is dated to ~6.8 ka (Levy et al., 2012; van Tatenhove et al., 1996). Timing and rates of retreat differ geographically; however, previously published cosmogenic ^{10}Be dates fit a common pattern with margins of

Greenland becoming ice free ~10 to 12 ka and ice retreating to close to its present position by ~7 to 8 ka (Figure 7) (Corbett et al., 2011; Hughes et al., 2012; Kelly et al., 2008; Levy et al., 2012; Rinterknecht et al., 2009; Roberts et al., 2009; Roberts et al., 2008; Young et al., 2011).

Retreat rates during the early Holocene, when temperatures were ~2°C warmer than today (Dahl-Jensen et al., 1998), range from 80 to 110 m a^{-1} (Corbett et al., 2011; Hughes et al., 2012; Young et al., 2011). During the warm mid-Holocene, ice retreated inland of its present position, and while the exact amount of retreat is unknown, it was likely on the order of 10s of kilometers (Weidick et al., 1990). Following the mid-Holocene climatic optimum, the ice sheet readvanced during the Neoglacial (~4 ka) and again during the Little Ice Age (AD 1300–1900) (Forman et al., 2007; van Tatenhove et al., 1996). In Kangerlussuaq, the Ørkendalen moraines (~6.8 ka) are cross cut by Little Ice Age moraines and Neoglacial moraines are obscured (Levy et al., 2012).

Since the Little Ice Age, retreat of land-based margins of the Greenland Ice Sheet has been variable, with 1 to 2 km of retreat punctuated by brief periods of readvance near Narsarsuaq (Weidick, 1968), and only limited retreat (<0.5 km) near Kangerlussuaq (Levy et al., 2012). 20th century melt has been pronounced with margins of the ice sheet south of Kangerlussuaq retreating 180 to 570 m between 1942 and 1978 (Gordon, 1981). In recent years, mass loss from the ice sheet has increased with ~80 km^3 a^{-1} of ice lost between 1997 and 2003 compared to losses of ~60 km^3 a^{-1} between 1993/4 and 1998/9 (Krabill et al., 2004). Ice sheet melt has accelerated in the 21st century yielding 0.46 to 0.75 mm a^{-1} of sea level equivalent (van den Broeke et al., 2009). Summer 2012 was one

of the warmest in recent history setting records for total melt, melt surface extent, and melt season duration (Tedesco et al., 2012).

5.8. Future

Global warming is expected to continue in the future – and at an accelerated rate – with temperature changes in the 21st century greater than those observed in the 20th century (IPCC, 2007). Model assessments indicate surface temperatures at the end of the next century will be 2 to 4.5ºC warmer than they are today (IPCC, 2007) and we can expect the Greenland Ice Sheet to be smaller in a world that is warmer. The 2007 IPCC report predicts sea level to rise ~0.2 to 0.6 m by 2100 due to glacial melt and thermal expansion; however, more recent publications have revised and increased this prediction. Nicholls et al. (2011) suggest that if Earth warms by 4ºC or more, sea level will rise 0.5 to 2 m by the end of the century due in part to increased ice discharge from the Greenland Ice Sheet. Similarly, Pfeffer et al. (2008) and Grinsted et al. (2010) predict sea level rise over the same period of 0.8 to 2 m. The discrepancy between IPCC sea level rise predictions and more recently published predictions is due to the inability of scientists, at the time of IPCC publication, to accurately predict contributions from large ice sheets – highlighting the importance of understanding how the Greenland Ice Sheet responds to changing climate.

6. Sediment Budgeting: An Overview

6.1. Definition and Importance

Accurately interpreting fluctuations in ice extent from ^{10}Be concentration in core sediment requires understanding the timing of sediment delivery to the coring site in the ocean. All processes related to sediment erosion and transportation are part of landscape's "sediment budget" which refers to "the sources and disposition of sediment as it travels from its point of origin to its eventual exit out of a defined landscape unit (Beylich, 2011)." To make a sediment budget, one must quantify and relate the processes that generate and transport sediment (Dietrich and Dunne, 1978). Sediment budgets are calculated most reliably through long term monitoring (Beylich, 2011) because surface processes are highly variable in time and space and act over long time scales (Dietrich and Dunne, 1978).

Sediment budgets can be considered on a variety of time scales. For my thesis, I am interpreting the ^{10}Be concentration in recently collected fluvial sediments to understand the glacial and non-glacial processes, which erode and transport surficial material across the landscape on the time scale of the Holocene. Cosmogenic ^{10}Be in fluvial sediment can be used as a tracer because isotope concentration will reflect source area exposure and contribution (Reusser and Bierman, 2010). For the larger project, we will be deciphering changes in ^{10}Be concentration over a 5 million-year sediment core record, so we will also need to understand how sediment budgets differ on a longer-term time scale that spans glacial and interglacial periods.

6.2. Part One: Sediment Budget over the Holocene

I am analyzing fluvial sediment samples collected in transects spanning the ice margin to the fjord mouth. For each sample, I am trying to understand (a) the sediment source, (b) the erosional history, and (c) the cosmic ray exposure history, which includes exposure as bedrock prior to erosion as well as exposure as sediment that is moving through and stored within the landscape. For the Holocene sediment budget, sediment exits the landscape when it is deposited into the fjords.

To assess Greenland's sediment budget during the most recent period of deglaciation, I need to understand sediment processes in the paraglacial environment, which is defined by Church et al. (1972) as an exposed landscape subject to rapid change due to glacial and non-glacial processes acting upon a landscape conditioned by glaciation. Ballantyne (2002a) further defines the paraglacial landscape as existing within a time frame over which glacially conditioned sediment is either released from the landscape or reaches an equilibrium, non-glacial state.

Margins of Greenland are partially glaciated and so are classified as "secondary paraglacial" environments, because sediment yield is determined by both the reworking of paraglacial sediment stores and the release of *in situ* glacially derived sediment (Ballantyne, 2002a). Kangerlussuaq is the most studied of my field areas, so I am using this location to illustrate the components of a secondary paraglacial system (Figure 1). The town of Kangerlussuaq, at the mouth of the Søndre Strømfjord, is separated from the Russell Glacier lobe of the Greenland Ice Sheet by a 25 km long valley. Outwash from the ice sheet is drained by several tributaries, which flow into the Watson River and down

valley into the fjord. Moraines in this region are well documented and the timing of Holocene ice retreat is well constrained (Levy et al., 2012; Ten Brink, 1975).

Storms et al. (2012) describe regional sedimentary processes during Holocene retreat as occurring in three phases. In phase one, the ice margin reached the sea and sediment deposition occurred within Søndre Strømfjord. In phase two, ice retreated to the present day fjord mouth ~7.5 to 8 ka and then became land-based and continued to retreat inward (Ten Brink and Weidick, 1974; Weidick et al., 1990). During this phase, sedimentation occurred within the valley where infill sequences are 40 to 80 m thick (Storms et al., 2012). During the latter part of phase two, ice retreated inland of its present position, briefly exposing to cosmic rays a portion of the landscape currently shielded by ice (Weidick et al., 1990) before readvancing during the Little Ice Age (Levy et al., 2012). Phase three spans the Little Ice Age to the present; in this phase, sediment has been largely bypassing the valley and deposition is occurring on the modern delta at the fjord mouth (Storms et al., 2012).

Our sediment samples fall along a spectrum that includes (a) *in situ* glacially derived sediment, (b) stored paraglacial sediments, and (c) paraglacial sediments sourced from the exposed hill slopes (Figure 8). Sediment sources can be further described by activity; frequently accessible and mobile sediment sources are characterized as "active" and sediment sources that only become mobile through periodic events are characterized as "semi-active" (Kelsey et al., 1987).

On the modern Greenland landscape, one of the primary sediment sources is derived *in situ* from beneath the ice sheet and alpine glaciers; this is an active source that produces glacial sediment seasonally when melt is occurring (Bartholomew et al., 2011).

Some studies have indicated that suspended sediment concentration in Arctic glacial environments is positively correlated to discharge (Bartholomew et al., 2011; Fausto et al., 2012; Hodson et al., 1998; Stott and Grove, 2001); however, suspended sediment concentration depends on subglacial sediment supply, which can be flushed and depleted, and so sediment concentration and discharge do not necessarily scale linearly (Cowton et al., 2012; Stott and Grove, 2001).

A second active sediment source is the glacial forelands, which are paraglacial storage reservoirs that become mobile through mass-movement, fluvial, and aeolian processes (Ballantyne, 2002b). Sediment stored within ice-cored moraines remobilizes seasonally, when melt occurs, through slumps, slides, and glacial outwash erosion (Ballantyne, 2002b; Etzelmuller, 2000; Rose, 1991). Ice cored moraines can be a significant sediment source; in a study of three glacial drainages in Svalbard, annual sediment mobilization due to thermo-erosion process is on the same order of magnitude as annual suspended sediment load (Etzelmuller, 2000).

Mass-movement and fluvial processes also act on gentler slopes, where sediment mobilizes towards the fluvial valley by frost-creep, gelifluction, and slopewash (Ballantyne, 2002b). Sediment stored in the channel bottoms and banks is also active during peak melt, when river discharge reaches or exceeds bankfull stage and erodes the banks (Hammer and Smith, 1983; Warburton, 1990). Aeolian processes can also mobilize glacial sediment, particularly during early stages of deglaciation when katabatic winds mobilize fine sediment on a non-vegetated landscape (Ballantyne, 2002b; Willemse et al., 2003)

Semi-active sediment sources include stored paraglacial sediment that only mobilizes periodically. Paraglacial sediment, stored in flood plains and in terraces, is *in situ* glacially derived sediment from a prior period of melt. These sediment sources are only active when the river exceeds bankfull stage because of jokulhaup or extreme melt or rain events. Other semi-active sediment sources include talus cones, which may be mobilized by fluvial reworking (Ballantyne, 2002b), and fjord-head deltas, where slope-failure occurs periodically (Prior et al., 1981).

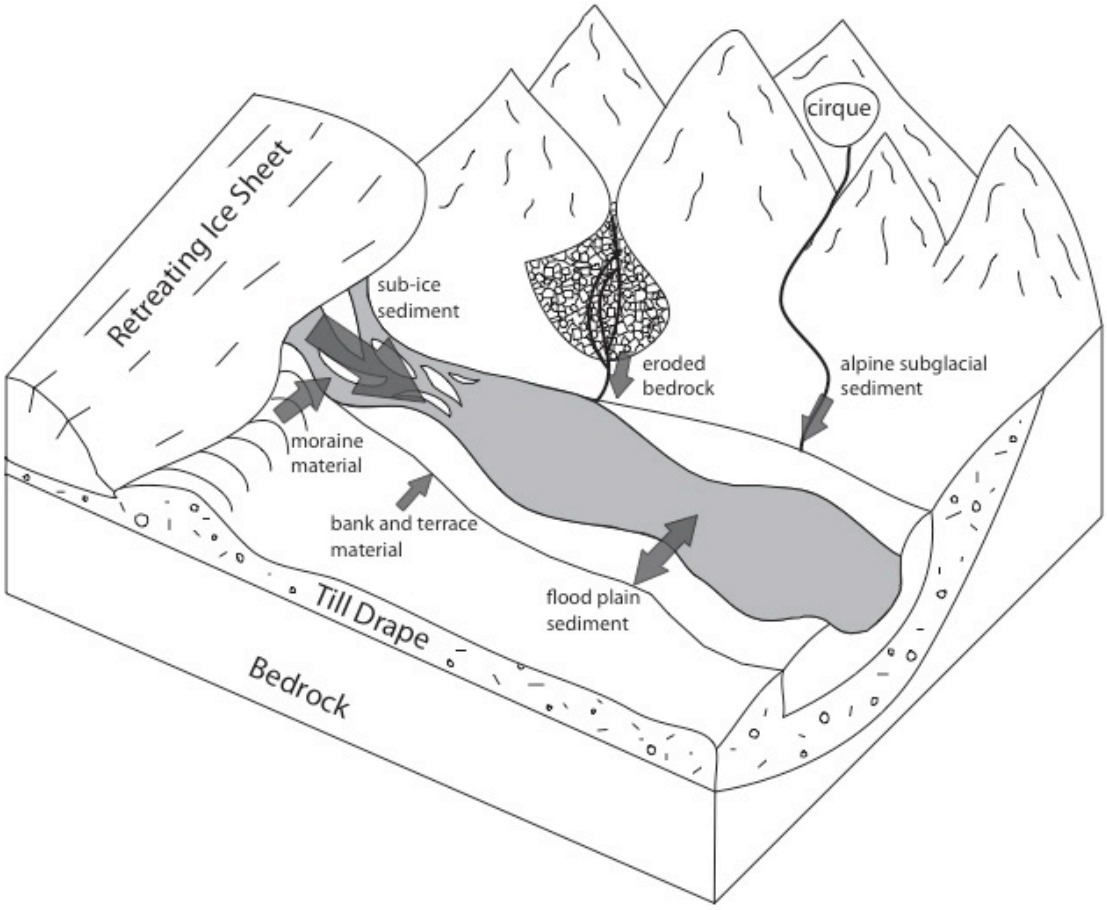

Figure 8: Schematic illustration showing sediment sources on the paraglacial landscape. The top of the picture represents mountainous terrain and the bottom of the picture represents a wide valley.

6.3. Part Two: Sediment Budget over the Pliocene and Pleistocene

The larger research project requires a longer-term sediment budget because the sediment we are going to analyze has been accumulating in the deep ocean for several million years. For this sediment budget, we need to consider the timing of sediment production, storage, and deposition at the coring site. Typically, sediment mobilized during deglaciation is stored within fjords and on the landscape (Harbor and Warburton, 1993) and is not evacuated to the deep ocean until the next period of glacial growth (Koppes et al., 2010). During a glacial-interglacial cycle, fjord infilling occurs in a series of sequential stages beginning with (1) occupancy by glacial ice, (2) proximal sedimentation from a marine-based glacier, (3) distal, pro-glacial sedimentation from a land-based glacier, and (4) distal sedimentation from the paraglacial environment (Syvitski and Shaw, 1995). With glacial regrowth, valley-infill and fjord sediment are evacuated to the deep ocean and the cycle begins again; thus, each glacial cycle resets the fjord and valley sediment infill sequence (Storms et al., 2012). When we interpret the marine sediment record, sediment delivery to the deep ocean will be coincident with a period of glacial advance.

At present, different stages of the sequence described by Syvitski et al. (1995) are occurring on Greenland where fjords are characterized along a continuum from stage 2 to 4 of the fjord-infill process. For example, three types of sources feed Sermilik Fjord on the east coast, and each of these sources represents a different stage in the infill sequence: the marine terminating Helheim lobe of the ice sheet is representative of stage 2, alpine glaciers and land-based tongues of the ice sheet are representative of stage 3, and fluvial

valleys where only small ice caps are present are an example of stage 4. Ultimately, sediment produced during each of these stages will mix together and be stored in the fjords until the next glacial advance (Desloges et al., 2002; O'Cofaigh et al., 2001; Smith and Andrews, 2000; Storms et al., 2012). Understanding the ^{10}Be concentration in sediment on the landscape, from different sources, will then allow us to infer the ^{10}Be concentration of sediment in the fjords and will then help us to interpret the ^{10}Be concentration in sediment in the deep ocean.

CHAPTER 3. DETAILED METHODOLOGY

1. Field Methods

1.1. Sampling Strategy

Sediment samples were collected near Kangerlussuaq and Narsarsuaq during the summer of 2011 (by Bierman, Portenga, Rood, and Shakun) and near Kangerlussuaq and Tasiilaq (by Bierman, Nelson, Rood, and Shakun) during the summer of 2012. Where possible, we collected samples in transects from the ice margin to the fjord mouth and from tributary valleys draining ice-free or partially glaciated basins. When possible, we also collected sediment stored in terraces and moraines (categorized as glacial). For terrace samples, we collected sediment at least several meters below the surface, a depth sufficient to minimize post depositional ^{10}Be accumulation; the ^{10}Be concentration measured in terrace samples represents the ^{10}Be concentration at the time of deposition, in the early Holocene.

The Kangerlussuaq sample sites from 2011 were resampled in 2012 to determine if there were temporal changes in concentration. Resampled sites are labeled by adding an "R" to the original sample number. Summer 2011 sampling happened in late May when the fluvial system was frozen. Most channels contained little if any water, and there was no connectivity; sampled sand for the most part represented the last material moved during summer and fall of 2010. The summer of 2012 had record warmth. Sampling took place in early June, and by then rivers and streams were almost completely ice free; water levels were near bankfull, sediment mobility was much higher than in 2011, and the sediment we sampled was moving rapidly downstream.

In Narsarsuaq, we also collected bedrock and boulder pairs for ^{10}Be exposure dating to estimate when the ice-free portion of the field area became ice-free. We collected bedrock and boulder samples in pairs because an erratic boulder will have a different pre-exposure history then the nearby bedrock, and so a paired analysis is a useful way to test for isotopic inheritance (Corbett et al., 2011).

1.2. Sample Collection

Sample locations were recorded using a Garmin 12 GPS. For sediment samples, we collected 1 to 2 kg (dry weight) of sand, which we then stored and transported in heavy-duty ziplock bags. At each sample site, we took notes about the sediment source, the proximity to the ice, and characteristics of the fluvial drainage. We also took multiple photos at each site, at least one of which included the sample name on a sign. This system allowed us to later match our field notes to the photographs and also to the sample location in Google Earth. In 2012, when we re-sampled sites in Kangerlussuaq, we had the photos from 2011 as well as GPS coordinates with us in the field so that we could accurately match the sample locations.

For bedrock and boulder samples, we used a chisel and hammer to chip off the top few centimeters of rock material. We chose flat-lying samples to avoid exposure histories that have been complicated by topographic shielding, and we chose intact surfaces that showed minimal signs of post-glacial erosion.

2. Laboratory Methods

2.1. Quartz Isolation

At the University of Vermont, bedrock and boulder samples were crushed and ground, and all samples were dried and sieved to isolate the 250 to 850 μm sand fraction. Samples were also magnetically separated to eliminate mafic minerals. In the mineral separation lab, samples were sonicated in a series of hot acid etches to remove "garden variety" ^{10}Be and to preferentially dissolve non-quartz minerals following a method adopted from Kohl and Nishiizumi (1992).

First, the samples were etched twice in 6N HCl to remove carbonate minerals and iron oxides. After each ~24 hour etch, the samples were thoroughly washed in deionized water and following the final rinse, the samples were dried in the oven. Next, ~40 g portions of each sample were etched in heated ultrasounds three times in 1% HF/HNO_3 to dissolve clays, feldspars, and other non-quartz minerals. Between each 24-hour etch, the samples were rinsed three times in deionized water. Following the third etch, the sample portions were recombined and etched for 72 hours and then one week in 0.5% HF/HNO_3. After this "long etch", the samples were rinsed, dried in the oven, and then visually inspected for quartz purity.

Samples containing abundant black or dark red non-quartz grains were further purified using density separation. Approximately 10 g portions of each sample were placed in conical, 50 ml tubes, to which we added ~15 ml of Lithium Sodium Polytungstate (LST), which was prepared to the density of quartz, about 2.7 g cm^{-3}. The samples were then sonicated for 10 minutes and centrifuged for 10 minutes. The combination of sonication and centrifuging created a clear separation between the quartz

grains, which rose to the top of the liquid, and the darker, heavier grains, which sank to the bottom.

The bottom of each sample tube was then dipped in liquid nitrogen, just deep enough to freeze the heavy minerals. With the sample tube partially frozen, the heavy mineral grains were locked in place at the bottom of the tube, and with the aid of a deonized water squirt bottle, we were able to pour the quartz grains and the liquid LST off the top and into a beaker. Sample aliquots were recombined and the samples were rinsed with deionized water and dried in the oven. The dilute LST was filtered and dried down to the density of quartz for reuse. Following density separation, samples underwent a second "long etch" for 72 hours plus one week in 0.5% in HF/HNO_3 to remove any impurities from the LST.

For all samples, quartz purity was tested by inductively coupled plasma optical emission spectrometry (ICP OES) using a 0.25 g sample aliquot. For samples that were not pure enough (more than 200 ppm Al), an additional long etch was done until desired quartz purity was achieved. Prior to Be isolation, samples were etched a final time, inside of the cosmogenic clean lab, in dilute HF/HNO_3, using acid-washed Teflon beakers. This final, ~4 hour etch, ensured that any dust or impurities from the mineral separation lab were removed prior to Be isolation.

2.2. Be Isolation

Beryllium was isolated in the University of Vermont Cosmogenic Laboratory, using ~20 to 40 g of purified quartz. All samples were processed in the dedicated, low-level sample hood using lab ware and equipment that is reserved for samples that contain

low isotope concentrations. Laboratory processing followed standard procedures outlined in Corbett et al. (2011) and described in detail on the cosmogenic lab website (www.uvm.edu/cosmolab).

Samples were processed in batches of 12, which included 2 process blanks. To each sample and blank, we added about 250 µg of beryl-derived ^{9}Be carrier and enough Al carrier to reach 2,500 µg total Al in the sample. If there were already at least 2,500 µg of native Al in the sample, then no additional Al was added. Over several days, samples were dissolved in HF, that was slowly heated to 140°C. Following complete dissolution and dry-down in the presence of HCl, HNO_3, and $HClO_4$ the samples were treated with three addtional $HClO_4$ dry-downs and two HCl dry-downs to break down any residual fluorides and convert the samples to chloride form.

Samples were then brought up in 6N HCl and passed through anion-exchange resin columns to remove iron. Following Fe-removal, samples were converted to sulfate-form and passed through cation-exchange resin columns to separate Be, Al, and Ti. The Ti fractions were discarded, and the Al and Be fractions were dried down, and then redissolved in 1% HNO_3. Using drop-wise addition of 30% and 15% NH_4OH in the presence of methyl red indicator, sample solutions were made basic, allowing for the precipitation of Be and Al hydroxide gels, which were washed in 18.2 Mohm water. Be gels were dried, ignited, and packed into stainless steel cathodes (LLNL) or copper cathodes (SUERC) for AMS measurement. Al gels have been archived.

2.3. AMS analysis

Samples collected during the summer of 2011 were measured at the Lawrence Livermore National Laboratory (LLNL) AMS facility and were normalized to standard 07KNSTD3110, with a reported ration of 2850 x 10^{-15} (Nishiizumi et al., 2007). Samples collected during the summer of 2012 were measured at the Scottish Universities Environmental Research Center (SUERC) and were normalized to the NIST standard with an assumed ratio of 2.79 x 10^{-11}, which is consistent with the 07KNSTD standard assuming a half-life of 1.36 My (Nishiizumi et al., 2007). For batches processed at LLNL, the average blank ratio of Be^{10}/Be^{9} was 6.44 ± 4.11 x 10^{-16} (n=9). For processing at SUERC, the average blank ratio was 1.24 x 10^{-15} ± 5.28 x 10^{-16} (n=7). Appropriate blank subtractions were made for all samples and the uncertainty of the blank was propagated quadratically.

3. Data Analysis

3.1. Sediment Samples

Using photographs, field notes, and landscape imagery, we classified the source for each sediment sample into the following categories: glacial, ice-free, mixture (glacial and non glacial sediment sources), or terrace. Glacial category samples include sediment collected from the ice, and sediment from lateral moraines, ground moraines, and outwash tunnels, as well as channels, and flood plains proximal to the ice margin. We categorized one sample from a sand dune as aeolian. To assess temporal variability, we compared channel replicates from Kangerlussuaq using a one-way analysis of variance (ANOVA) and we removed GLX-04 and GLX-04R from the comparison

because the GLX-04 concentration is an extreme outlier (more than three times the inter quartile range outside of third quartile).

A student's t-test indicated that means of 2011 and 2012 temporal replicate fluvial sediment sample concentrations are statistically inseparable (p=0.08). The two sample groups passed the Brown-Forsythe test for equal variance (p=0.22); however, the percent standard deviation for 2011 samples was higher (46%) than for 2012 samples (23%). The greater variability in 2011 channel sediment compared to 2012 channel sediment is likely due to seasonality, so we used the 2012 concentration data for categorical comparisons because we believe that sediment collected at or near bankfull flow is likely to be better mixed. We compared the mean sediment concentration of the source categories using Tukey's Honestly Significant Difference test; concentrations were first transformed using a log base-10 transformation to ensure equal variance. The terrace category was not included in the statistical comparison because the sample size (n=3) is small.

To determine relative contribution of glacial versus ice-free sediment sources to the channels, we use a simple two component mixing model:

$$C_g x + C_i y = C_m \quad (1)$$

in which C_g= glacial concentration (atoms g^{-1}), C_i= ice-free concentration (atoms g^{-1}), C_m= mixed concentration (atoms g^{-1}), and x and y are fractions, which add to one. To analyze how ^{10}Be concentration in sediment could have accumulated, we considered the sample's potential exposure history. In our analyses, we used three different equations: spallation production at the surface and shallow depths (Equation 2), "steady-state" muogenic production for long periods of exposure and depths ≥10 m below the

surface (Equation 3), and spallation production on a surface that is eroding (Equation 4). For each of the equations, we used parameters that are well defined – concentration, production rate, density, attenuation, and decay –to solve for the parameters that are unknown – such as exposure duration and erosion.

For production by spallation in glacial sediment, we integrated the concentration at depth equation (Lal, 1988) and took the average over a specified erosion depth

$$\frac{1}{b-a}\int_{a}^{b}\left(P_{s,m}S_e e^{-\frac{x\rho}{\Lambda}}\right)t \qquad (2)$$

where a=0 (surface), b=depth (cm), $P_{s,m}$=production by spallation (3.98 atoms g^{-1} a^{-1}, S_e=elevation scaling factor (Lal, 1991), x=depth (cm), ρ=density (2.7 g cm^{-3}), Λ=attenuation (160 g cm^{-1}), and t=exposure duration (years). For glacial samples, to scale production with elevation, we used the ice margin elevation.

At depths below 10 m, isotope production by spallation and negative muon capture become negligible and production by fast muons dominates. Over long periods of exposure, ^{10}Be concentration reaches a "steady-state", during which erosion equals decay and concentration by fast muon production can be approximated by the following linear equation (Braucher et al., 2003):

$$\ln[C] = -\frac{x}{\Lambda_{\mu f}} + \ln\left(\frac{P_{\mu f}}{\frac{\varepsilon}{\Lambda_{\mu f}} + \lambda}\right) \qquad (3)$$

where C=concentration (atoms g^{-1}), x=depth (g cm^{-2}), $\Lambda_{\mu f}$=fast muon attenuation (4,320 g cm^{-2}), $P_{\mu f}$= fast muon production (0.093 atoms g^{-1} a^{-1}), ε=erosion (g cm^{-2} a^{-1}), and λ=decay constant (4.9867 x 10^{-7}). The parameters we use for fast muon attenuation and production are estimated for ^{10}Be in SiO_2 at sea level and high latitude (Heisinger et al., 2002a; Heisinger et al., 2002b). We use the "steady-state" equation (2) because deeply sourced ^{10}Be produced by fast muons would have accumulated over a long period of exposure, prior to Greenland Ice Sheet inception. Using a ^{10}Be half-life of 1.39 My (Chmeleff et al., 2009; Korschinek et al., 2009), we decay-corrected the concentration measured in glacial and terrace sediment assuming that production ceased at ice sheet inception (~3.5 Ma). From the decay-corrected concentration, we calculate the depth at which sediment is sourced using pre-Greenland Ice Sheet erosion rate estimates of 5, 10, 15, and 20 m my^{-1}.

For ice-free samples we use the production by spallation equation for a surface that is eroding (Lal, 1991)

$$C = C_i + \frac{P_{s,m} S_e}{\Lambda^{-1}\varepsilon} e^{-\Lambda}\left(1 - e^{-\Lambda^{-1}\varepsilon t}\right) \qquad (4)$$

where C=concentration, C_i=inherited concentration, $P_{s,m}$=production by spallation (3.98 atoms g^{-1} a^{-1}, S_e=elevation scaling factor (Lal, 1991), Λ=attenuation (160 g cm^{-1}), ε= erosion (g cm^{-2}), and t=exposure duration. For the scaling factor, we use the basin averaged elevation calculated in ArcGIS from a 5 km bedrock digital elevation model

(Bamber et al., 2001), and for inherited isotope concentration we used $4.6 \pm 1.8 \times 10^3$ atoms g^{-1}, which is the low-elevation glacial average. Using measured ^{10}Be concentration data for sediment sourced from ice-free terrain and the estimated exposure age of the ice-free landscape (7 to 8 ky for Kangerlussuaq, 9.5 ky for Narsarsuaq, and 11 ky for Tasiilaq), we then solved the equation iteratively for the erosion rate of unconsolidated material using a regolith density of 1.8 g cm^{-3}.

3.2. Bedrock and Boulder Samples

For bedrock and boulder samples from Narsarsuaq, we calculated exposure age using the CRONUS Earth online exposure age calculator, version 2.2, constants version 2.2.1 (Balco et al., 2008). We used the regionally calibrated Northeast North America production rate (Balco et al., 2009) found to be accurate for Greenland (Briner et al., 2012) and the Lal/Stone constant production rate and scaling scheme (Lal, 1991; Stone, 2000). We assumed no erosion after exposure and we did not make any corrections for topographic shielding because the samples were flat-lying and fully exposed. A comparison of paired boulder/bedrock exposure ages (n=4) indicated that the means are statistically inseparable ($p=0.43$) and a matched pairs test showed that exposure ages of paired samples are within 1σ (internal AMS) uncertainty. For exposure ages of paired samples, we used the average of the bedrock and the boulder age.

CHAPTER 4. MANUSCRIPT FOR "EARTH SURFACE PROCESSES AND LANDFORMS"

Using in situ cosmogenic ^{10}Be as a sediment source tracer in Greenland's paraglacial environment

Alice Nelson[1*]
Paul Bierman[2]
Jeremy Shakun[3]
Dylan Rood[4,5]

[1]Department of Geology, University of Vermont, 180 Colchester Avenue, Burlington, VT 05405, USA
[2]Department of Geology and Rubenstein School of Environment and Natural Resources, University of Vermont, 180 Colchester Avenue, Burlington, VT 05404 USA
[3]Department of Earth and Environmental Sciences, Boston College, 140 Commonwealth Avenue, Chestnut Hill, MA 02467, USA
[4]Scottish Universities Environmental Research Centre (SUERC), East Kilbride, G75 0QF, Scotland, UK
[5]Earth Research Institute, University of California Santa Barbara, Santa Barbara, CA 93016, USA
[*]*Contact Author: ahnelson@uvm.edu, (802) 656-4411*

1. Abstract

We use the concentration of *in situ* ^{10}Be in fluvial and morainal quartz sand to trace sediment sources and to determine the relative contribution of glaciers and deglaciated hillslopes to Greenland's paraglacial sediment budget. We sampled along the western, eastern, and southern margins of the Greenland Ice Sheet, and collected sediment sourced from glacial (*n*=19) and ice-free terrain (*n*=10), from channels where sediment from glaciers and ice-free terrain is mixed (*n*=28), from Holocene fluvial terraces (*n*=4), and from one sand dune. *In situ* ^{10}Be concentrations range from 1,600 to 34,000 atoms g^{-1}. The concentration of *in situ* ^{10}Be in sediment sourced from ice-free terrain is significantly higher than in glacially sourced sediment, in mixed channel sediment, and in terrace sediment that was deposited during the Holocene. To constrain the timing of landscape exposure for the ice-free portion of the Narsarsuaq field area in southern Greenland, we measured *in situ* ^{10}Be concentration in bedrock (*n*=5) and boulder (*n*=6) samples. Paired bedrock and boulder ages are indistinguishable at 1σ uncertainty and indicate rapid exposure of the upland slopes at ~10.5 ka.

The isotope concentration in sediment sourced from ice-free terrain is higher than in sediment sourced from glacial terrain because the ice-free landscape has been exposed to cosmic radiation since early Holocene deglaciation. Glacial sediment contains a low, but measurable concentration of ^{10}Be that likely accumulated at depth during a prolonged period of exposure, probably before the establishment of the Greenland Ice Sheet. The concentration of ^{10}Be in mixed fluvial sediment and in terrace sediment is low, and similar to the concentration in glacial sediment, which indicates that the Greenland Ice Sheet is the dominant source of sediment moving through the paraglacial landscape.

2. Introduction

Paraglacial landscapes, exposed by retreating glaciers, are thought to be unstable and susceptible to rapid geomorphic change and extensive sediment redistribution (Ballantyne, 2002b; Church and Ryder, 1972). As Earth's climate continues to warm, there will be more land area classified as paraglacial (Mercier, 2008), and rivers and channels will likely receive increased sediment load from the paraglacial environment (Stott et al., 2013). Understanding the sediment budget of deglaciating landscapes will be important for managing downstream ecosystems and infrastructure, such as fisheries, reservoirs, and dams (Morche et al., 2013).

Greenland is an appropriate place to study sediment processes in the paraglacial environment because large portions of the exposed landscape are paraglacial and large areas of land, now under ice, are likely to become ice free in the next few centuries. Some estimates suggest that just a few degrees of warming could make the ice sheet there melt completely (Alley et al., 2010). The Greenland Ice Sheet margin provides a key setting to predict future sediment mobility, and it is also the best analog we have for the past; studying how the current landscape is responding to current warming will improve understanding of landscape response during the Pleistocene when large ice sheets were melting. Erosion and sediment transport during repeated glaciations have carved the Greenlandic landscape that we see today (Weidick et al., 2004) and through which paraglacial sediment is routed. Sediment eroded during previous glacial cycles is now offshore, and understanding modern sediment sourcing may inform interpretations of the marine record of glaciation.

2.1. Greenland Ice Sheet History

The Greenland Ice Sheet first formed during the Pliocene (~3.5 Ma) when global cooling caused isolated alpine glaciers to grow and coalesce into one large ice sheet (DeConto et al., 2008). The ice sheet has since responded to changes in regional and global average temperature – growing during periods of cooling and retreating during periods of warming (Alley et al., 2010). Ice sheet extent has fluctuated throughout the Pleistocene (~2.5 Ma to 12 ka) in response to cyclical changes in climate (Lisiecki and Raymo, 2005).

During the Holocene (~12 ka to present), temperatures warmed and the Greenland Ice Sheet retreated inland, then re-advanced during the Neoglacial (beginning ~4 to 5 ka), and is now retreating again. Cosmogenic ^{10}Be ages from around Greenland indicate a common pattern of early and mid Holocene retreat (Figure 1). The margins of Greenland became ice-free between 10 to 12 ka leaving behind paraglacial environments. By ~7 to 8 ka, the ice sheet was close to the location of the current margin, and it then continued to retreat inland, exposing additional paraglacial landscape (Weidick et al., 1990).

Retreat inland of the current margin likely varied spatially. Quantifying the extent and duration of retreat is difficult because landforms such as moraines, which constrain ice sheet size, have been overrun by ice sheet re-advances. Subsurface mapping (Weidick et al., 1990), cultural evidence (Weidick et al., 1990), modeling (Fleming and Lambeck, 2004; Simpson et al., 2009), and ice-contact deposits (van Tatenhove et al., 1996; Weidick et al., 2004) suggest ice retreated 5 to 80 km inland of

the current margin in the middle Holocene (Simpson et al., 2009; van Tatenhove et al., 1996; Weidick et al., 2004; Weidick et al., 1990).

When the ice sheet re-advanced during the Neoglacial (beginning ~4 to 5 ka) (Kaufman et al., 2004) and the Little Ice Age (AD 1300–1900) (Forman et al., 2007; van Tatenhove et al., 1996), it overrode subaerially exposed landscapes, entraining and mobilizing mid-Holocene paraglacial sediment. Today the ice sheet is again retreating, increasing the extent of paraglacial landscapes. Recently, ice sheet melt has accelerated (Gordon, 1981; Krabill et al., 2004; van den Broeke et al., 1999). The summer of 2012 was the warmest in recent history setting records for total melt, melt surface extent, and melt season duration (Tedesco et al., 2012).

As the Greenland Ice Sheet advanced and retreated, it eroded the underlying landscape and deposited sediment. The amount and style of erosion and deposition that occurs during glaciation influences topography and the distribution of sediment stored on the landscape after glacial retreat. Inherent to the concept of a paraglacial environment is that landscape behavior continues to be influenced by glaciation, even after ice retreat (Church and Ryder, 1972).

On Greenland, the efficacy of sub-glacial erosion varies depending on whether the ice sheet is warm- or cold-based. More erosion occurs under areas of warm-based ice because sliding and regelation promote evacuation of debris from beneath the ice (Hallet et al., 1996; Sugden, 1978). Cold-based ice, being frozen to the bed, does little if any erosion. During the last glacial cycle, the Greenland Ice Sheet eroded non-uniformly with at least 2 m of erosion at some locations (Corbett et al., 2011; Goehring et al., 2010), but little if any erosion at other sites (Corbett et al., 2013; Hakansson et al., 2011).

2.2. Sediment Sources on Greenland

On the modern Greenlandic landscape, sediment is either sourced from outboard of the current ice margin, the paraglacial landscape that has been exposed since Holocene deglaciation, or it is sourced subglacially from the landscape within the ice margin, a small area of which was exposed during the mid-Holocene. Paraglacial sediment sources on the landscape in front of the ice margin include steep slopes, which may fail periodically, gentler slopes, which are blanketed by unconsolidated debris, and the valleys and glacier forelands, where glacially-derived sediment from the early Holocene is stored within valley fills, deltas, terraces, and moraines (Ballantyne, 2002b) (Figure 2). Glacially sourced sediment from within the ice margin could come from a variety of sources including: paraglacial sediment such as moraines that were deposited inland during the mid-Holocene thermal maximum and have since been remobilized by ice sheet readvance during the Neoglacial, unconsolidated surficial material and bedrock surfaces that may have been exposed during the mid-Holocene, or deeply eroded bedrock that has not been exposed since it was first covered by the ice sheet in the early Pleistocene or late Pliocene.

2.3. In situ produced cosmogenic ^{10}Be

In situ produced cosmogenic ^{10}Be is a dosimeter of cosmic ray exposure. ^{10}Be is produced *in situ* in near-surface rocks and sediment by exposure to cosmic radiation, dominantly, fast neutrons. For Greenland, the sea-level, high-latitude production rate of ^{10}Be in quartz is estimated to be 3.98 ± 0.24 atoms g^{-1} a^{-1} (Briner et al., 2012), and isotope

production scales spatially with geographic location (latitude and longitude), elevation, and depth (Lal, 1991; Lal and Peters, 1967). The neutron spallation reactions that dominantly produce ^{10}Be near Earth's surface decrease exponentially with depth such that spallation production is almost completely attenuated 2 to 3 m below rock surfaces (Lal and Peters, 1967). Muon production, at much lower production rates, continues for tens of meters below the surface (Heisinger et al., 2002a; Heisinger et al., 2002b; Lal and Peters, 1967). Non-cosmogenic processes, which are not controlled by cosmic-ray exposure, can also produce ^{10}Be by exotic decay, fission, and alpha-induced nuclear reactions of U-Th; however, these radiogenic processes produce at most a steady state isotope concentration $\leq 5 \times 10^2$ atoms g^{-1} (Sharma and Middleton, 1989), which is significantly lower than concentrations measured in this study.

When glaciers advance, they often erode enough surficial material to remove regolith and the upper portion of near-surface rock where the highest concentration of cosmogenic isotopes accumulated prior to ice advance; however, if the ice is cold-based, the former land surface may be preserved and so when the glacier retreats, isotopes are inherited from prior periods of exposure (Bierman et al., 1999; Briner et al., 2006; Briner and Swanson, 1998; Colgan et al., 2002; Davis et al., 2006). Large ice masses, such as the Greenland Ice Sheet, shield the underlying landscape from most cosmic radiation, so glacially sourced sediment is likely to have a lower concentration of ^{10}Be than sediment sourced from ice-free terrain.

Sediment samples contain thousands of sand grains, and so the ^{10}Be concentration in sediment represents an average for the source area. If different sediment sources have different characteristic concentrations of ^{10}Be, then the isotope concentration can be used

to trace the relative contribution of each source to the paraglacial sediment budget (c.f., Clapp et al., 2002; Nichols et al., 2005). In bedrock and boulder samples, the concentration of *in situ* ^{10}Be can be used to date landscape exposure to cosmic radiation following ice sheet retreat (Balco, 2011; Gosse and Phillips, 2001).

3. Study Areas

We collected sediment samples from three regions along the Greenland Ice Sheet margin: Kangerlussuaq (67° N) on the west coast, Narsarsuaq (61° N) near the southern tip of Greenland, and Tasiilaq (65.5° N) on the southeast coast (Figure 1). The lithology, climate, vegetation, and Holocene glacial history of each region is generally similar; however, topography and ice margin configurations differ, so each field area represents a different paraglacial environment (Figure 3).

The Greenland Ice Sheet is the largest ice sheet in North America and at present, it covers 78% of Greenland (Escher and Watt, 1976; Thomas and Investigators, 2001). The bedrock geology of Greenland is predominantly crystalline rocks of the Precambrian shield (Henriksen et al., 2009), and rock outcrops in our field areas are primarily granulite and amphibolite facies gneisses (Escher and Pulvertaft, 1995). Greenland's climate is characterized as Arctic and the mean annual temperature for each field area is below 0°C (Anderson et al., 2001; Mernild et al., 2008; Sparrenbom et al., 2006). Vegetation on Greenland is primarily dwarf-shrubs, moss, and lichen (Anderson et al., 2001; Mernild et al., 2008; Sparrenbom et al., 2006), which in our field areas are limited to the low elevations and valleys; the uplands and slopes are predominantly bare rock outcrop with limited cover of unconsolidated material.

The coldest and driest of our three field areas is Kangerlussuaq, which is in the zone of continuous permafrost (Weidick, 1968). The average annual temperature at Kangerlussuaq is -6°C, and annual precipitation is less than 150 mm a^{-1} (Anderson et al., 2001). Compared to Kangerlussuaq, Narsarsuaq and Tasiilaq are slightly warmer and more humid because they are at lower latitudes and are closer to the coast. Narsarsuaq and Tasiilaq are both in the zone of discontinuous permafrost, and average temperature/precipitation in the two field areas is -3°C/~600 mm a^{-1} and -2°C/~980 mm a^{-1}, respectively (Mernild et al., 2008; Sparrenbom et al., 2006; Weidick, 1968).

Greenland's ice-free margins are dissected by fjords and glacially over-deepened valleys (Weidick et al., 2004), which have been carved during successive glaciations. At present, the ice sheet is inland of the coast and each of our field areas is located where glacial outwash flows into a fjord. Each field area fits into a generalized model of paraglacial sediment production (Figure 2); however, landscape relief and sediment storage in each region are different (Figure 3).

3.1. Kangerlussuaq

The Kangerlussuaq field area represents a paraglacial environment with low relief where the ice margin is at a low elevation and is significantly inland from the coast. The town is in central west Greenland at the head of the 190 km long Søndre Strømfjord and the Greenland Ice Sheet margin is ~25 km to the east (Figure 4). The current ice margin configuration consists of three main lobes and drainages of the ice sheet, all of which sit in low elevation valleys where Holocene sediment infill sequences are 40 to 80 m thick (Storms et al., 2012). Radiocarbon dates from the Umîvît-Keglen moraine system show

that the ice sheet was near the fjord head at ~8.1 ka (7,500 ^{14}C yr BP) (van Tatenhove et al., 1996), and cosmogenic ^{10}Be exposure dating of the Ørkendalen moraine system indicates that ice was near the present day margin at ~6.8 ka (Levy et al., 2012). These two moraine systems provide age constraints for the ice-free portion of our field area and indicate that sediment from ice-free terrain is sourced from a landscape exposed to cosmic radiation for 7 to 8 ky (Levy et al., 2012; van Tatenhove et al., 1996).

3.2. Narsarsuaq

The Narsarsuaq field area represents a paraglacial environment with high relief where inland ice sheet margins are primarily at high elevations, 900 to >1500 m asl, though some narrow, low-elevation outlet glaciers approach the fjord (Weidick et al., 2004). The village is situated at the head of the Tunulliarfik Fjord, which is ~75 km inland in a region where the Greenland Ice Sheet has retreated ~100 km from the outer coastal islands (Figure 5). The ice-free margin of southern Greenland is mountainous and relatively narrow, generally ~40 to 75 km wide, and is dissected by numerous fjords and glacially over-deepened troughs (Weidick et al., 2004). The field area is bordered to the west by the Qassimiut lobe of the ice sheet and to the east by the Julianehåb Ice Cap. The ice-free slopes are predominantly bare outcrops of proterozoic gneiss with granite intrusions (Escher and Pulvertaft, 1995), and low elevations are a mixture of glaciated and ice-free terrain.

In southern Greenland, as temperatures warmed in the early Holocene, the ice margin retreated and also thinned, which means that outer land margins and inland peaks may have been exposed around the same time (Weidick et al., 2004). Radiocarbon dates

of basal lake sediment near the coast yield minimum deglaciation ages between 10.2 and 11.2 ka (Anderson et al., 1999; Kelly and Funder, 1974; Weidick et al., 2004), which correspond to ^{10}Be ages south of our field area, indicating rapid emergence of southern Greenland ~11 ka (Bierman et al., 2012; Carlson et al., 2012). Our field area is inland of the coast, and radiocarbon dates of >9.5 and >9.7 ka provide minimum deglaciation ages for the low elevations of our field area near the head of Tunulliarfik Fjord (Kelly, 1973).

3.3. Tasiilaq

In the Tasiilaq region, the ice-free margin is relatively narrow and coastal islands are glaciated, but local ice there is not connected to the mainland ice sheet. The town of Tasiilaq is located on Ammassalik Island, which separates the larger Sermilik Fjord to the west from the smaller Angmagssalik Fjord to the east (Figure 6). At present, the Greenland Ice Sheet is limited to the western side of Sermilik Fjord, and of our three field areas, this is the region where the Greenland Ice Sheet is closest to the fjord. Age constraints of the inland ice margin are few; cosmogenic ^{10}Be dating of bedrock and boulders along Sermilik Fjord and the tributary Torqulertivit Imiat Valley, have been recalculated using CRONUS version 2.2 (Hughes et al., 2012) and yield exposure ages which are clustered in time, indicating that ice retreated rapidly from the valleys at 12.8 to 10.3 ka (Hughes et al., 2012; Roberts et al., 2008). Margins of the inland ice are within 1 km of what is assumed to be a Little Ice Age moraine and tight clustering of exposure ages indicates that ice-free portions of the landscape have been exposed for ~11 ky (Hughes et al., 2012; Roberts et al., 2008).

To the east, coastal islands are partially covered by ice caps and valley glaciers, which are not attached to the mainland ice sheet. Cosmogenic ^{10}Be ages along Sermilik Fjord provide a maximum exposure age for the ice-free landscape to the east of ~10.9 to 12.8 ka (Hughes et al., 2012), and it is possible that extent of valley glaciers and ice caps has varied during the Holocene. Hasholt et al. (2008) propose that during the Medieval Warm Period, Mittivakkat Glacier either melted completely or was significantly reduced before re-advancing almost to the fjord mouth during the Little Ice Age. If glacial extent on coastal islands fluctuated significantly during the Holocene, then there would have been periods of complete landscape exposure, followed by enhanced erosion and sediment mobility as glaciers were reestablished and then advanced over the once-paraglacial environment.

4. Methods

4.1. Field Work

We collected fluvial sediment samples near Kangerlussuaq and Narsarsuaq during the summer of 2011 and near Kangerlussuaq and Tasillaq during the summer of 2012 (Figure 1). Samples were collected directly from channels. In Narsarsuaq, we also collected bedrock (n=5) and boulder (n=6) samples for exposure dating to estimate when the landscape became ice-free (Figure 5). One bedrock and boulder pair is from Igaliku, ~20 km south of our field area, one boulder is from the floor of the Kiattuut Sermia glacial valley and the remainder of the samples are from the upland slopes north of the Tunulliarfik Fjord head. For all field areas, where possible, we collected fluvial sediment samples in transects from the ice margin to the fjord mouth and from tributary valleys

draining ice-free or partially glaciated basins. At some sites, we collected sediment stored in terraces and moraines (classified as glacial). For terrace samples, we collected sediment at least several meters below the surface, a depth sufficient to minimize post depositional ^{10}Be accumulation; the ^{10}Be concentration measured in terrace samples represents the ^{10}Be concentration at the time of deposition, in the early Holocene.

Some Kangerlussuaq sample sites from 2011 were re-sampled in 2012 to determine if there were temporal changes in sediment ^{10}Be concentration, and re-sampled sites are labeled by adding an "R" to the original sample number. Summer 2011 sampling happened in late May when the fluvial system was frozen. Most channels contained little if any water, and there was no connectivity; sampled sand for the most part represented the last material moved during summer and fall of 2010. The summer of 2012 had record warmth. Sampling took place in early June, and by then rivers and streams were almost completely ice free; water levels were near bankfull, sediment mobility was much higher than in 2011, and the sediment we sampled was moving rapidly downstream.

4.2. Laboratory Work

We measured the concentration of ^{10}Be in quartz sand, which is ubiquitous on the Greenland landscape. To isolate quartz grains, the 250 to 850 μm sand fraction was first magnetically separated to eliminate mafic minerals and then was sonicated in a series of heated (HF, HNO_3) etches to remove adhered meteoric ^{10}Be and to preferentially dissolve non-quartz minerals following a method adapted from that of Kohl and Nishiizumi (1992). Beryllium was isolated in the University of Vermont cosmogenic clean lab, using

~20 to 40 g of purified quartz (Corbett et al., 2011). Samples were processed in batches of 12, each of which included two process blanks.

Samples collected during summer of 2011 were measured at the Lawrence Livermore National Laboratory (LLNL) Accelerator Mass Spectrometry (AMS) facility and were normalized to standard 07KNSTD3110, with a reported ratio of 2850 x 10^{-15} (Nishiizumi et al., 2007). Samples collected during summer of 2012 were measured at the Scottish Universities Environmental Research Center (SUERC) AMS facility and were normalized to the NIST standard with an assumed ratio of 2.79 x 10^{-11}, which is consistent with the 07KNSTD standard assuming a half-life of 1.36 My (Nishiizumi et al., 2007). For batches processed at LLNL, the average blank ratio of $^{10}Be/^{9}Be$ was 6.44 ± 4.11 x 10^{-16} (n=9). For processing at SUERC, the average blank ratio was 1.24 ± 0.53 x 10^{-15} (n=7). Appropriate blank subtractions were done for all samples and the uncertainty of the blank was propagated in quadrature.

4.3. Data Analysis

Using photographs, field notes, and landscape imagery, we classified the source for each sediment sample into the following categories: glacial, ice-free, mixture (glacial and ice-free sediment sources), or terrace. Glacial category samples include sediment collected from the ice, and sediment from lateral moraines, ground moraines, and outwash tunnels, as well as channels, and flood plains proximal to the ice margin. We categorized one sample from a sand dune as aeolian. We compared channel replicates from Kangerlussuaq using a one-way analysis of variance (ANOVA) and we

removed GLX-04 and GLX-04R from the comparison because the GLX-04 concentration is an extreme outlier.

A student's t-test indicated that means of 2011 and 2012 temporal replicate fluvial sediment sample concentrations are statistically inseparable (p=0.08). The two sample groups passed the Brown-Forsythe test for equal variance (p=0.22); however, we used the 2012 concentration data for categorical comparisons because we believe that sediment collected at or near bankfull flow is more likely to be well mixed and indicative of material in transport.

We compared the mean sediment concentration of the source categories using Tukey's Honestly Significant Difference test; concentrations were first transformed using a log base-10 transformation in order to ensure equal variance. The terrace category was not included in the statistical comparison because the sample size (n=3) is small.

For bedrock and boulder samples from Narsarsuaq, we calculated exposure age using the CRONUS Earth online exposure age calculator, version 2.2, constants version 2.2.1 (Balco et al., 2008). We used the regionally calibrated Northeast North America production rate (Balco et al., 2009) found to be accurate for Greenland (Briner et al., 2012) and the Lal/Stone constant production rate and scaling scheme (Lal, 1991; Stone, 2000). We assumed no erosion after exposure and we did not make any corrections for topographic shielding because the samples were flat-lying and fully exposed. A comparison of paired boulder/bedrock exposure ages (n=4) indicated that the means are statistically inseparable (p=0.45) and a matched pairs test showed that exposure ages of paired samples are within 1σ uncertainty. For exposure ages of paired samples, we used the average of the bedrock and the boulder age.

To analyze ^{10}Be concentration in sediment, we used a series of mathematical equations, and the detailed methods are described in the online data repository. To determine relative contribution of glacial versus ice-free sediment sources to the channels, we used a simple two component mixing model:

$$C_g x + C_i y = C_m \quad (1)$$

in which C_g= glacial concentration (atoms g^{-1}), C_i= ice-free concentration (atoms g^{-1}), C_m= mixed concentration (atoms g^{-1}), and x and y are fractions, which add to one. To analyze how the ^{10}Be concentrations in sediment could have accumulated, we considered the sample's potential exposure history. To analyze the concentration produced by spallation in glacial sediment, we integrated the concentration at depth equation (Lal, 1988) and took the average over a specified erosion depth

$$\frac{1}{b-a}\int_a^b \left(P_{s,m} S_e e^{-\frac{x\rho}{\Lambda}} \right) t \quad (2)$$

where a=0 (surface), b=depth (cm), $P_{s,m}$=surface production by spallation (3.98 atoms g^{-1} a^{-1}, S_e=elevation scaling factor (Lal, 1991), x=depth (cm), ρ=density (2.7 g cm^{-3}), Λ=attenuation (160 g cm^{-2}), and t=exposure duration (years). For glacial samples, to interpret the concentration that we measured, we scaled production to the ice margin elevation and experimented with different durations of mid-Holocene exposure.

At depths below 10 m, isotope production by spallation and negative muon capture becomes negligible and production by fast muons dominates. Over long periods of exposure, ^{10}Be concentration reaches a "steady-state", during which erosion equals decay and concentration by fast muon production can be approximated by the following

linear equation (Braucher et al., 2003):

$$\ln[C] = -\frac{x}{\Lambda_{\mu f}} + \ln\left(\frac{P_{\mu f}}{\frac{\varepsilon}{\Lambda_{\mu f}} + \lambda}\right) \quad (3)$$

where C=concentration (atoms g^{-1}), x=depth (g cm^{-2}), $\Lambda_{\mu f}$=fast muon attenuation (4,320 g cm^{-2}), $P_{\mu f}$= fast muon production (0.093 atoms g^{-1} a^{-1}), ε=erosion (g cm^{-2} a^{-1}), and λ=decay constant (4.9867 x 10^{-7}). The parameters we used for fast muon attenuation and production are estimated for ^{10}Be in SiO_2 at sea level and high latitude (Heisinger et al., 2002a; Heisinger et al., 2002b). We used the "steady-state" equation (3) because deeply sourced ^{10}Be produced by fast muons would have accumulated over a long period of exposure, prior to Greenland Ice Sheet inception. To determine if glacial and terrace sediment could be deeply sourced, we used the ^{10}Be half-life of 1.39 My (Chmeleff et al., 2009; Korschinek et al., 2009) to decay-correct the concentration measured because we assumed that cosmogenic isotope production ceased at ice sheet inception (~3.5 Ma). From the decay-corrected concentration, we calculated the depth at which sediment is sourced using pre-Greenland Ice Sheet erosion rate estimates of 5, 10, 15, and 20 m my^{-1}, a reasonable range for tectonically stable regions (Portenga and Bierman, 2011)

For ice-free samples we used the production by spallation equation for a surface that is eroding (Lal, 1991)

$$C = C_i + \frac{P_{s,m} S_e}{\Lambda^{-1}\varepsilon} e^{-\Lambda}\left(1 - e^{-\Lambda^{-1}\varepsilon t}\right) \quad (4)$$

where C=concentration, C_i=inherited concentration, $P_{s,m}$=production by spallation (3.98 atoms g^{-1} a^{-1}), S_e=elevation scaling factor (Lal, 1991), Λ=attenuation (160 g cm^{-1}), ε= erosion (g cm^{-2}), and t=exposure duration (years). For the scaling factor, we used the basin averaged elevation calculated in ArcGIS from a 5 km bedrock digital elevation model (Bamber et al., 2001), and for inherited isotope concentration we used 4.6 ± 1.8 x10^3 atoms g^{-1}, which is the low-elevation glacial average. Using measured ^{10}Be concentration data for sediment sourced from ice-free terrain and the estimated exposure age of the ice-free landscape (7 to 8 ky for Kangerlussuaq, 10.5 ky for Narsarsuaq, and 11 ky for Tasiilaq), we then solved the equation iteratively for the erosion rate of unconsolidated material using a regolith density of 1.8 g cm^{-3}.

5. Results

The concentration of cosmogenic ^{10}Be in quartz sand from 62 sediment samples collected from and near the Greenland Ice Sheet along the west, east and south coasts of Greenland ranges from 1.6 ± 0.5 x 10^3 to 34.1 ± 1.6 x 10^3 atoms g^{-1} (Figures 4-6). The samples with the lowest and highest concentrations came from Narsarsuaq. We measured the lowest ^{10}Be concentration in a mixed category sample from the outwash channel of a narrow outlet glacier (GLX-37) and the highest in an ice-free category sample (GLX-18) from an upland basin (Figure 5).

Across the three field sites, measured ^{10}Be concentrations are similar within the source categories and the median concentration for all samples in each region is similar (Table 1). For replicate samples (n=8) from 2011 and 2012, concentrations are not correlated (r^2=0.04; Figure 7). Seven of the replicates are channel samples, and means of 2011 and 2012 channel sediment ^{10}Be concentrations are statistically inseparable (p=0.08).

For all regions, average concentrations of glacial (n=19) and mixed (n=20) category samples are statistically inseparable (p=0.64), and the average concentration in sediment sourced from ice-free terrain (n=10) is higher, and significantly different (p<0.0001; Figure 8). ^{10}Be concentration in glacial sediment ranges from 2.2 ± 0.05 x 10^3 to 18.7 ± 0.7 x 10^3 atoms g^{-1}, and on average, glacial category ^{10}Be concentration is less than half that of the ice-free category. ^{10}Be concentration in mixed samples is similar to glacial samples, though the mixed category has a lower percent standard deviation (40%) than the glacial category (63%).

The distribution of ^{10}Be concentration in glacial category samples shows two groupings (Figure 9); the majority of glacially sourced sediment samples have concentrations (n=14) between 2.2 x 10^3 and 6.1 x 10^3 atoms g^{-1}, five samples have concentrations >9.0 x 10^3 atoms g^{-1}, and differences in concentration are associated with sub-groupings within the glacial source category. ^{10}Be concentration in quartz sediment from low-elevation (<500 m asl) ice sheet margins (n=15, μ=4.6 ± 1.8 x 10^3 atoms g^{-1}) is lower than the ^{10}Be concentration in quartz sediment from high-elevation (>500 m asl) ice sheet margins (n=2, μ=15.5 ± 4.5 x 10^3 atoms g^{-1}) and margins of smaller glaciers,

which are not contiguous with the mainland ice sheet (n=2, μ=9.8 ± 0.3 x 10^3 atoms g^{-1}; Figure 9).

For channel transects containing mixed category samples, two channels in Narsarsuaq show increasing downstream trends in concentration, though the sample size in both transects (n=3) is small and the correlations of downstream position and concentration are not significant. For two channels in Kangerlussuaq, sample size within transects is greater (n=5 and n=6) and there are no downstream trends in concentration (r^2=<0.01 for both transects).

Terrace samples are not included in the statistical comparison because there are only 3 such samples, but concentration in this category is similar to the average concentration of glacial and mixed category samples (Table 1; Figure 8). Concentration in the single aeolian sample is also similar to the concentration of glacial, mixed, and terrace samples (Table 1; Figure 8). In contrast to the previously described categories, average concentration of ^{10}Be in quartz from the ice-free category (n=10) is 14.9 ± 8.6 x 10^3 atoms g^{-1}, which is more than twice the average concentration in glacial, mixed, or terrace sediment (Table 1; Figure 8).

^{10}Be concentrations in bedrock and boulder samples from Narsarsuaq (n=11) indicate that the ice-free portion of that field area has been exposed for ~10.5 ka (Table 2). Concentration in bedrock and boulders agree within 1σ uncertainty, which suggests a simple exposure history and indicates that inheritance from prior exposure is unlikely (Bierman et al., 1999; Corbett et al., 2011). One pair of samples was collected in Igaliku, ~20 km south of our field area, and the rest of the samples are from within our field area, close to where we collected sediment. One young boulder (GLX-36A; 1.5 ± 0.1 ka) is

from the valley floor down stream of the Kiattuut Sermia glacier, and the exposure age indicates neoglacial ice advance. The remainder of the samples are from upland slopes north of Tunulliarfik Fjord, from the same basin as many of our ice-free sediment samples. For all samples in Narsarsuaq and Igaliku, with the exception of the one young boulder, ^{10}Be ages range from 9.6 ± 0.8 to 11.3 ± 0.6 ka (Table 2). For upland slope samples (330 to 970 m asl; n=8) there are no elevation related trends in concentration (r^2=0.007), indicating that ice retreat here was rapid.

6. Discussion

Across the three regions studied, the average ^{10}Be concentration in sediment is 5.9 x 10^3 atoms g^{-1}. *In situ* ^{10}Be concentration in sediment is low compared to concentrations previously measured in bedrock and boulder samples from Greenland (3.2 x 10^3–1.7 x 10^6; μ=1.4 ± 3.6 x 10^5; Figure 1), indicating that fluvial and morainal sediment has had either very little near-surface exposure and/or that the sediment is deeply sourced. Within each of the three regions studied, ^{10}Be concentration in sediment is variable. This variability suggests that sediment is sourced from different places on the landscape that have different cosmic-ray exposure histories (Figures 4–6).

6.1. ^{10}Be as a Tracer

We are able to use *in situ* ^{10}Be as a tracer because sediment from ice-free and glacial source categories have significantly different concentrations of ^{10}Be (Figure 8). *In situ* ^{10}Be concentration in glacial sediment is consistently low, as is the concentration in terrace and mixed sediment (Table 1). This finding indicates that glacially-sourced

sediment dominates not only the contemporary fluvial system draining the ice sheet but also that glacially-sourced sediment dominated early Holocene outwash streams. The concentration of ^{10}Be in aeolian sand is similar to glacial, mixed, and terrace sample concentrations (Table 1; Figure 8), suggesting that the aeolian sand we sampled is either directly or indirectly glacial in origin.

The ^{10}Be concentration in ice-free sediment is on average more than twice that of mixed category sediment (Table 1). Input of sediment from ice-free terrain is not great enough to increase ^{10}Be concentration in fluval sediment downstream - even though in some cases channels flow through several tens of kilometers of ice-free, paraglacial landscape. Mixed category samples are all from low-elevation channels and a two component mixing model using the average concentration of low-elevation glacial sediment and the average concentration of ice-free sediment indicates that ~90% of mixed sediment is glacial in origin. For ice-free sediment to raise the mixed category concentration by at least one standard deviation, the ice-free contribution would have to be at least 30%, which is three times greater than the contribution we estimate from the mixing model.

Previous studies of paraglacial sediment processes suggest that sediment contribution from the ice-free landscape can be high because ice-free slopes are often unstable (eg Ballantyne, 2002a, b; Caine, 1982; McColl and Davies, 2012), but ^{10}Be concentrations in fluvial sediment show that in our field areas, the vast majority of this sediment is sourced from the glacier rather than from the ice-free slopes. Our findings imply that in the past (at least for other tectonically inactive regions with hard rocks), when large ice sheets melted, the majority of sediment evacuated to the oceans and left

on the landscape would have been glacial in origin; however relative sediment budget contribution from ice-free terrain is likely to increase as ice sheet size diminishes.

The paucity of fluvial sediment sourced from Greenland's ice-free terrain could be due to the relative strength of the bedrock (Augustinus, 1995; Escher and Pulvertaft, 1995) or a lack of connectivity between paraglacial hillslopes and the fluvial system (Cossart, 2013). We collected the greatest number of ice-free samples in Narsarsuaq, where landscape relief is greater than in our other field areas, and thus where there is the greatest potential for slope failure and significant sediment sourcing from the ice-free landscape. Yet even though ice-free category samples such as GLX-18 and GLX-20 have high ^{10}Be concentrations ($> 20 \times 10^3$ atoms g^{-1}), the downstream concentration in GLX-12 is low ($<10 \times 10^3$ atoms g^{-1}), indicating that while sediment is produced in ice-free terrain, there is not enough sediment mobility – or volume – in this category to affect channel concentration of ^{10}Be.

In two steeply sided glacial valleys, also in Narsarsuaq, we measured a slight downstream increase in sediment ^{10}Be concentration (e.g., GLX-21, 22, and 23) consistent with the input of sediment with higher ^{10}Be concentration from the ice-free landscape. With a simple mixing model using the glacial concentration (GLX-21; 4.3×10^3 atoms g^{-1}) and the ice-free average (14.9×10^3 atoms g^{-1}), we calculated that ice-free sediment contribution increased downstream from 0% at the glacier to 15% at the end of the channel (GLX-23; 5.9×10^3 atoms g^{-1}). Even in steep terrain, glacial sediment still dominates the load carried by channels draining the ice margin.

6.2. Temporal Variability

We are able to use ^{10}Be concentration as a tracer because different sediment sources have different characteristic isotope concentrations (Figure 8); however, the ^{10}Be concentration in samples collected 13 months apart from the same sites in Kangerlussuaq are not correlated (Figure 7), indicating that there is temporal variability in ^{10}Be concentration.

Variability in sediment concentration could be due to differences in the subglacial sediment source, even at a single outwash tunnel. Over the course of a melt season, a glacier will evacuate sediment from different sources because subglacial sediment stores change or become exhausted, depending on subglacial channel migration (Cowton et al., 2012). Different subglacial sediment sources might be eroded from different depths, resulting in variability in ^{10}Be concentration in glacial sediment. Such variability is not limited to contemporary fluvial sediment but was also present in two samples collected within tens of meters of one another from the same terrace; the concentration in GLX-8 is $8.7 \pm 0.5 \times 10^3$ atoms g^{-1} and in GLX-8R is $4.5 \pm 0.6 \times 10^3$ atoms g^{-1} (Figure 4). Terrace replicates do not represent consecutive years of deposition, but do show that over the course of terrace deposition, ^{10}Be concentration was variable.

6.3. Source of ^{10}Be in Glacial, Mixed, Terrace, and Aeolian Sediment

Glacial, mixed, and terrace samples all contain low ($\mu=5.9 \times 10^3$ atoms g^{-1}), but measurable concentrations of ^{10}Be indicating the sediment source area had prior exposure to cosmic radiation (Table 1). Our data are consistent with similar data collected in east central Greenland where early Holocene deltaic sediment from Scoresby Sund contains 4.3 to 6.5 x 10^3 atoms g^{-1} of inherited *in situ* produced ^{10}Be (Goehring et al., 2010). To

determine where and when these low concentrations of ^{10}Be were produced, we explore two possibilities: 1) that measured ^{10}Be accumulated at depth during a prolonged period of exposure that happened several million years ago, before the Greenland Ice Sheet existed, and 2) that the measured ^{10}Be accumulated during a more recent period of exposure such as the mid-Holocene or the last interglacial.

The concentration of ^{10}Be in contemporary glacial sediment (n=19; 6.5 ± 4.9 x 10^3 atoms g^{-1}) is statistically the same as that measured in early Holocene terrace sediment (n=3; 5.2 ± 2.4 x 10^3 atoms g^{-1}), which because of its age could not have been exposed during the mid-Holocene warm period. Because sediment sourced from the ice sheet in the early Holocene has a concentration of *in situ* ^{10}Be similar to that of sediment sourced from the ice today, mid-Holocene exposure (Weidick et al., 1990) is likely not the predominant source of ^{10}Be in contemporary glacial sediment. During the mid-Holocene, the landscape surface behind the ice margin would have accumulated ^{10}Be concentrations between ~10 x 10^3 atoms g^{-1} (2 ky of surficial exposure) and ~30 x 10^3 atoms g^{-1} (6 ky) of ^{10}Be. In order for mid-Holocene exposure to not affect the concentration of ^{10}Be in glacial sediment, the mass of sediment sourced from the interior of the ice sheet must be many times greater than the mass of sediment derived near the ice margin - or sediment exposed during the Holocene has already been exported from the system.

It is possible that ^{10}Be measured in both contemporary sediment and in early Holocene terrace and deltaic deposits, was formed by subaerial exposure during the last interglacial (130–115 ka) when the Greenland Ice Sheet retreated inland, likely exposing much of southern Greenland for at least a short period of time (Alley et al., 2010; de

Vernal and Hillaire-Marcel, 2008; Otto-Bliesner et al., 2006). Concentration in terrace and glacial sediment (~5.5 x 10^3 atoms g^{-1}) is consistent with sourcing from 1.5 meters below a land surface exposed for ~15 ky during the last interglacial, but it is unlikely sediment sourced from this depth remains on the landscape. Measured cosmogenic isotope concentrations in numerous bedrock and boulder samples from southern Greenland indicate little or no inheritance of cosmogenic isotopes from prior periods of exposure (Hughes et al., 2012; Levy et al., 2012). The lack of inheritance implies at least 2 to 3 m of erosion, at least at the ice margin, in the areas we sampled.

We conclude that glacially-derived sediment is most likely to be sourced deeply, from a depth where ^{10}Be accumulated as a result of muogenic production. Because muon-induced production rates of ^{10}Be are very low, measured isotope concentrations of many thousands of atoms per gram must be inherited from a prolonged period of exposure, which could only have happened before the ice sheet was established. If we assume the pre-glacial Greenland landscape eroded steadily are rates between 5 and 20 m my^{-1}, erosion rates typical of passive margins and tectonically inactive regions (Portenga and Bierman, 2011), then decay-corrected ^{10}Be concentrations are consistent with steady-state production by muons 15 to 30 m below the initial rock surface. We assume that nuclide production ceased at 3.5 Ma with the establishment of the Greenland Ice Sheet because while muons are able to penetrate deeply, ^{10}Be production in bedrock shielded an ice sheet is effectively zero; beneath 3 km of ice, the steady-state inventory of ^{10}Be would be 3 to 7 atoms g^{-1} (John Stone, personal communication).

During marine isotope stages 5, 9, 11, and perhaps 25, 31, and 47, the Greenland Ice Sheet likely retreated briefly within the Holocene ice margin (Alley et al., 2010; de

Vernal and Hillaire-Marcel, 2008; Otto-Bliesner et al., 2006; Raymo et al., 2011; Roberts et al., 2012; Steig and Wolfe, 2008), but over the short time frame of exposure (~10 ky), the only significant ^{10}Be accumulation on the landscape would have been by spallation reactions in the upper few meters, which in many regions, at least near the margin, would have eroded during the next glacial advance.

The concentration of *in situ* ^{10}Be we measured in glacial sediment is generally consistent with 10 m my^{-1} of glacial erosion since Greenland Ice Sheet inception 3.5 Ma,. The concentration ^{10}Be in glacial sediment varies with elevation (Figure 9), consistent with lower rates of sub-ice erosion and less cumulative erosion in uplands compared to lowlands (Bierman et al., 1999; Corbett et al., 2013; Corbett et al., 2011). Subglacial erosion is generally greater at low elevations where ice is thickest, and there is often less erosion at the high elevations where the ice is thinner (Sugden, 1978).

Glacial sediment ^{10}Be concentration is also higher than the category average at the margins of smaller glaciers, not attached to the Greenland Ice Sheet. Previous research suggests that these smaller glaciers are less stable than the nearby ice sheet (Hasholt et al., 2008) and thus, the underlying landscape was likely exposed to more cosmic radiation during past warm periods than the landscape beneath the mainland ice sheet. Small ice caps may also be less erosive than the Greenland Ice Sheet.

6.4. Sediment from ice-free drainages

Sediment sourced from ice-free terrain contains higher concentrations of ^{10}Be than glacial sediment because the landscape from which ice-free sediment is sourced is exposed to rather than shielded from cosmic radiation (Table 1; Figure 8). The

concentration of ^{10}Be in sediment sourced from ice-free terrain is dependent on the inherited isotope concentration (~5 x 10^3 atoms g^{-1}), source area elevation, landscape erosion rate, and duration of exposure to cosmic radiation, which in our field areas ranges from ~6.8 to 12.8 ky (Hughes et al., 2012; Levy et al., 2012). Outcrops in our field areas are fresh and so we assume that ice-free sediment is unconsolidated surficial material that has been eroding since deglaciation.

From the nuclide concentration measured in samples from ice-free drainages (*n*=10) and using a deglacial age for each field area based on extant data (Figure 1), we calculated an average regolith erosion rate for the ice-free landscape of 2.75 ± 5 mm a^{-1}. Our calculated regolith erosion rates are consistent with the low end of poorly constrained erosion estimates for other paraglacial sediment-mantled slopes (Ballantyne, 2002b). For example in Norway, erosion inferred from debris cone accumulation in newly deglaciated terrain ranges from 8 to 44 mm a^{-1} and gully erosion ranges from 2.5 to 169 mm a^{-1}, with the caveat that these high erosion rates are likely only sustained for a few decades immediately following deglaciation (Ballantyne, 2002b).

7. Conclusion

Sediment collected in paraglacial environments near Kangerlussuaq, Narsarsuaq, and Tasiilaq contains characteristically different concentrations of *in situ* produced ^{10}Be depending on the sediment source. There is spatial and temporal variability in the ^{10}Be concentration of glacial, mixed, and terrace sediment, but ^{10}Be concentration in these categories is consistently and characteristically low because for most of the last 3.5 My, the Greenland Ice Sheet has shielded the subglacial sediment source from cosmic

radiation. We speculate that the low concentrations of ^{10}Be in glacially sourced sediment accumulated 20 to 30 meters below the pre Greenland Ice Sheet land surface as the result of fast muon-induced production, and are inherited from a prolonged period of exposure that pre-dates formation of the Greenland Ice Sheet.

In contrast to the glacial, mixed, and terrace categories, sediment sourced from ice-free terrain contains significantly higher concentrations of ^{10}Be then glacial sediment, but there is not enough sediment sourced from ice-free terrain to affect the concentration of ^{10}Be leaving the landscape and entering the fjords. Using *in situ* ^{10}Be as a tracer, we find the ice sheet to be the dominant sediment source in the paraglacial environment, contributing ~90% of the sediment that is moving through channels and into the fjords. The low concentration of ^{10}Be in terrace samples indicates that glacially-sourced sediment also dominated the fluvial system during the early Holocene. Our findings imply that concentration of ^{10}Be in marine sediment will be controlled by the efficacy and timing of glacial erosion because the concentration of ^{10}Be in glacial sediment is controlled by the depth to which the pre-ice sheet landscape has been eroded. Duration and extent of paraglacial landscape exposure are not likely to have a measurable effect on the ^{10}Be concentration of marine sediment, unless the extent and duration of ice sheet retreat was significantly greater than it is today.

8. Acknowledgements

Funding for this research was provided by National Science Foundation award number ARC-1023191 to Bierman and the University of Vermont.

9. References

Alley, R. B., Andrews, J. T., Brigham-Grette, J., Clarke, G. K. C., Cuffey, K. M., Fitzpatrick, J. J., Funder, S., Marshall, S. J., Miller, G. H., Mitrovica, J. X., Muhs, D. R., Otto-Bliesner, B. L., Polyak, L., and White, J. W. C. 2010. History of the Greenland Ice Sheet: paleoclimatic insights. *Quaternary Science Reviews* **29**: 1728-1756. Doi 10.1016/J.Quascirev.2010.02.007

Anderson, N. J., Bennike, O., Christoffersen, K., Jeppesen, E., Markager, S., Miller, G., and Renberg, I. 1999. Limnological and paleolimnological studies of lakes in south-western Greenland. *Geology of Greenland Survey Bulletin* **183**: 68-74.

Anderson, N. J., Harriman, R., Ryves, D. B., and Patrick, S. T. 2001. Dominant factors controlling variability in the ionic composition of West Greenland Lakes. *Arctic Antarctic and Alpine Research* **33**: 418-425. Doi 10.2307/1552551

Augustinus, P. 1995. Rock Mass Strength and the Stability of Some Glacial Valley Slopes. *Zeitschrift Fur Geomorphologie* **39**: 55-68.

Balco, G. 2011. Contributions and unrealized potential contributions of cosmogenic-nuclide exposure dating to glacier chronology, 1990-2010. *Quaternary Science Reviews* **30**: 3-27. Doi 10.1016/J.Quascirev.2010.11.003

Balco, G., Briner, J., Finkel, R. C., Rayburn, J. A., Ridge, J. C., and Schaefer, J. M. 2009. Regional ^{10}Be production rate calibration for late-glacial northeastern North America. *Quaternary Geochronology* **4**: 93-107. Doi 10.1016/J.Quageo.2008.09.001

Balco, G., Stone, J. O., Lifton, N. A., and Dunai, T. J. 2008. A complete and easily accessible means of calculating surface exposure ages or erosion rates from ^{10}Be and ^{26}Al measurements. *Quaternary Geochronology* **3**: 174-195. Doi 10.1016/J.Quageo.2007.12.001

Ballantyne, C. K. 2002a. A general model of paraglacial landscape response. *Holocene* **12**: 371-376. Doi 10.1191/0959683602hl553fa

-. 2002b. Paraglacial geomorphology. *Quaternary Science Reviews* **21**: 1935-2017.

Bamber, J. L., Layberry, R. L., and Gogineni, S. 2001. A new ice thickness and bedrock elevation data set for Greenland, part I. *Journal of Geophysical Research* **106**: 33,773-733,780. Doi 10.1029/2001jd900054

Bierman, P., Rood, D., and Corbett, L. B. 2012. High-precision, high-resolution emergence curves for southern Greenland generated with in situ cosmogenic ^{10}Be. Abstract C53E-06 presented at 2012 Fall Meeting, AGU, San Fransciso, California, 3–7 December.

Bierman, P. R., Marsella, K. A., Patterson, C., Davis, P. T., and Caffee, M. 1999. Mid-Pleistocene cosmogenic minimum-age limits for pre-Wisconsinan glacial surfaces in southwestern Minnesota and southern Baffin island: a multiple nuclide approach. *Geomorphology* **27**: 25-39.

Braucher, R., Brown, E. T., Bourles, D. L., and Colin, F. 2003. In situ produced ^{10}Be measurements at great depths: implications for production rates by fast muons. *Earth and Planetary Science Letters* **211**: 251-258. Doi 10.1016/S0012-821x(03)00205-X

Briner, J., Young, N. E., Goehring, B. M., and Schaefer, J. M. 2012. Constraining Holocene ^{10}Be Production Rates in Greenland. *Journal of Quaternary Science* **27**: 2-6.

Briner, J. P., Miller, G. H., Davis, P. T., and Finkel, R. C. 2006. Cosmogenic radionuclides from fiord landscapes support differential erosion by overriding ice sheets. *Geological Society of America Bulletin* **118**: 406-420. Doi 10.1130/B25716.1

Briner, J. P., and Swanson, T. W. 1998. Using inherited cosmogenic ^{36}Cl to constrain glacial erosion rates of the Cordilleran ice sheet. *Geology* **26**: 3-6.

Caine, N. 1982. Toppling Failures from Alpine Cliffs on Ben Lomond, Tasmania. *Earth Surface Processes and Landforms* **7**: 133-152. Doi 10.1002/Esp.3290070207

Carlson, A. E., Winsor, K., Brook, E., Ullman, D. J., LeGrande, A., Anslow, F., Rood, D., and Axford, Y. 2012. Holocene Southwest Greenland Ice-Sheet Retreat Suggests Recent Ice Retreat Is A Response To Global Warming. Abstract PP23B-2046 presented at 2012 Fall Meeting, AGU, San Francisco, California, 3–7 December.

Chmeleff, J., von Blanckenburg, F., Kossert, K., and Jakob, D. 2009. Determination of the ^{10}Be half-life by Multi Collector ICP-mass spectrometry and liquid scintillation counting. *Geochimica Et Cosmochimica Acta* **73**: A221-A221.

Church, M., and Ryder, J. 1972. Paraglacial Sedimentation: A consideration of Fluvial Processes Conditioned by Glaciation. *Geological Society of America Bulletin* **83**: 3059-3072.

Clapp, E. M., Bierman, P. R., and Caffee, M. 2002 Using ^{10}Be and ^{26}Al to determine sediment generation rates and identify sediment source areas in an arid region drainage basin. *Geomorphology* **45**: 89-104. Doi 10.1016/S0169-555x(01)00191-X

Colgan, P. M., Bierman, P. R., Mickelson, D. M., and Caffee, M. 2002. Variation in glacial erosion near the southern margin of the Laurentide Ice Sheet, south-central Wisconsin, USA: Implications for cosmogenic dating of glacial terrains. *Geological Society of America Bulletin* **114**: 1581-1591.

Corbett, L. B. 2011. Investigating the timing of deglaciation and the efficiency of subglacial erosion in central-western Greenland with cosmogenic ^{10}Be and ^{26}Al. Master's Thesis, The University of Vermont, USA.

Corbett, L. B., Bierman, P., Graly, J. A., Neumann, T. A., and Rood, D. 2013. Using cosmogenic nuclides to study subglacial erosion efficiency and landscape history in western Greenland. In *Proceedings Geologic Society of American Northeast Section Meeting*. Bretton Woods, NH.

Corbett, L. B., Young, N. E., Bierman, P. R., Briner, J. P., Neumann, T. A., Rood, D. H., and Graly, J. A. 2011. Paired bedrock and boulder ^{10}Be concentrations resulting from early Holocene ice retreat near Jakobshavn Isfjord, western Greenland. *Quaternary Science Reviews* **30**: 1739-1749. Doi 10.1016/J.Quascirev.2011.04.001

Cossart, E. 2013. Do deglaciated mountainslopes contribute significantly to paraglacial sediment fluxes? Presented at EGU General Assembly, 2013, Vienna, Austria. *Geophysical Research Abstracts* **15**.

Cowton, T., Nienow, P., Bartholomew, I., Sole, A., and Mair, D. 2012. Rapid erosion beneath the Greenland ice sheet. *Geology* **40**: 343-346. Doi 10.1130/G32687.1

Davis, P. T., Briner, J. P., Coulthard, R. D., Finkel, R. W., and Miller, G. H. 2006. Preservation of Arctic landscapes overridden by cold-based ice sheets. *Quaternary Research* **65**: 156-163. Doi 10.1016/J.Yqres.2005.08.019

de Vernal, A., and Hillaire-Marcel, C. 2008. Natural variability of Greenland climate, vegetation, and ice volume during the past million years. *Science* **320**: 1622-1625. Doi 10.1126/Science.1153929

DeConto, R. M., Pollard, D., Wilson, P. A., Palike, H., Lear, C. H., and Pagani, M. 2008. Thresholds for Cenozoic bipolar glaciation. *Nature* **455**: 652-U652. Doi 10.1038/Nature07337

Escher, A., and Watt, W. S. 1976. Geology of Greenland, Copenhagen. *The Geologic Survey of Greenland*.

Escher, J. C., and Pulvertaft, T. C. 1995. Geologic map of Greenland, scale 1 :2500000. *Geologic Survey of Greenland*.

Fleming, K., and Lambeck, K. 2004. Constraints on the Greenland Ice Sheet since the Last Glacial Maximum from sea-level observations and glacial-rebound models. *Quaternary Science Reviews* **23**: 1053-1077. Doi 10.1016/J.Quascirev.2003.11.001

Forman, S. L., Marin, L., van der Veen, C., Tremper, C., and Csatho, B. 2007. Little ice age and neoglacial landforms at the Inland Ice margin, Isunguata Sermia, Kangerlussuaq, west Greenland. *Boreas* **36**: 341-351. Doi 10.1080/00173130601173301

Goehring, B. M., Kelly, M. A., Schaefer, J. M., Finkel, R. C., and Lowell, T. V. 2010. Dating of raised marine and lacustrine deposits in east Greenland using ^{10}Be depth profiles and implications for estimates of subglacial erosion. *Journal of Quaternary Science* **25**: 865-874. Doi 10.1002/Jqs.1380

Gordon, J. E. 1981. Glacier Margin Fluctuations during the 19th and 20th Centuries in the Ikamiut Kangerdluarssuat Area, West Greenland. *Arctic and Alpine Research* **13**: 47-62. Doi 10.2307/1550625

Gosse, J. C., and Phillips, F. M. 2001. Terrestrial in situ cosmogenic nuclides: theory and application. *Quaternary Science Reviews* **20**: 1475-1560. Doi 10.1016/S0277-3791(00)00171-2

Hakansson, L., Briner, J., Alexanderson, H., Aldahan, A., and Possnert, G. 2007a. ^{10}Be ages from central east Greenland constrain the extent of the Greenland ice sheet during the Last Glacial Maximum. *Quaternary Science Reviews* **26**: 2316-2321. Doi 10.1016/J.Quascirev.2007.08.001

Hakansson, L., Briner, J. P., Aldahan, A., and Possnert, G. 2011. ^{10}Be data from meltwater channels suggest that Jameson Land, east Greenland, was ice-covered during the last glacial maximum. *Quaternary Research* **76**: 452-459. Doi 10.1016/J.Yqres.2011.06.007

Hakansson, L., Graf, A., Strasky, S., Ivy-Ochs, S., Kubik, P. W., Hjort, C., and Schluchter. 2007b. Cosmogenic ^{10}Be-ages from the Store Koldewey island, NE Greenland. *Geografiska Annaler Series a-Physical Geography* **89A**: 195-202.

Hallet, B., Hunter, L., and Bogen, J. 1996. Rates of erosion and sediment

evacuation by glaciers: A review of field data and their implications. *Global and Planetary Change* **12**: 213-235. Doi 10.1016/0921-8181(95)00021-6

Hasholt, B., Kruger, J., and Skjernaa, L. 2008. Landscape and sediment processes in a proglacial valley, the Mittivakkat Glacier area, Southeast Greenland. *Geografisk Tidsskrift-Danish Journal of Geography* **108**: 97-110.

Heisinger, B., Lal, D., Jull, A. J. T., Kubik, P., Ivy-Ochs, S., Knie, K., and Nolte, E. 2002a. Production of selected cosmogenic radionuclides by muons: 2. Capture of negative muons. *Earth and Planetary Science Letters* **200**: 357-369.

Heisinger, B., Lal, D., Jull, A. J. T., Kubik, P., Ivy-Ochs, S., Neumaier, S., Knie, K., Lazarev, V., and Nolte, E. 2002b. Production of selected cosmogenic radionuclides by muons 1. Fast muons. *Earth and Planetary Science Letters* **200**: 345-355. Doi 10.1016/S0012-821x(02)00640-4.

Henriksen, N., Higgins, A., Kalsbeek, F., and Pulvertaft, T. 2009. Greenland from Archaen to Quaternary. *Geological Survey of Denmark and Greenland Bulletin* **18**.

Hughes, A. L. C., Rainsley, E., Murray, T., Fogwill, C. J., Schnabel, C., and Xu, S. 2012. Rapid response of Helheim Glacier, southeast Greenland, to early Holocene climate warming. *Geology* **40**: 427-430. Doi 10.1130/G32730.1

Kaufman, D. S., Ager, T.A., Anderson, N.J., Anderson, P.M., Andrews, J.T., Bartlein, P.J., Brubaker, L.B., Coats, L.L., Cwynar, L.C., Duvall, M.L., Dyke, A.S., Edwards, M.E., Eisner, W.R., Gajewski, K., Geirsdottir, A., Hu, F.S., Jennings, A.E., Kaplan, M.R., Kerwin, M.N., Lozhkin, A.V., MacDonald, G.M., Miller, G.H., Mock, C.J., Oswald, W.W., Otto-Bleisner, B.L., Porinchu, D.F., Ruhland, K., Smol, J.P., Steig, E.J., Wolfe, B.B. 2004. Holocene thermal maximum in the western Arctic (0-180° W). *Quaternary Research* **23**: 529-560.

Kelly, M. 1973. The marine limit in Julianehab district, south Greenland and its iostatic implications: Crustal structure of the Gardar rift, south Greenland. *Report on fieldwork*.

Kelly, M., and Funder, S. 1974. The pollen stratigraphy of late Quaternary lake sediments of South-West Greenland.

Kelly, M. A., Lowell, T. V., Hall, B. L., Schaefer, J. M., Finkel, R. C., Goehring, B. M., Alley, R. B., and Denton, G. H. 2008. A ^{10}Be chronology of lateglacial and Holocene mountain glaciation in the Scoresby Sund region, east Greenland: implications for seasonality during lateglacial time. *Quaternary Science Reviews* **27**: 2273-2282. Doi 10.1016/J.Quascirev.2008.08.004

Kohl, C. P., and Nishiizumi, K. 1992. Chemical Isolation of Quartz for Measurement of Insitu-Produced Cosmogenic Nuclides. *Geochimica Et Cosmochimica Acta* **56**: 3583-3587.

Korschinek, G., Bergmaier, A., Dillmann, I., Faestermann, T., Gerstmann, U., Knie, K., von Gostomski, C. L., Maiti, M., Poutivtsev, M., Remmert, A., Rugel, G., and Wallner, A. 2009. Determination of the ^{10}Be half-life by HI-ERD and Liquid Scintillation Counting. *Geochimica Et Cosmochimica Acta* **73**: A685-A685.

Krabill, W., Hanna, E., Huybrechts, P., Abdalati, W., Cappelen, J., Csatho, B., Frederick, E., Manizade, S., Martin, C., Sonntag, J., Swift, R., Thomas, R., and Yungel, J. 2004. Greenland Ice Sheet: Increased coastal thinning. *Geophysical Research Letters* **31**. Doi 10.1029/2004gl021533
Lal, D. 1988. *In situ* Produced Cosmogenic Isotopes in Terrestrial Rocks. *Annual Review of Earth and Planetary Sciences* **16**: 355-388.

-. 1991. Cosmic-Ray Labeling of Erosion Surfaces: *in situ* nuclide production rates and eosion models. *Earth and Planetary Science Letters* **104**: 424-439. Doi 10.1016/0012-821x(91)90220-C

Lal, D., and Peters, B. 1967. Cosmic Ray Produced Radioactivity on the Earth. *Handbuch der Physik* **Band XLV1/2**: 551-612.

Levy, L. B., Kelly, M. A., Howley, J. A., and Virginia, R. A. 2012. Age of the Orkendalen moraines, Kangerlussuaq, Greenland: constraints on the extent of the southwestern margin of the Greenland Ice Sheet during the Holocene. *Quaternary Science Reviews* **52**: 1-5. Doi 10.1016/J.Quascirev.2012.07.021

Lisiecki, L. E., and Raymo, M. E. 2005. A Pliocene-Pleistocene stack of 57 globally distributed benthic delta ^{18}O records. *Paleoceanography* **20**
Doi 10.1029/2005pa001164

McColl, S., and Davies, T. R. 2012. Large ice-contact slope movements: glacial buttressing, deformation, and erosion. *Earth Surface Processes and Landforms*. Doi: 10.1002/esp.3346

Mercier, D. 2008. Paraglacial and paraperiglacial landsystems: concepts, temporal scales and spatial distribution. *Geomorphologie-Relief Processus Environnement* **4**: 223-233.

Mernild, S. H., Hansen, B. U., Jakobsen, B. H., and Hasholt, B. 2008. Climate conditions at the Mittivakkat Glacier catchment (1994-2006), Ammassalik Island, SE Greenland, and in a 109-year perspective (1898–2006). *Geografisk Tidsskrift-Danish Journal of Geography* **108**: 51–72.

Morche, D., Baewert, H., Weber, M., and Schmidt, K. H. 2013. On the hydrology of fluvial sediment transport of the proglacial river Riffler Bach (Weibseeferner, Ötztal Alps, Tyrol). Presented at EGU General Assembly, 2013, Vienna, Austria. *Geophysical Research Abstracts* **15**.

Nichols, K. K., Bierman, P. R., Caffee, M., Finkel, R., and Larsen, J. 2005. Cosmogenically enabled sediment budgeting. *Geology* **33**: 133-136. Doi 10.1130/G21006.1

Nishiizumi, K., Imamura, M., Caffee, M. W., Southon, J. R., Finkel, R. C., and McAninch, J. 2007. Absolute calibration of ^{10}Be AMS standards: Nuclear Instruments & Methods. In *Physics Research Section B-Beam Interactions with Materials and Atoms* **258**: 403-413. Doi 10.1016/J.Nimb.2007.01.297

Otto-Bliesner, B. L., Marsha, S. J., Overpeck, J. T., Miller, G. H., Hu, A. X., and Mem, C. L. I. P. 2006. Simulating arctic climate warmth and icefield retreat in the last interglaciation. *Science* **311**: 1751-1753. Doi 10.1126/Science.1120808

Portenga, E., and Bierman, P. 2011. Understanding Earth's eroding surface with ^{10}Be. *GSA Today* **21**: 4–10.

Raymo, M. E., Mitrovica, J. X., O'Leary, M. J., DeConto, R. M., and Hearty, P. L. 2011. Departures from eustasy in Pliocene sea-level records. *Nature Geoscience* **4**: 328-332. Doi 10.1038/Ngeo1118

Rinterknecht, V., Gorokhovich, Y., Schaefer, J., and Caffee, M. 2009. Preliminary ^{10}Be chronology for the last deglaciation of the western margin of the Greenland Ice Sheet. *Journal of Quaternary Science* **24**: 270-278. Doi 10.1002/Jqs.1226

Roberts, D. H., Long, A. J., Schnabel, C., Davies, B. J., Xu, S., Simpson, M. J. R., and Huybrechts, P. 2009. Ice sheet extent and early deglacial history of the southwestern sector of the Greenland Ice Sheet. *Quaternary Science Reviews* **28**: 2760-2773. Doi 10.1016/J.Quascirev.2009.07.002

Roberts, D. H., Long, A. J., Schnabel, C., Freeman, S., and Simpson, M. J. R. 2008. The deglacial history of southeast sector of the Greenland Ice Sheet during the Last Glacial Maximum. *Quaternary Science Reviews* **27**: 1505-1516. Doi 10.1016/J.Quascirev.2008.04.008

Roberts, D. L., Karkanas, P., Jacobs, Z., Marean, C., and Roberts, R. 2012. Melting ice sheets 400,000 yr ago raised sea level by 13 m: Past analogue for future trentds. *Earth and Planetary Science Letters* **357-358**: 226-237. Doi 10.1016/j.epsl.2012.09.006

Sharma, P., and Middleton, R. 1989. Radiogenic Production of ^{10}Be and ^{26}Al in

Uranium and Thorium Ores - Implications for Studying Terrestrial Samples Containing Low-Levels of ^{10}Be and ^{26}Al. *Geochimica Et Cosmochimica Acta* **53**: 709-716. Doi 10.1016/0016-7037(89)90013-6

Simpson, M. J. R., Milne, G. A., Huybrechts, P., and Long, A. J. 2009. Calibrating a glaciological model of the Greenland ice sheet from the Last Glacial Maximum to present-day using field observations of relative sea level and ice extent. *Quaternary Science Reviews* **28**: 1631-1657. Doi 10.1016/J.Quascirev.2009.03.004

Sparrenbom, C. J., Bennike, O., Bjorck, S., and Lambeck, K. 2006. Holocene relative sea-level changes in the Qaqortoq area, southern Greenland. *Boreas* **35**: 171-187. Doi 10.1080/03009480600578032

Steig, E. J., and Wolfe, A. P. 2008. Sprucing up Greenland. *Science* **320**: 1595-1596. Doi 10.1126/Science.1160004

Stone, J. O. 2000. Air pressure and cosmogenic isotope production. *Journal of Geophysical Research-Solid Earth* **105**: 23753-23759.

Storms, J. E. A., de Winter, I. L., Overeem, I., Drijkoningen, G. G., and Lykke-Andersen, H. 2012. The Holocene sedimentary history of the Kangerlussuaq Fjord-valley fill, West Greenland. *Quaternary Science Reviews* **35**: 29-50. Doi 10.1016/J.Quascirev.2011.12.014

Stott, T., Leggat, M., Owens, P., Forrester, B., and Déry, S. 2013. Suspended sediment dynamics in the forefield of the rapidly deglaciating Castle Creek Glacier, Bristish Columbia. Presented at EGU General Assembly, 2013, Vienna, Austria. *Geophysical Research Abstracts* **15**.

Sugden, D. E. 1978. Glacial erosion by the Laurentide Ice Sheet. *Journal of Glaciology* **20**: 367–390.

Tedesco, M., Fettweis, X., Mote, T., Wahr, J., Alexander, P., Box, J., and Wouters, B. 2012. Evidence and analysis of 2012 Greenland records from spaceborne observations, a regional climate model and reanalysis data. *The Cryosphere Discussions* **6**: 4939-4976.

Thomas, R. H., and Investigators, P. 2001. Program for arctic regional climate assessment (PARCA): Goals, key findings, and future directions. *Journal of Geophysical Research-Atmospheres* **106**: 33691-33705.

van den Broeke, M. R., Winther, J. G., Isaksson, E., Pinglot, J. F., Karlof, L., Eiken, T., and Conrads, L. 1999. Climate variables along a traverse line in Dronning Maud Land, East Antarctica. *Journal of Glaciology* **45**: 295-302.

van Tatenhove, F. G. M., van der Meer, J. J. M., and Koster, E. A. 1996. Implications for deglaciation chronology from new AMS age determinations in central west Greenland. *Quaternary Research* **45**: 245-253. Doi 10.1006/Qres.1996.0025

Weidick, A. 1968. Observations on Some Holocene Glacier Fluctuations in West Greenland. *Meddelelser om Grønland* **165**: 6-212.

Weidick, A., Kelly, M., and Bennike, O. 2004. Late Quaternary development of the southern sector of the Greenland Ice Sheet, with particular reference to the Qassimiut lobe. *Boreas* **33**: 284-299. Doi 10.1080/03009480410001947

Weidick, A., Oerter, H., Reeh, N., Thomsen, H. H., and Thorning, L. 1990. The Recession of the Inland Ice Margin during the Holocene Climatic Optimum in the Jakobshavn-Isfjord Area of West Greenland. *Global and Planetary Change* **82**: 389-399.

Young, N. E., Briner, J. P., Stewart, H. A. M., Axford, Y., Csatho, B., Rood, D. H., and Finkel, R. C. 2011. Response of Jakobshavn Isbrae Greenland, to Holocene climate change. *Geology* **39**: 131-134. Doi 10.1130/G31399.1

Table 1: Summary of the average ^{10}Be concentration and standard deviation of each source category.

Region	Ice-free (atoms g^{-1} x 10^3)	Glacial (atoms g^{-1} x 10^3)	Mixed (atoms g^{-1} x 10^3)	Terrace (atoms g^{-1} x 10^3)	Aeolian (atoms g^{-1} x 10^3)	Median (atoms g^{-1} x 10^3)
K[a]	14.8 ± 2.6	5.2 ± 2.0	5.9 ± 1.8	6.6 ± 3.0	8.9	5.9
	n=2	*n=7*	*n=14*	*n=1*	*n=1*	*n=26*
N[b]	15.7 ± 11.3	11.7 ± 7.2	3.5 ± 1.8	3.7 ± 0.7		5.2
	n=6	*n=3*	*n= 5*	*n=2*		*n=16*
T[c]	12.3 ± 1.4	5.3 ± 2.8	9.1			5.6
	n=2	*n=9*	*n=1*			*n=12*
All	14.9 ± 8.6	6.5 ± 4.1	5.5 ± 2.2	5.2 ± 2.4	8.9	5.9
	n=10	*n=19*	*n=20*	*n=3*	*n=1*	*n=54*

[a]Some sites from Kangerlussuaq were sampled twice. For "mixed" category samples, which were measured in 2011 and 2012, the 2012 value is used for calculations. For the terrace, we use the average of the 2011 and 2012 concentrations**.**
[b]Narsarsuaq
[c]Tasiilaq

Table 2: Sample and exposure age calculation information for bedrock and boulder samples collected near Narsarsuaq, southern Greenland.

Sample Name	Sample Type	Latitude[a] (°N)	Longitude[a] (°E)	Elevation[a] (m asl)	Thickness (cm)	^{10}Be Conc. (atoms g^{-1})[b]	Uncertainty[c]	Exposure age (ka)[d]	Uncertainty (ka)
GLX14B	bedrock	61.296	-45.571	307	4	5.96×10^4	1.16×10^3	10.3	0.5
GLX15A	boulder	61.343	-45.546	969	4	1.15×10^5	2.15×10^3	10.9	0.6
GLX16A	boulder	61.323	-45.537	467	3	6.96×10^4	1.37×10^3	10.3	0.5
GLX16B	bedrock	61.323	-45.537	469	3	7.27×10^4	1.41×10^3	10.7	0.6
GLX17A	boulder	61.331	-45.543	724	1	9.11×10^4	2.47×10^3	10.5	0.6
GLX17B	bedrock	61.331	-45.543	720	6	8.00×10^4	5.61×10^3	9.6	0.8
GLX25A	boulder	61.193	-45.302	556	5	8.17×10^4	2.00×10^3	11.3	0.6
GLX25B	bedrock	61.193	-45.302	554	3	7.79×10^4	1.19×10^3	10.6	0.5
GLX28A	boulder	60.995	-45.431	52	2	4.71×10^4	1.96×10^3	10.4	0.6
GLX28B	bedrock	60.995	-45.431	50	2.5	4.67×10^4	1.19×10^3	10.4	0.6
GLX36A	boulder	61.182	-45.386	80	2.5	7.11×10^3	5.29×10^2	1.5	0.1

[a] Locations and elevations were recorded in the field with a Garmin-12 GPS

[b] Sample ^{10}Be/^{9}Be ratios were measured at the Lawrence Livermore National Laboratory and were normalized to the standard 07KNSTD3110 (Nishiizumi et al., 2007), blank-corrections have been made and the blank-corrected ^{10}Be concentration is reported

[c] Reported uncertainties are internal AMS uncertainties

[d] Exposure ages were calculated using the CRONUS Earth online calculator (Balco et al., 2008). We use the North American production rate and the Lal (1991)/Stone (2000) and production is scaled for elevation, sample density, thickness, latitude, and longitude

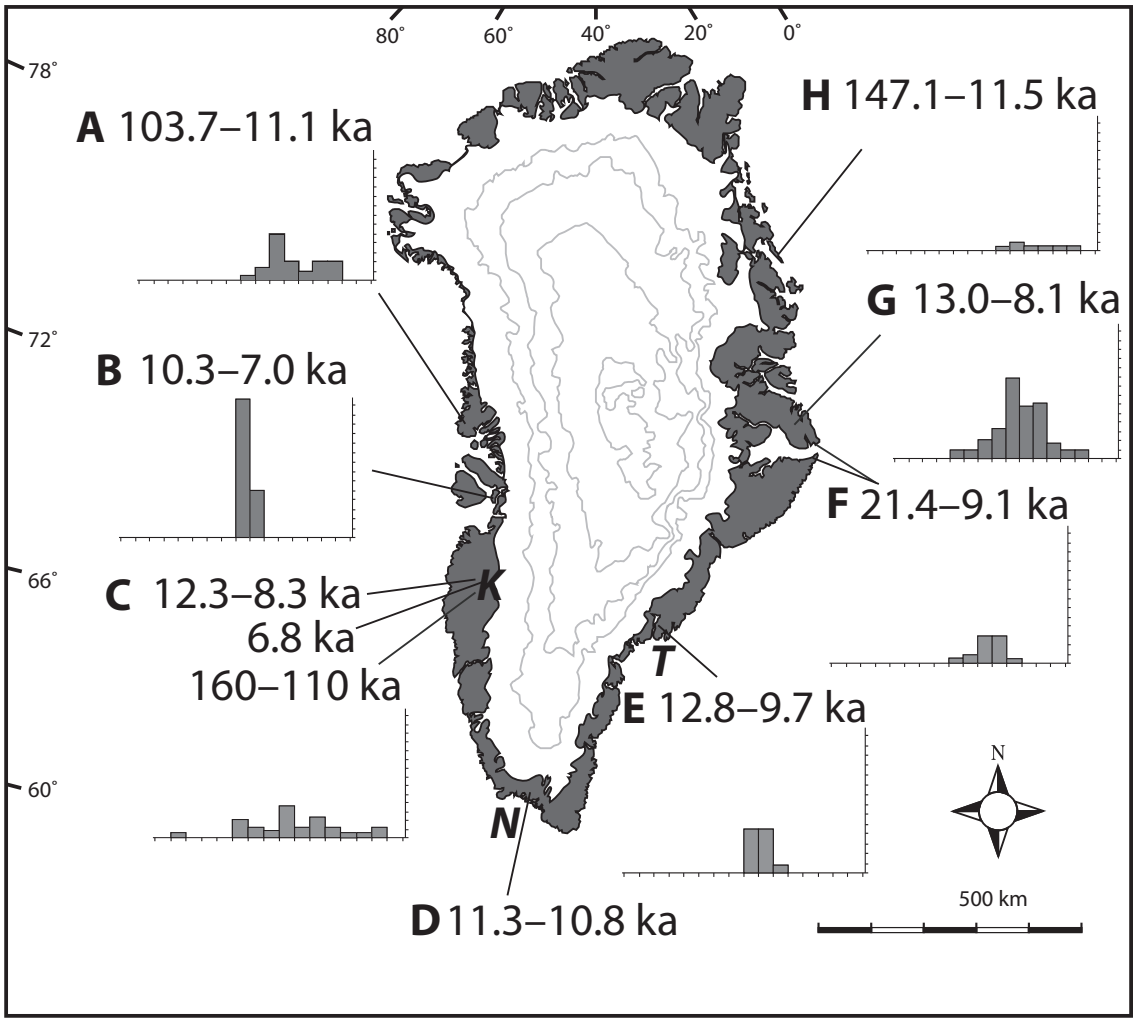

Figure 1: Map of Greenland showing showing single nuclide exposure age ranges (cosmogenic ^{10}Be data) as reported in previously published papers (*n=242*). Histograms show the log-scale distribution of ^{10}Be concentration for each region. The count scale on the y-axis goes from 0 to 35 and the log-scale of concentration on the x-axis ranges from 2.5–6.5, which represents ^{10}Be concentrations ranging from 3.2 x 10^3 to 1.7 x 10^6 atoms g^{-1}. Data are from A (Corbett, 2011), B (Corbett et al., 2011; Young et al., 2011), C (Levy et al., 2012; Rinterknecht et al., 2009; Roberts et al., 2009), D (Carlson et al., 2012), E (Roberts et al., 2008), F (Hakansson et al., 2007a; Hakansson et al., 2011; Hughes et al., 2012), G (Goehring et al., 2010; Kelly et al., 2008), H (Hakansson et al., 2007b). Fieldwork locations are Kangerlussuaq (*K*) on the west coast, Narsarsuaq (*N*) at the southern margin, and Tasiilaq (*T*) on the southeast coast. The base map was modified from worldofmaps.net.

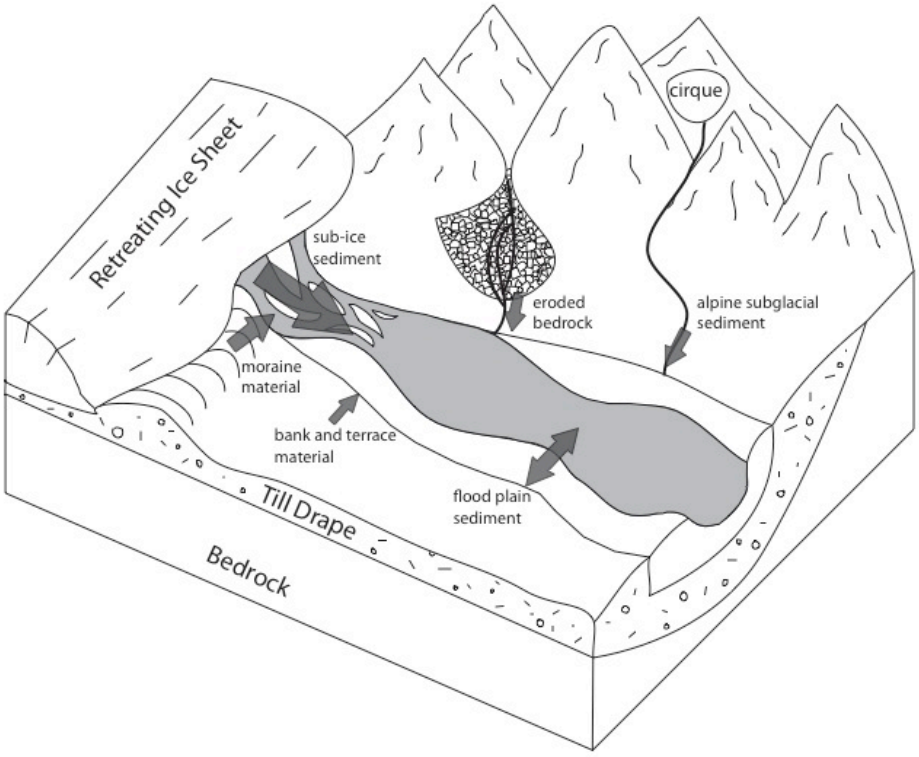

Figure 2: Schematic illustration showing sediment sources on the paraglacial landscape. The top of the picture represents mountainous terrain and the bottom of the picture represents a wide ice marginal valley.

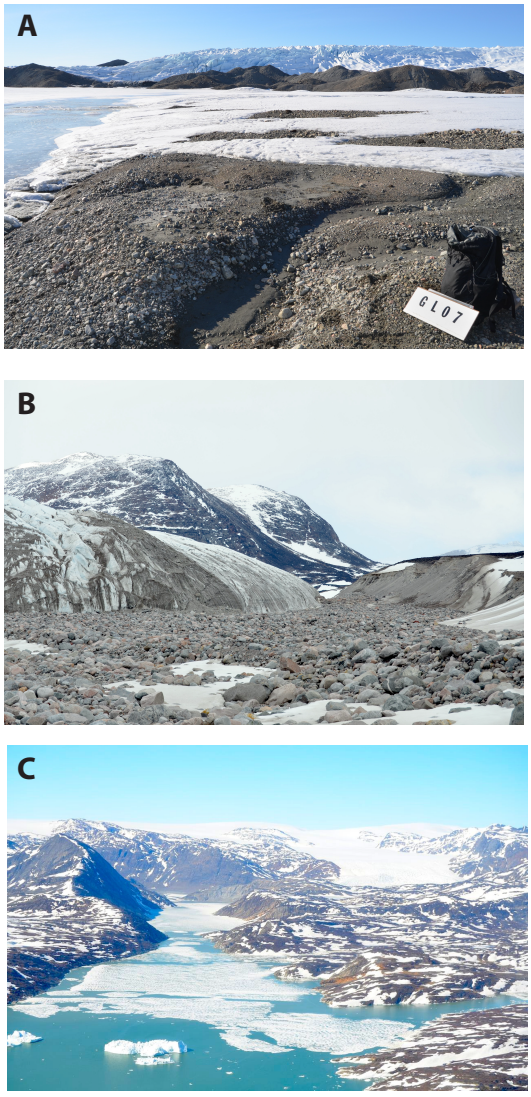

Figure 3: Field photographs showing the landscape in each study area. In Kangerlussuaq (A), the ice sheet margin is inland and glacial outwash flows into wide fluvial valleys that cross ice-free lowlands to the fjord. The photograph is from the GLX-07 (2011) sampling site, which is a wide glacial outwash plain close to the ice sheet margin. In Narsarsuaq (B) the ice sheet margin is primarily at high elevations in the uplands, the relief in this field area is greater than in the others and fluvial valleys are narrower. The photograph is from the GLX-19 sampling site, where the ice margin is ~600 m asl. In Tasiilaq (C) the ice margin sits at low elevations close to the coast. This photograph was taken looking across Sermilik Fjord, toward the Greenland Ice Sheet.

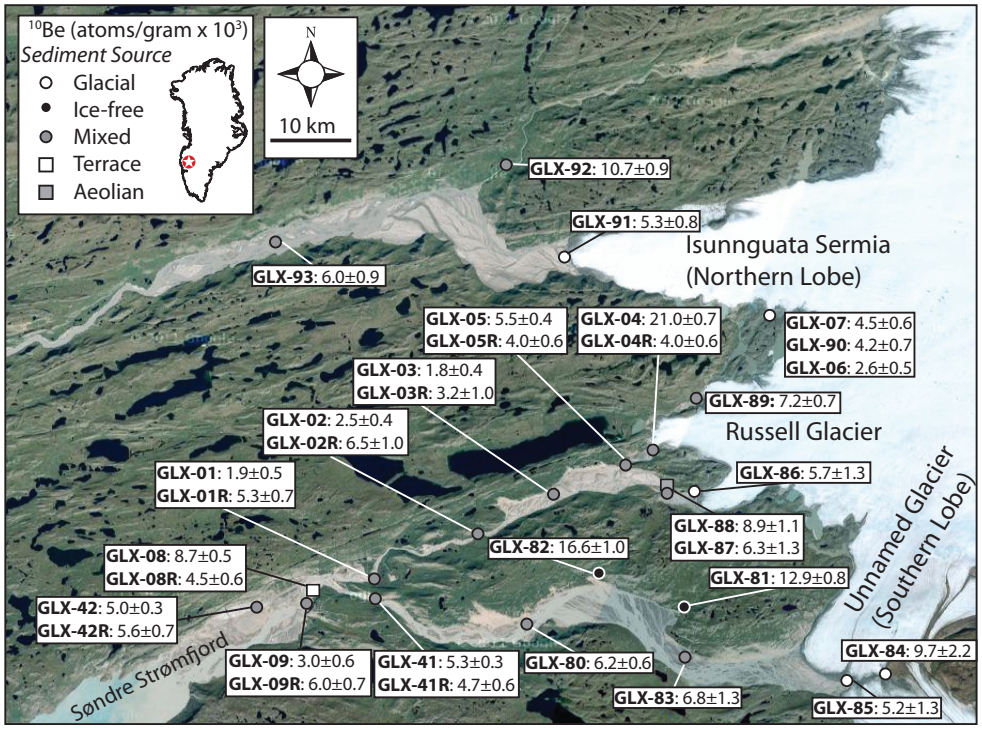

Figure 4: Google Earth image of the Kangerlussuaq field area showing sample sites and ^{10}Be concentration (atoms g^{-1} x 10^3) and 1σ internal AMS uncertainty (atoms g^{-1} x 10^3). Sample sites are labeled according to the sediment source category; white circles are glacial sediment, black circles are ice-free sediment, grey circles are mixed sediment, the white square is a terrace, and the grey square is an aeolian sample.

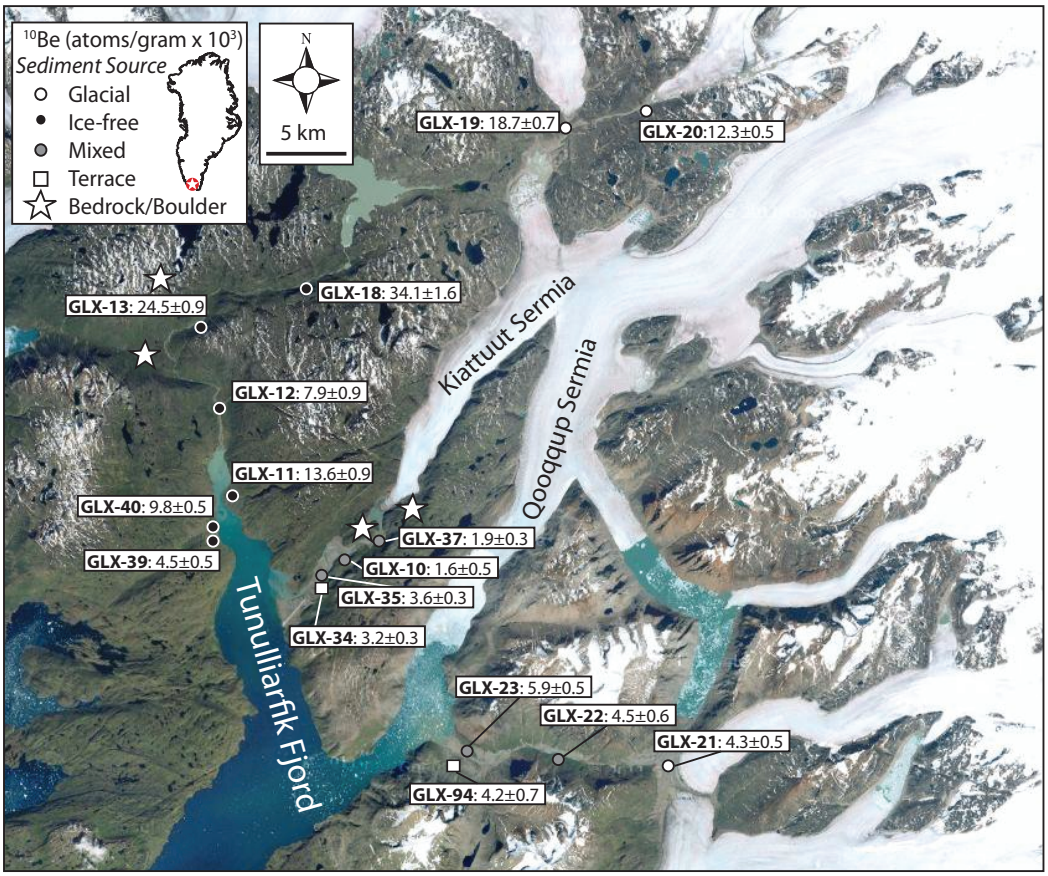

Figure 5: Google Earth image of the Narsarsuaq field area showing sample sites and ^{10}Be concentration (atoms g^{-1} x 10^3) and 1σ internal AMS uncertainty (atoms g^{-1} x 10^3). Sample sites are labeled according to the sediment source category; white circles are glacial sediment, black circles are ice-free sediment, grey circles are mixed sediment, and the white squares are terraces. The stars represent locations where we collected bedrock and boulder samples for exposure dating (Table 2).

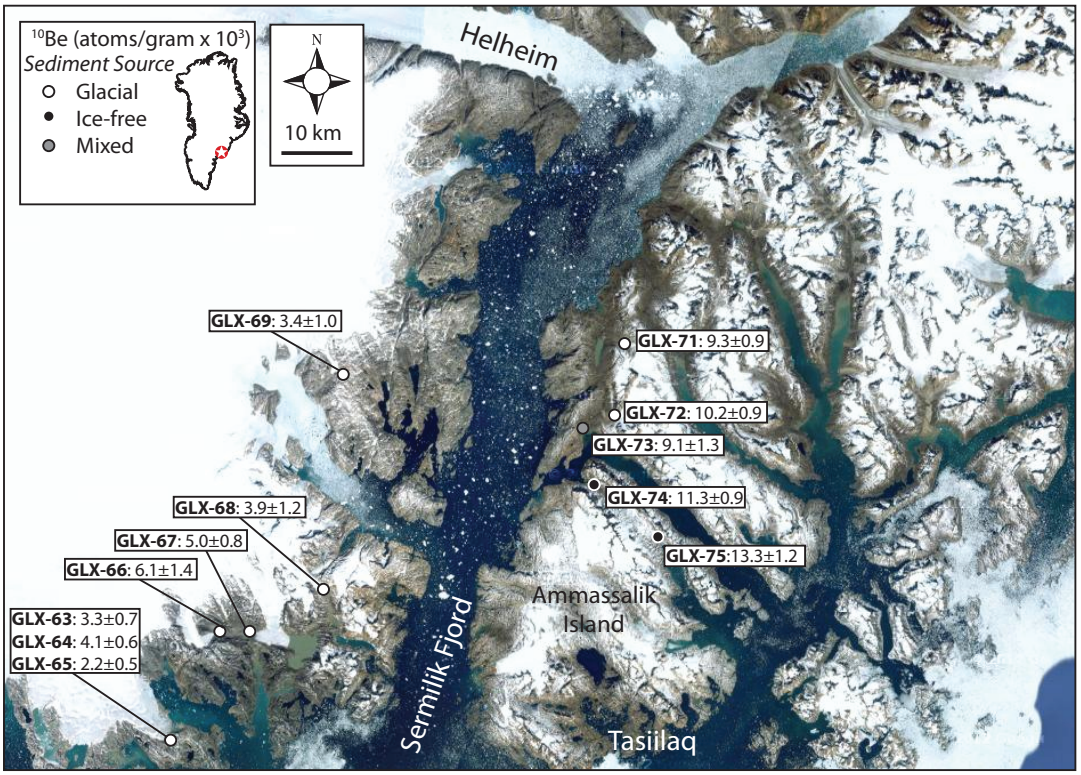

Figure 6: Google Earth image of the Tasiilaq region where the Greenland Ice Sheet to the west of Sermilik Fjord and coastal islands to the east are glaciated by isolated alpine glaciers. ^{10}Be concentration (atoms g^{-1} x 10^3) and 1σ internal AMS uncertainty (atoms g^{-1} x 10^3) is given for each sample site, which are labeled according to the sediment source category; white circles are glacial sediment, black circles are ice-free sediment, and the grey circle is mixed sediment.

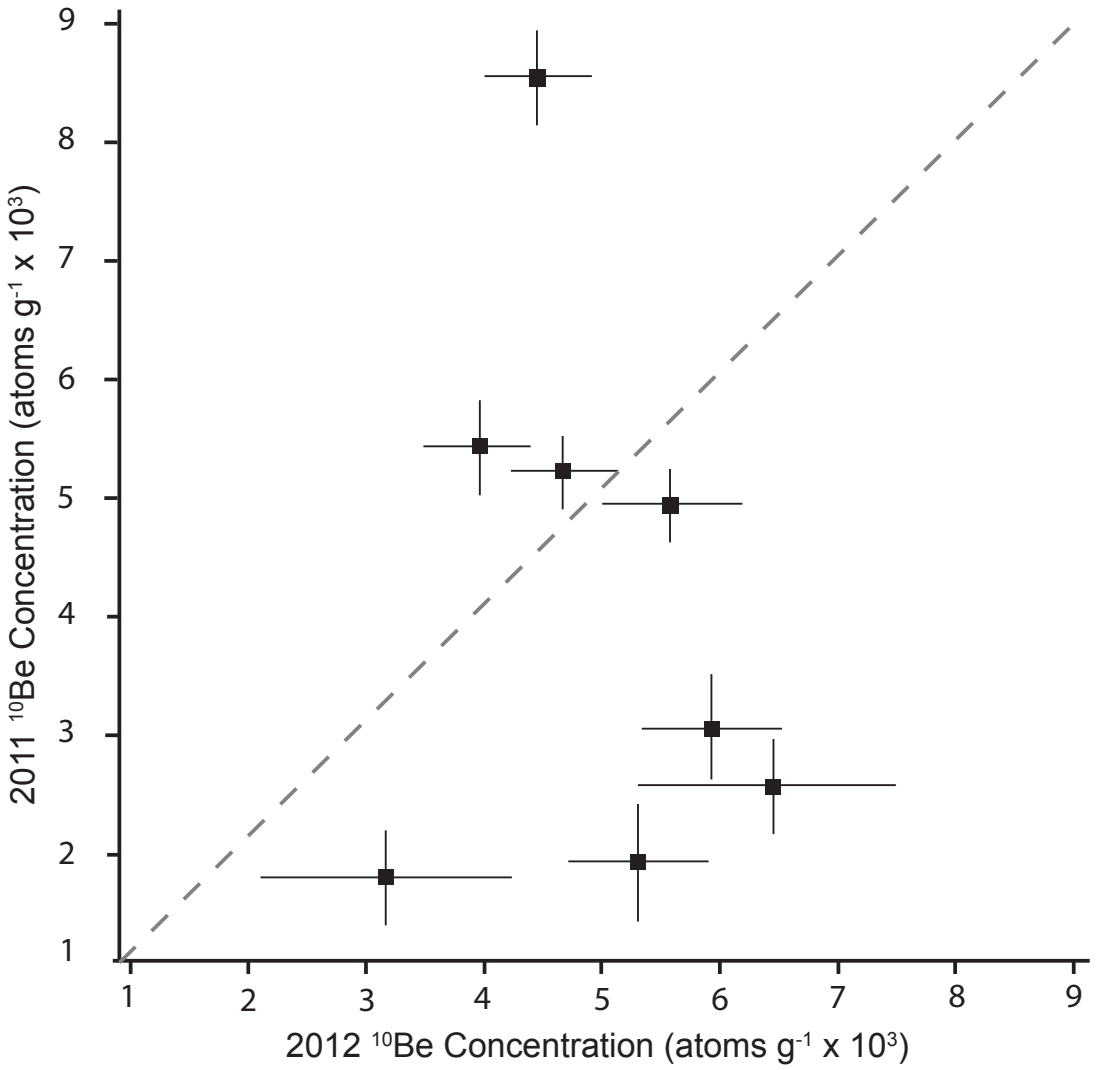

Figure 7: Scatter plot showing replicate sample concentration and uncertainty (*n=8*) from Kangerlussuaq. There is no correlation in concentration ($r^2=0.04$) between samples from 2011 (y-axis) and 2012 (x-axis). Seven of the eight replicates are channel samples, and means of 2011 channel concentrations and 2012 channel concentrations are statistically inseparable (p=0.08).

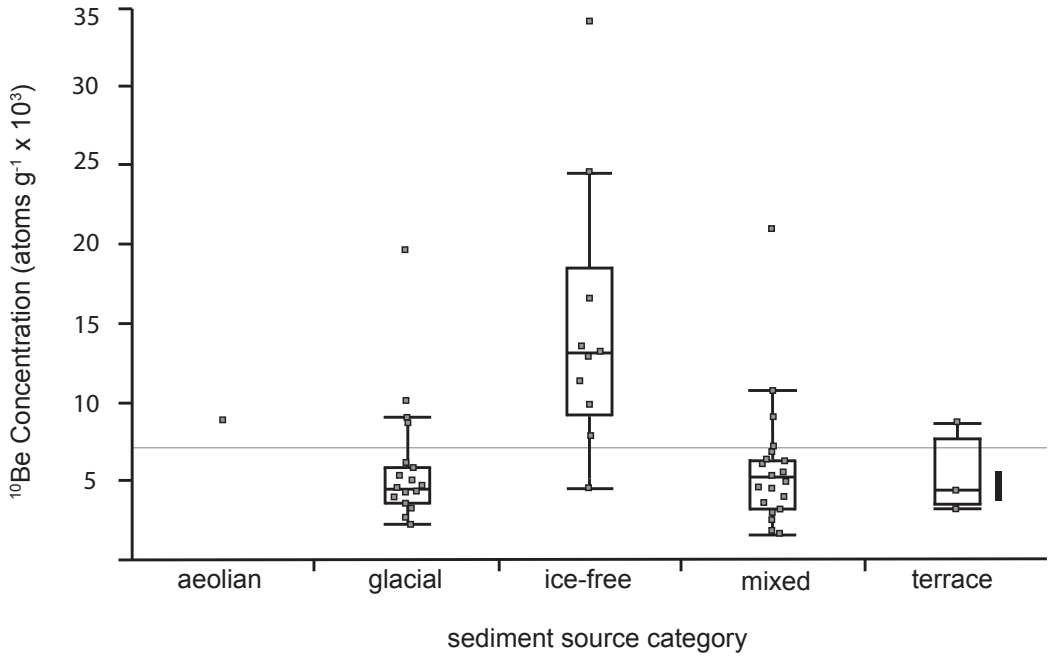

Figure 8: Box and whisker plots showing concentration for each of the source categories. The box encloses the data that fall between the first and third quartiles, the horizontal line is the median, and the whiskers span one standard deviation. The line, which spans the entire plot horizontally, is the grand mean of all samples. Concentration in aeolian (*n*=1), glacial (*n*=19), mixed (*n*=20), and terrace (*n*=3) samples is similar and the concentration in ice-free samples (*n*=10) is higher. The black bar next to the terrace category shows the range of inherited concentrations in deltaic sediment from Scoresby Sund, which is similar to the concentrations measured in glacial, mixed, and terrace sediment at our field sites.

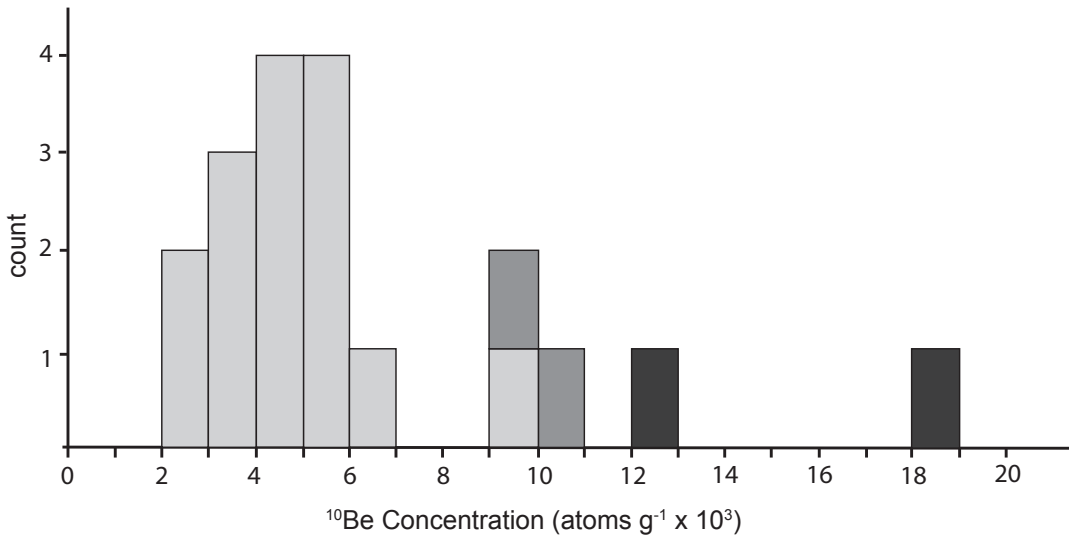

Figure 9: Histogram showing the concentration distribution for glacial category sediment. The different shades of grey represent glacial sample sub-categories; low-elevation ice sheet margins are pale grey, high-elevation ice sheet margins are the darkest shade of grey, and glacial margins not connected to the mainland ice sheet are the medium shade of grey.

CHAPTER 5. CONCLUSIONS

1. Conclusions

We analyzed 62 sediment samples from three different ice marginal locations on Greenland and found the average ^{10}Be concentration in sediment to be 5.9 x 10^3 atoms g^{-1}. We were able to use the concentration of *in situ* ^{10}Be to trace the relative contribution of different sediment sources to the paraglacial sediment budget because ^{10}Be concentrations in glacial and ice-free sediment are characteristically different. We compared the ^{10}Be concentrations of different sediment source categories and found that for all three of our field areas, the concentration in glacial, mixed, and terrace sediment is similar, and ice-free sediment concentration is significantly higher, indicating that glacial sediment dominates the modern fluvial system, and also dominated the fluvial system earlier in the Holocene when terraces were deposited.

Glacial sediment contains low concentrations of ^{10}Be that accumulated at depth, by muogenic production, over a prolonged period of exposure that happened before the ice sheet was established. The isotope concentration in glacial sediment is low because the landscape from which the sediment is sourced has been shielded from cosmic radiation for much of the last ~3.5 My and because ^{10}Be has been decaying since production ceased when the ice sheet was established. In contrast to glacial sediment, ice-free sediment contains significantly higher concentrations of ^{10}Be because ice-free sediment is old glacial sediment that has since accumulated additional ^{10}Be from cosmic ray exposure on the landscape surface following early Holocene ice sheet retreat.

Using ^{10}Be concentration as a tracer, we find that ~90% of mixed source sediment is glacial in origin. Concentration in ice-free category sediment is on average more than twice that of glacial category sediment, but there is not enough sediment sourced from ice-free terrain to affect channel concentration, even though the channels flow through the ice-free landscape. Our findings imply that most sediment currently stored in the fjords, and thus evacuated to the oceans, is also glacial in origin.

2. Implications for long-term marine records of ^{10}Be

This thesis is part of a larger research project that will use the concentration of *in situ* ^{10}Be in marine sediment to create a 5 to 6 My record of Greenland glaciation. Previous studies indicate that the timing of sediment delivery to coring sites in the ocean is controlled by the timing of glacial advance; during ice sheet retreat, eroded material accumulates on the landscape and within the coastal fjords, and during advance, sediment is evacuated to the ocean (Harbor and Warburton, 1993; Koppes et al., 2010; Storms et al., 2012). Our findings suggest that the majority of sediment in fjords is glacial in origin and so ^{10}Be concentration in the marine record will likely be controlled by the efficacy and timing of ice sheet erosion. In our field areas, with the current amount of land exposure, the majority of sediment deposited in the fjords is glacial in origin.

From our understanding of the modern paraglacial environment, we expect that during the next period of glacial advance, the sediment evacuated to the ocean will contain ~5 x 10^3 atoms g^{-1} of ^{10}Be because this is the concentration in sediment that is currently being deposited in the fjords. In the past, however, decay-corrected ^{10}Be concentration in marine sediment is likely to have been higher. We calculated that the

low concentrations of ^{10}Be in glacial sediment accumulated 20 to 30 meters below the land surface by steady-state muogenic production before the Greenland Ice Sheet was established. If ~30 m of bedrock have since been eroded by the ice sheet, then earlier in the marine record, sediment will be sourced closer to the surface, and will contain higher concentrations of ^{10}Be then the modern glacial sediment. Initial establishment of the ice sheet may be recorded in the marine record as a pulse of high-concentration ^{10}Be, the timing of which would be concurrent with erosion and evacuation of the upper few meters of the land surface, where high concentrations of ^{10}Be had accumulated by steady-state spallation production. Over time, ^{10}Be concentration in marine sediment will likely decline as subglacial erosion exhumed sediment sourced deeper and deeper below the initial surface. In marine core samples, depending on sample resolution and frequency, decline in ^{10}Be concentration may occur as step-wise pulses associated with specific periods of glacial advance.

Past warm periods are not likely to be recorded in the marine record, unless duration and extent of interglacial ice sheet retreat was significantly greater than it is today. At present, there is a much greater volume of glacial sediment on the landscape then there is ice-free sediment, and so the ice-free concentration is averaged out in the channels and thus also in the fjords. If the ice sheet was ever significantly reduced – or if it melted completely – as has been proposed during MIS 11 (Berger and Loutre, 1991; de Vernal and Hillaire-Marcel, 2008; Hearty et al., 1999; Kaufman et al., 2004; Nishiizumi et al., 1996; Poore and Dowsett, 2001; Raymo et al., 2011; Roberts et al., 2012; Steig and Wolfe, 2008), then the relative contribution of sediment from glacial and ice-free terrain would have been different then it is today. With a much reduced - or absent - ice sheet,

the sediment contribution from the ice-free landscape would have been greater than it is today, and concentration in mixed sediment in channels and fjords would also have been higher, as would the concentration in marine sediment. Thus, there is potential that the ^{10}Be concentration in marine sediment could improve our understanding of Greenland Ice Sheet stability by recording instances in the past when the ice sheet retreated more in response to warming than it has today.

COMPREHENSIVE BIBLIOGRAPHY

Alley, R. B., Andrews, J. T., Brigham-Grette, J., Clarke, G. K. C., Cuffey, K. M., Fitzpatrick, J. J., Funder, S., Marshall, S. J., Miller, G. H., Mitrovica, J. X., Muhs, D. R., Otto-Bliesner, B. L., Polyak, L., and White, J. W. C., 2010, History of the Greenland Ice Sheet: paleoclimatic insights: Quaternary Science Reviews, v. 29, no. 15-16, p. 1728-1756. Doi 10.1016/J.Quascirev.2010.02.007

Anderson, N. J., Harriman, R., Ryves, D. B., and Patrick, S. T., 2001, Dominant factors controlling variability in the ionic composition of West Greenland Lakes: Arctic Antarctic and Alpine Research, v. 33, no. 4, p. 418-425. Doi 10.2307/1552551

Andrews, J., 2000, Icebergs and iceberg rafted detritus (IRD) in the North Atlantic: facts and assumptions: Oceanography, v. 13, no. 3, p. 100-108.

Balco, G., Briner, J., Finkel, R. C., Rayburn, J. A., Ridge, J. C., and Schaefer, J. M., 2009, Regional beryllium-10 production rate calibration for late-glacial northeastern North America: Quaternary Geochronology, v. 4, no. 2, p. 93-107. Doi 10.1016/J.Quageo.2008.09.001

Balco, G., Stone, J. O., Lifton, N. A., and Dunai, T. J., 2008, A complete and easily accessible means of calculating surface exposure ages or erosion rates from ^{10}Be and ^{26}Al measurements: Quaternary Geochronology, v. 3, no. 3, p. 174-195. Doi 10.1016/J.Quageo.2007.12.001

Ballantyne, C. K., 2002a, A general model of paraglacial landscape response: Holocene, v. 12, no. 3, p. 371-376. Doi 10.1191/0959683602hl553fa

-, 2002b, Paraglacial geomorphology: Quaternary Science Reviews, v. 21, no. 18-19, p. 1935-2017.

Bamber, J. L., Layberry, R. L., and Gogineni, S., 2001, A new ice thickness and bedrock elevation data set for Greenland, part I.: Journal of Geophysical Research, v. 106, no. D24, p. 33,773-733,780. Doi 10.1029/2001jd900054

Bamber, J. L., Riva, R. E. M., Vermeersen, B. L. A., and LeBrocq, A. M., 2009, Reassessment of the Potential Sea-Level Rise from a Collapse of the West Antarctic Ice Sheet: Science, v. 324, no. 5929, p. 901-903. Doi 10.1126/Science.1169335

Bartholomew, I., Nienow, P., Sole, A., Mair, D., Cowton, T., Palmer, S., and Wadham, J., 2011, Supraglacial forcing of subglacial drainage in the ablation zone of the Greenland ice sheet: Geophysical Research Letters, v. 38. Artn L08502
Doi 10.1029/2011gl047063

Berger, A., and Loutre, M. F., 1991, Insolation Values for the Climate of the Last 10,000,000 Years: Quaternary Science Reviews, v. 10, no. 4, p. 297-317.

Beylich, A. A., 2011, Mass transfers, sediment budgets and relief development in cold environments: Results of long-term geomorphologic drainage basin studies in Iceland, Swedish Lapland and Finnish Lapland: Zeitschrift Fur Geomorphologie, v. 55, no. 2, p. 145-174. Doi 10.1127/0372-8854/2011/0055-0046

Braucher, R., Brown, E. T., Bourles, D. L., and Colin, F., 2003, In situ produced ^{10}Be measurements at great depths: implications for production rates by fast muons:

Earth and Planetary Science Letters, v. 211, no. 3-4, p. 251-258. Doi 10.1016/S0012-821x(03)00205-X

Briner, J., Young, N. E., Goehring, B. M., and Schaefer, J. M., 2012, Constraining Holocene ^{10}Be Production Rates in Greenland: Journal of Quaternary Science, v. 27, no. 1, p. 2-6.

Briner, J. P., Miller, G. H., Davis, P. T., and Finkel, R. C., 2006, Cosmogenic radionuclides from fiord landscapes support differential erosion by overriding ice sheets: Geological Society of America Bulletin, v. 118, no. 3-4, p. 406-420. Doi 10.1130/B25716.1

Cane, M. A., and Molnar, P., 2001, Closing of the Indonesian seaway as a precursor to east African aridircation around 3-4 million years ago: Nature, v. 411, no. 6834, p. 157-162.

Carlson, A. E., Winsor, K., Brook, E., Ullman, D. J., LeGrande, A., Anslow, F., Rood, D., and Axford, Y., 2012, Holocene Southwest Greenland Ice-Sheet Retreat Suggests Recent Ice Retreat Is A Response To Global Warming, 2012 Fall Meeting, AGU: San Francisco, California.

Chmeleff, J., von Blanckenburg, F., Kossert, K., and Jakob, D., 2009, Determination of the ^{10}Be half-life by Multi Collector ICP-mass spectrometry and liquid scintillation counting: Geochimica Et Cosmochimica Acta, v. 73, no. 13, p. A221-A221.

Church, M., and Ryder, J., 1972, Paraglacial Sedimentation: A consideration of Fluvial Processes Conditioned by Glaciation: Geological Society of America Bulletin, v. 83, p. 3059-3072.

Clark, P. U., and Huybers, P., 2009, Interglacial and Future Sea Level: Nature, v. 462, no. 7275, p. 856-857. Doi 10.1038/462856a

Colgan, P. M., Bierman, P. R., Mickelson, D. M., and Caffee, M., 2002, Variation in glacial erosion near the southern margin of the Laurentide Ice Sheet, south-central Wisconsin, USA: Implications for cosmogenic dating of glacial terrains: Geological Society of America Bulletin, v. 114, no. 12, p. 1581-1591.

Colville, E. J., Carlson, A. E., Beard, B. L., Hatfield, R. G., Stoner, J. S., Reyes, A. V., and Ullman, D. J., 2011, Sr-Nd-Pb Isotope Evidence for Ice-Sheet Presence on Southern Greenland During the Last Interglacial: Science, v. 333, no. 6042, p. 620-623. Doi 10.1126/Science.1204673

Corbett, L. B., 2011, Investigating the timing of deglaciation and the efficiency of subglacial erosion in central-western Greenland with cosmogenic ^{10}Be and ^{26}Al [Master of Science Specializing in Geology: The University of Vermont, 174 p.

Corbett, L. B., Young, N. E., Bierman, P. R., Briner, J. P., Neumann, T. A., Rood, D. H., and Graly, J. A., 2011, Paired bedrock and boulder ^{10}Be concentrations resulting from early Holocene ice retreat near Jakobshavn Isfjord, western Greenland: Quaternary Science Reviews, v. 30, no. 13-14, p. 1739-1749. Doi 10.1016/J.Quascirev.2011.04.001

Cowton, T., Nienow, P., Bartholomew, I., Sole, A., and Mair, D., 2012, Rapid erosion beneath the Greenland ice sheet: Geology, v. 40, no. 4, p. 343-346. Doi 10.1130/G32687.1

Cuffey, K. M., and Marshall, S. J., 2000, Substantial contribution to sea-level rise during the last interglacial from the Greenland ice sheet: Nature, v. 404, no. 6778, p. 591-594. Doi 10.1038/35007053

Dahl-Jensen, D., Mosegaard, K., Gundestrup, N., Clow, G. D., Johnsen, S. J., Hansen, A. W., and Balling, N., 1998, Past temperatures directly from the Greenland Ice Sheet: Science, v. 282, no. 5387, p. 268-271. Doi 10.1126/Science.282.5387.268

Davis, P. T., Briner, J. P., Coulthard, R. D., Finkel, R. W., and Miller, G. H., 2006, Preservation of Arctic landscapes overridden by cold-based ice sheets: Quaternary Research, v. 65, no. 1, p. 156-163. Doi 10.1016/J.Yqres.2005.08.019

de Vernal, A., and Hillaire-Marcel, C., 2008, Natural variability of Greenland climate, vegetation, and ice volume during the past million years: Science, v. 320, no. 5883, p. 1622-1625. Doi 10.1126/Science.1153929

de Winter, I. L., Storms, J. E. A., and Overeem, I., 2012, Numerical modeling of glacial sediment production and transport during deglaciation: Geomorphology, v. 167, p. 102-114. Doi 10.1016/J.Geomorph.2012.05.023

DeConto, R. M., Pollard, D., Wilson, P. A., Palike, H., Lear, C. H., and Pagani, M., 2008, Thresholds for Cenozoic bipolar glaciation: Nature, v. 455, no. 7213, p. 652-U652. Doi 10.1038/Nature07337

Desloges, J. R., Gilbert, R., Nielsen, N., Christiansen, C., Rasch, M., and Ohlenschlager, R., 2002, Holocene glacimarine sedimentary environments in fiords of Disko Bugt, West Greenland: Quaternary Science Reviews, v. 21, no. 8-9, p. 947-963.

Dietrich, W. E., and Dunne, T., 1978, Sediment budget for a small catchment in mountainous terrain: Zeitschrift Fur Geomorphologie, Supplement, v. 29, p. 191-206.

Drewry, D., 1986, Glacial Geological Processes, London, Edward Arnold.

Escher, A., and Watt, W. S., 1976, Geology of Greenland, Copenhagen, The Geologic Survey of Greenland.

Escher, J. C., and Pulvertaft, T. C., 1995, Geologic map of Greenland: Geologic Survey of Greenland, scale 1:2500000.

Etzelmuller, B., 2000, Quantification of thermo-erosion in pro-glacial areas - examples from Svalbard: Zeitschrift Fur Geomorphologie, v. 44, no. 3, p. 343-361.

Fausto, R. S., Mernild, S. H., Hasholt, B., Ahlstrom, A. P., and Knudsen, N. T., 2012, Modeling Suspended Sediment Concentration and Transport, Mittivakkat Glacier, Southeast Greenland: Arctic Antarctic and Alpine Research, v. 44, no. 3, p. 306-318. Doi 10.1657/1938-4246-44.3.306

Forman, S. L., Marin, L., van der Veen, C., Tremper, C., and Csatho, B., 2007, Little ice age and neoglacial landforms at the Inland Ice margin, Isunguata Sermia, Kangerlussuaq, west Greenland: Boreas, v. 36, no. 4, p. 341-351. Doi 10.1080/00173130601173301

Friedlander, M., 1990, Cosmic Rays, Cambridge, MA, Harvard University Press.

Funder, S., Hjort, C., Landvik, J. Y., Nam, S. I., Reeh, N., and Stein, R., 1998, History of a stable ice margin - East Greenland during the Middle and Upper Pleistocene: Quaternary Science Reviews, v. 17, no. 1-3, p. 77-123.

Gilbert, R., 1990, Rafting in glacimarine environments: Geological Society, London, Special Publications, v. 53, p. 105-120.

Goehring, B. M., Kelly, M. A., Schaefer, J. M., Finkel, R. C., and Lowell, T. V., 2010, Dating of raised marine and lacustrine deposits in east Greenland using ^{10}Be depth profiles and implications for estimates of subglacial erosion: Journal of Quaternary Science, v. 25, no. 6, p. 865-874. Doi 10.1002/Jqs.1380

Gordon, J. E., 1981, Glacier Margin Fluctuations during the 19th and 20th Centuries in the Ikamiut Kangerdluarssuat Area, West Greenland: Arctic and Alpine Research, v. 13, no. 1, p. 47-62. Doi 10.2307/1550625

Gosse, J. C., and Phillips, F. M., 2001, Terrestrial in situ cosmogenic nuclides: theory and application: Quaternary Science Reviews, v. 20, no. 14, p. 1475-1560. Doi 10.1016/S0277-3791(00)00171-2

Grinsted, A., Moore, J. C., and Jevrejeva, S., 2010, Reconstructing sea level from paleo and projected temperatures 200 to 2100 AD: Climate Dynamics, v. 34, no. 4, p. 461-472. Doi 10.1007/S00382-008-0507-2

Gurnell, A., Hannah, D., and Lawler, D., 1996, Suspended sediment yield from glacier basins: IAHS Publications-Series of Proceedings and Reports-Intern Assoc Hydrological Sciences, v. 236, p. 97-104.

Hakansson, L., Briner, J., Alexanderson, H., Aldahan, A., and Possnert, G., 2007a, ^{10}Be ages from central east Greenland constrain the extent of the Greenland ice sheet during the Last Glacial Maximum: Quaternary Science Reviews, v. 26, no. 19-21, p. 2316-2321. Doi 10.1016/J.Quascirev.2007.08.001

Hakansson, L., Briner, J. P., Aldahan, A., and Possnert, G., 2011, ^{10}Be data from meltwater channels suggest that Jameson Land, east Greenland, was ice-covered during the last glacial maximum: Quaternary Research, v. 76, no. 3, p. 452-459. Doi 10.1016/J.Yqres.2011.06.007

Hakansson, L., Graf, A., Strasky, S., Ivy-Ochs, S., Kubik, P. W., Hjort, C., and Schluchter, 2007b, Cosmogenic ^{10}Be-ages from the Store Koldewey island, NE Greenland: Geografiska Annaler Series a-Physical Geography, v. 89A, no. 3, p. 195-202.

Hallet, B., 1979, A Theoretical Model of Glacial Abrasion: Journal of Glaciology, v. 23, no. 89, p. 39-50.

Hallet, B., Hunter, L., and Bogen, J., 1996, Rates of erosion and sediment evacuation by glaciers: A review of field data and their implications: Global and Planetary Change, v. 12, no. 1-4, p. 213-235. Doi 10.1016/0921-8181(95)00021-6

Hammer, K. M., and Smith, N. D., 1983, Sediment Production and Transport in a Proglacial Stream - Hilda Glacier, Alberta, Canada: Boreas, v. 12, no. 2, p. 91-106.

Harbor, J., and Warburton, J., 1993, Relative Rates of Glacial and Nonglacial Erosion in Alpine Environments: Arctic and Alpine Research, v. 25, no. 1, p. 1-7.

Harbor, J. M., 1993, Glacial Geomorphology - Modeling Processes and Landforms: Geomorphology, v. 7, no. 1-3, p. 129-140. Doi 10.1016/0169-555x(93)90014-S

Haug, G. H., and Tiedemann, R., 1998, Effect of the formation of the Isthmus of Panama on Atlantic Ocean thermohaline circulation: Nature, v. 393, no. 6686, p. 673-676.

Haywood, A. M., Valdes, P. J., and Sellwood, B. W., 2000, Global scale palaeoclimate reconstruction of the middle Pliocene climate using the UKMO GCM: initial

results: Global and Planetary Change, v. 25, no. 3-4, p. 239-256. Doi 10.1016/S0921-8181(00)00028-X
Hearty, P. J., Kindler, P., Cheng, H., and Edwards, R. L., 1999, A +20 m middle Pleistocene sea-level highstand (Bermuda and the Bahamas) due to partial collapse of Antarctic ice: Geology, v. 27, no. 4, p. 375-378.
Heisinger, B., Lal, D., Jull, A. J. T., Kubik, P., Ivy-Ochs, S., Knie, K., and Nolte, E., 2002a, Production of selected cosmogenic radionuclides by muons: 2. Capture of negative muons: Earth and Planetary Science Letters, v. 200, no. 3-4, p. 357-369.
Heisinger, B., Lal, D., Jull, A. J. T., Kubik, P., Ivy-Ochs, S., Neumaier, S., Knie, K., Lazarev, V., and Nolte, E., 2002b, Production of selected cosmogenic radionuclides by muons 1. Fast muons: Earth and Planetary Science Letters, v. 200, no. 3-4, p. 345-355. Pii S0012-821x(02)00640-4
Doi 10.1016/S0012-821x(02)00640-4
Henriksen, N., Higgins, A., Kalsbeek, F., and Pulvertaft, T., 2009, Greenland from Archaen to Quaternary: Geological Survey of Denmark and Greenland Bulletin, v. 18.
Hicks, D. M., Mcsaveney, M. J., and Chinn, T. J. H., 1990, Sedimentation in Proglacial Ivory Lake, Southern Alps, New-Zealand: Arctic and Alpine Research, v. 22, no. 1, p. 26-42.
Hodson, A., Gurnell, A., Tranter, M., Bogen, J., Hagen, J. O., and Clark, M., 1998, Suspended sediment yield and transfer processes in a small High-Artic glacier basin, Svalbard: Hydrological Processes, v. 12, no. 1, p. 73-86. Doi 10.1002/(Sici)1099-1085(199801)12:1<73::Aid-Hyp564>3.0.Co;2-S
Hughes, A. L. C., Rainsley, E., Murray, T., Fogwill, C. J., Schnabel, C., and Xu, S., 2012, Rapid response of Helheim Glacier, southeast Greenland, to early Holocene climate warming: Geology, v. 40, no. 5, p. 427-430. Doi 10.1130/G32730.1
Imbrie, J., Hays, J. D., Martinson, D. G., Mcintyre, A., Mix, A., Morley, J. J., Pisias, N. G., Prell, W. L., and Shackleton, N. J., 1984, The orbital theory of Pleistocene climate: support from a revised chronology of the marine delta ^{18}O record, *in* Proceedings NATO Advanced Research Workshop, Palisades, NY, 1982, Reidel Publishing, p. 269.
IPCC, 2007, Climate Change 2007: The Physical Science Basis. Contribution of Working Group I to the Fourth Assessment Report of the Intergovernmnetal Panel on Climate Change.
Jakobsson, M., Nilsson, J., O'Regan, M., Backman, J., Lowemark, L., Dowdeswell, J. A., Mayer, L., Polyak, L., Colleoni, F., Anderson, L. G., Bjork, G., Darby, D., Eriksson, B., Hanslik, D., Hell, B., Marcussen, C., Sellen, E., and Wallin, A., 2010, An Arctic Ocean ice shelf during MIS 6 constrained by new geophysical and geological data: Quaternary Science Reviews, v. 29, no. 25-26, p. 3505-3517. Doi 10.1016/J.Quascirev.2010.03.015
Kaufman, D. S., Ager, T. A., Anderson, N. J., Anderson, P. M., Andrews, J. T., Bartlein, P. J., Brubaker, L. B., Coats, L. L., Cwynar, L. C., Duvall, M. L., Dyke, A. S., Edwards, M. E., Eisner, W. R., Gajewski, K., Geirsdottir, A., Hu, F. S., Jennings, A. E., Kaplan, M. R., Kerwin, M. N., Lozhkin, A. V., MacDonald, G. M., Miller, G. H., Mock, C. J., Oswald, W. W., Otto-Bliesner, B. L., Porinchu, D. F.,

Ruhland, K., Smol, J. P., Steig, E. J., and Wolfe, B. B., 2004, Holocene thermal maximum in the western Arctic (0-180 degrees W): Quaternary Science Reviews, v. 23, no. 5-6, p. 529-560. Doi 10.1016/J.Quascirev.2003.09.007

Keigwin, L., 1982, Isotopic Paleo-Oceanography of the Caribbean and East Pacific - Role of Panama Uplift in Late Neogene Time: Science, v. 217, no. 4557, p. 350-352.

Kelly, M., 1985, A review of the Quaternary geology of western Greenland, *in* Andrews, J., ed., Quaternary Environments Eastern Canadian Arctic, Baffin Bay and Western Greenland: Boston, Allen and Unwin, p. 461–501.

Kelly, M. A., Lowell, T. V., Hall, B. L., Schaefer, J. M., Finkel, R. C., Goehring, B. M., Alley, R. B., and Denton, G. H., 2008, A ^{10}Be chronology of lateglacial and Holocene mountain glaciation in the Scoresby Sund region, east Greenland: implications for seasonality during lateglacial time: Quaternary Science Reviews, v. 27, no. 25-26, p. 2273-2282. Doi 10.1016/J.Quascirev.2008.08.004

Kelsey, H. M., Lamberson, R., and Madej, M. A., 1987, Stochastic-Model for the Long-Term Transport of Stored Sediment in a River Channel: Water Resources Research, v. 23, no. 9, p. 1738-1750. Doi 10.1029/Wr023i009p01738

Kleiven, H. F., Jansen, E., Fronval, T., and Smith, T. M., 2002, Intensification of Northern Hemisphere glaciations in the circum Atlantic region (3.5-2.4 Ma) - ice-rafted detritus evidence: Palaeogeography Palaeoclimatology Palaeoecology, v. 184, no. 3-4, p. 213-223.

Kohl, C. P., and Nishiizumi, K., 1992, Chemical Isolation of Quartz for Measurement of Insitu-Produced Cosmogenic Nuclides: Geochimica Et Cosmochimica Acta, v. 56, no. 9, p. 3583-3587.

Kopp, R. E., Simons, F. J., Mitrovica, J. X., Maloof, A. C., and Oppenheimer, M., 2009, Probabilistic assessment of sea level during the last interglacial stage: Nature, v. 462, no. 7275, p. 863-U851. Doi 10.1038/Nature08686

Koppes, M., Sylwester, R., Rivera, A., and Hallet, B., 2010, Variations in sediment yield over the advance and retreat of a calving glacier, Laguna San Rafael, North Patagonian Icefield: Quaternary Research, v. 73, no. 1, p. 84-95. Doi 10.1016/J.Yqres.2009.07.006

Korschinek, G., Bergmaier, A., Dillmann, I., Faestermann, T., Gerstmann, U., Knie, K., von Gostomski, C. L., Maiti, M., Poutivtsev, M., Remmert, A., Rugel, G., and Wallner, A., 2009, Determination of the ^{10}Be half-life by HI-ERD and Liquid Scintillation Counting: Geochimica Et Cosmochimica Acta, v. 73, no. 13, p. A685-A685.

Krabill, W., Hanna, E., Huybrechts, P., Abdalati, W., Cappelen, J., Csatho, B., Frederick, E., Manizade, S., Martin, C., Sonntag, J., Swift, R., Thomas, R., and Yungel, J., 2004, Greenland Ice Sheet: Increased coastal thinning: Geophysical Research Letters, v. 31, no. 24. Artn L24402

Doi 10.1029/2004gl021533

Lal, D., 1988, *In situ* Produced Cosmogenic Isotopes in Terrestrial Rocks: Annual Review of Earth and Planetary Sciences, v. 16, p. 355-388.

-, 1991, Cosmic-Ray Labeling of Erosion Surfaces: *in situ* nuclide production rates and eosion models: Earth and Planetary Science Letters, v. 104, no. 2-4, p. 424-439. Doi 10.1016/0012-821x(91)90220-C

Lal, D., and Peters, B., 1967, Cosmic Ray Produced Radioactivity on the Earth: Handbuch der Physik, v. Band XLV1/2, p. 551-612.

Larsen, H. C., Saunders, A. D., Clift, P. D., Beget, J., Wei, W., Spezzaferri, S., Ali, J., Cambray, H., Demant, A., Fitton, G., Fram, M. S., Fukuma, K., Gieskes, J., Holmes, M. A., Hunt, J., Lacasse, C., Larsen, L. M., Lykkeanderson, H., Meltser, A., Morrison, M. L., Nemoto, N., Okay, N., Saito, S., Sinton, C., Stax, R., Vallier, T. L., Vandamme, D., Werner, R., and Cliff, P. D., 1994, 7-Million Years of Glaciation in Greenland: Science, v. 264, no. 5161, p. 952-955.

Levy, L. B., Kelly, M. A., Howley, J. A., and Virginia, R. A., 2012, Age of the Orkendalen moraines, Kangerlussuaq, Greenland: constraints on the extent of the southwestern margin of the Greenland Ice Sheet during the Holocene: Quaternary Science Reviews, v. 52, p. 1-5. Doi 10.1016/J.Quascirev.2012.07.021

Lisiecki, L. E., and Raymo, M. E., 2005, A Pliocene-Pleistocene stack of 57 globally distributed benthic delta ^{18}O records: Paleoceanography, v. 20, no. 2. Artn Pa2007 Doi 10.1029/2005pa001164

-, 2007, Plio-Pleistocene climate evolution: trends and transitions in glacial cycle dynamics: Quaternary Science Reviews, v. 26, no. 1-2, p. 56-69. Doi 10.1016/J.Quascirev.2006.09.005

Loutre, M. F., 2003, Clues from MIS 11 to predict the future climate - a modelling point of view: Earth and Planetary Science Letters, v. 212, no. 1-2, p. 213-224. Doi 10.1016/S0012-821x(03)00235-8

Lunt, D. J., Foster, G. L., Haywood, A. M., and Stone, E. J., 2008, Late Pliocene Greenland glaciation controlled by a decline in atmospheric CO_2 levels: Nature, v. 454, no. 7208, p. 1102-U1141. Doi 10.1038/Nature07223

Lunt, D. J., Haywood, A. M., Schmidt, G. A., Salzmann, U., Valdes, P. J., and Dowsett, H. J., 2010, Earth system sensitivity inferred from Pliocene modelling and data: Nature Geoscience, v. 3, no. 1, p. 60-64. Doi 10.1038/Ngeo706

Mernild, S. H., Hansen, B. U., Jakobsen, B. H., and Hasholt, B., 2008, Climate conditions at the Mittivakkat Glacier catchment (1994-2006), Ammassalik Island, SE Greenland, and in a 109-year perspective (1898–2006): Geografisk Tidsskrift-Danish Journal of Geography, v. 108, no. 1, p. 51–72.

Montgomery, D. R., 2002, Valley formation by fluvial and glacial erosion: Geology, v. 30, no. 11, p. 1047-1050. Doi 10.1130/0091-7613(2002)030<1047:Vfbfag>2.0.Co;2

Moran, K., Backman, J., Brinkhuis, H., Clemens, S. C., Cronin, T., Dickens, G. R., Eynaud, F., Gattacceca, J., Jakobsson, M., Jordan, R. W., Kaminski, M., King, J., Koc, N., Krylov, A., Martinez, N., Matthiessen, J., McInroy, D., Moore, T. C., Onodera, J., O'Regan, M., Palike, H., Rea, B., Rio, D., Sakamoto, T., Smith, D. C., Stein, R., St John, K., Suto, I., Suzuki, N., Takahashi, K., Watanabe, M., Yamamoto, M., Farrell, J., Frank, M., Kubik, P., Jokat, W., and Kristoffersen, Y., 2006, The Cenozoic palaeoenvironment of the Arctic Ocean: Nature, v. 441, no. 7093, p. 601-605. Doi 10.1038/Nature04800

Muhs, D. R., 2002, Evidence for the timing and duration of the last interglacial period from high-precision uranium-series ages of corals on tectonically stable

coastlines: Quaternary Research, v. 58, no. 1, p. 36-40. Doi 10.1006/Qres.2002.2339
Nishiizumi, K., Finkel, R., Ponganis, K., Graf, T., Kohl, C., and Marti, K., 1996, *In situ* produced cosmogenic nuclides in GISP2 rock core from Greenland summit: EOS, v. 77, p. OS41B-10.
Nishiizumi, K., Imamura, M., Caffee, M. W., Southon, J. R., Finkel, R. C., and McAninch, J., 2007, Absolute calibration of Be-10 AMS standards: Nuclear Instruments & Methods in Physics Research Section B-Beam Interactions with Materials and Atoms, v. 258, no. 2, p. 403-413. Doi 10.1016/J.Nimb.2007.01.297
O'Cofaigh, C., Dowdeswell, J. A., and Grobe, H., 2001, Holocene glacimarine sedimentation, inner Scoresby Sund, East Greenland: the influence of fast-flowing ice-sheet outlet glaciers: Marine Geology, v. 175, no. 1-4, p. 103-129.
Otto-Bliesner, B. L., Marsha, S. J., Overpeck, J. T., Miller, G. H., Hu, A. X., and Mem, C. L. I. P., 2006, Simulating arctic climate warmth and icefield retreat in the last interglaciation: Science, v. 311, no. 5768, p. 1751-1753. Doi 10.1126/Science.1120808
Ovenshine, A. T., 1970, Observations of Iceberg Rafting in Glacier Bay, Alaska, and the Identification of Ancient Ice-Rafted Deposits: Geologic Society of America Bulletin, v. 81, no. 3, p. 891-894.
Pfeffer, W. T., Harper, J. T., and O'Neel, S., 2008, Kinematic constraints on glacier contributions to 21st-century sea-level rise: Science, v. 321, no. 5894, p. 1340-1343. Doi 10.1126/Science.1159099
Phillips, F. M., Zreda, M. G., Smith, S. S., Elmore, D., Kubik, P. W., and Sharma, P., 1990, Cosmogenic Chlorine-36 Chronology for Glacial Deposits at Bloody Canyon, Eastern Sierra-Nevada: Science, v. 248, no. 4962, p. 1529-1532. Doi 10.1126/Science.248.4962.1529
Poore, R. Z., and Dowsett, H. J., 2001, Pleistocene reduction of polar ice caps: Evidence from Cariaco Basin marine sediments: Geology, v. 29, no. 1, p. 71-74.
Prior, D. B., Wiseman, W. J., and Bryant, W. R., 1981, Submarine Chutes on the Slopes of Fjord Deltas: Nature, v. 290, no. 5804, p. 326-328. Doi 10.1038/290326a0
Raymo, M. E., Lisiecki, L. E., and Nisancioglu, K. H., 2006, Plio-pleistocene ice volume, Antarctic climate, and the global delta ^{18}O record: Science, v. 313, no. 5786, p. 492-495. Doi 10.1126/Science.1123296
Raymo, M. E., Mitrovica, J. X., O'Leary, M. J., DeConto, R. M., and Hearty, P. L., 2011, Departures from eustasy in Pliocene sea-level records: Nature Geoscience, v. 4, no. 5, p. 328-332. Doi 10.1038/Ngeo1118
Reusser, L. J., and Bierman, P. R., 2010, Using meteoric ^{10}Be to track fluvial sand through the Waipaoa River basin, New Zealand: Geology, v. 38, no. 1, p. 47-50. Doi 10.1130/G30395.1
Rinterknecht, V., Gorokhovich, Y., Schaefer, J., and Caffee, M., 2009, Preliminary ^{10}Be chronology for the last deglaciation of the western margin of the Greenland Ice Sheet: Journal of Quaternary Science, v. 24, no. 3, p. 270-278. Doi 10.1002/Jqs.1226
Roberts, D. H., Long, A. J., Schnabel, C., Davies, B. J., Xu, S., Simpson, M. J. R., and Huybrechts, P., 2009, Ice sheet extent and early deglacial history of the

southwestern sector of the Greenland Ice Sheet: Quaternary Science Reviews, v. 28, no. 25-26, p. 2760-2773. Doi 10.1016/J.Quascirev.2009.07.002
Roberts, D. H., Long, A. J., Schnabel, C., Freeman, S., and Simpson, M. J. R., 2008, The deglacial history of southeast sector of the Greenland Ice Sheet during the Last Glacial Maximum: Quaternary Science Reviews, v. 27, no. 15-16, p. 1505-1516. Doi 10.1016/J.Quascirev.2008.04.008
Roberts, D. L., Karkanas, P., Jacobs, Z., Marean, C., and Roberts, R., 2012, Melting ice sheets 400,000 yr ago raised sea level by 13 m: Past analogue for future trentds: Earth and Planetary Science Letters, v. 357-358, p. 226-237. http://dx.doi.org/10.1016/j.epsl.2012.09.006
Rose, J., 1991, Subaerial modification of glacier bedforms immediately following ice wastage: Norsk Geologisk Tidsskrift, v. 45, no. 3, p. 143-153.
Ruddiman, W. F., 1977, Late Quaternary Deposition of Ice-Rafted Sand in Subpolar North-Atlantic (lat 40˚ to 65˚N): Geological Society of America Bulletin, v. 88, no. 12, p. 1813-1827. Doi 10.1130/0016-7606(1977)88<1813:Lqdois>2.0.Co;2
Salzmann, U., Williams, M., Haywood, A. M., Johnson, A. L. A., Kender, S., and Zalasiewicz, J., 2011, Climate and environment of a Pliocene warm world: Palaeogeography Palaeoclimatology Palaeoecology, v. 309, no. 1-2, p. 1-8. Doi 10.1016/J.Palaeo.2011.05.044
Serreze, M. C., Walsh, J. E., Chapin, F. S., Osterkamp, T., Dyurgerov, M., Romanovsky, V., Oechel, W. C., Morison, J., Zhang, T., and Barry, R. G., 2000, Observational evidence of recent change in the northern high-latitude environment: Climatic Change, v. 46, no. 1-2, p. 159-207. Doi 10.1023/A:1005504031923
Shackleton, N. J., Backman, J., Zimmerman, H., Kent, D. V., Hall, M. A., Roberts, D. G., Schnitker, D., Baldauf, J. G., Desprairies, A., Homrighausen, R., Huddlestun, P., Keene, J. B., Kaltenback, A. J., Krumsiek, K. A. O., Morton, A. C., Murray, J. W., and Westbergsmith, J., 1984, Oxygen Isotope Calibration of the Onset of Ice-Rafting and History of Glaciation in the North-Atlantic Region: Nature, v. 307, no. 5952, p. 620-623.
Smith, L. M., and Andrews, J. T., 2000, Sediment characteristics in iceberg dominated fjords, Kangerlussuaq region, East Greenland: Sedimentary Geology, v. 130, no. 1-2, p. 11-25.
Sparrenbom, C. J., Bennike, O., Bjorck, S., and Lambeck, K., 2006, Holocene relative sea-level changes in the Qaqortoq area, southern Greenland: Boreas, v. 35, no. 2, p. 171-187. Doi 10.1080/03009480600578032
St John, K. E. K., and Krissek, L. A., 2002, The late Miocene to Pleistocene ice-rafting history of southeast Greenland: Boreas, v. 31, no. 1, p. 28-35.
Steig, E. J., and Wolfe, A. P., 2008, Sprucing up Greenland: Science, v. 320, no. 5883, p. 1595-1596. Doi 10.1126/Science.1160004
Stone, J. O., 2000, Air pressure and cosmogenic isotope production: Journal of Geophysical Research-Solid Earth, v. 105, no. B10, p. 23753-23759.
Storms, J. E. A., de Winter, I. L., Overeem, I., Drijkoningen, G. G., and Lykke-Andersen, H., 2012, The Holocene sedimentary history of the Kangerlussuaq Fjord-valley fill, West Greenland: Quaternary Science Reviews, v. 35, p. 29-50. Doi 10.1016/J.Quascirev.2011.12.014

Stott, T. A., and Grove, J. R., 2001, Short-term discharge and suspended sediment fluctuations in the proglacial Skeldal River, north-east Greenland: Hydrological Processes, v. 15, no. 3, p. 407-423. Doi 10.1002/Hyp.156
Sugden, D. E., 1977, Reconstructions of morphology, dynamics, and thermal characteristics of the Laurentide Ice Sheet at its maximum: Arctic and Alpine Research, v. 9, no. 1, p. 21–47.
-, 1978, Glacial erosion by the Laurentide Ice Sheet: Journal of Glaciology, v. 20, no. 83, p. 367–390.
Syvitski, J. P. M., and Shaw, J., 1995, Sedimentology and Geomorphology of Fjords, *in* Perillo, G. M. E., ed., Geomorphology and Sedimentology of Estuaries. Developments in Sedimentology, Volume 53: Amsterdam, Elsevier Science, p. 113-178.
Tedesco, M., Fettweis, X., Mote, T., Wahr, J., Alexander, P., Box, J., and Wouters, B., 2012, Evidence and analysis of 2012 Greenland records from spaceborne observations, a regional climate model and reanalysis data: The Cryosphere Discussions, v. 6, p. 4939-4976.
Ten Brink, N. W., 1975, Holocene history of the Greenland Ice Sheet based on radiocarbon-dated moraines in West Greenland: Meddelelser om Grønland, v. 201, no. 4, p. 1-44.
Ten Brink, N. W., and Weidick, A., 1974, Greenland ice sheet history since the last glaciation: Quaternary Research, v. 4, no. 4, p. 429-440.
Thomas, R. H., and Investigators, P., 2001, Program for arctic regional climate assessment (PARCA): Goals, key findings, and future directions: Journal of Geophysical Research-Atmospheres, v. 106, no. D24, p. 33691-33705.
van den Broeke, M., Bamber, J., Ettema, J., Rignot, E., Schrama, E., van de Berg, W. J., van Meijgaard, E., Velicogna, I., and Wouters, B., 2009, Partitioning Recent Greenland Mass Loss: Science, v. 326, no. 5955, p. 984-986. Doi 10.1126/Science.1178176
van Tatenhove, F. G. M., van der Meer, J. J. M., and Koster, E. A., 1996, Implications for deglaciation chronology from new AMS age determinations in central west Greenland: Quaternary Research, v. 45, no. 3, p. 245-253. Doi 10.1006/Qres.1996.0025
Warburton, J., 1990, An Alpine Proglacial Fluvial Sediment Budget: Geografiska Annaler Series A-Physical Geography, v. 72, no. 3-4, p. 261-272. Doi 10.2307/521154
Weertman, J., 1961, Mechanisms for the formation of inner moraines found near the edge of cold ice caps and ice sheets: Journal of Glaciology, v. 3, no. 30, p. 965-978.
Weidick, A., 1968, Observations on Some Holocene Glacier Fluctuations in West Greenland: Meddelelser om Grønland, v. 165, no. 6, p. 6-212.
Weidick, A., Kelly, M., and Bennike, O., 2004, Late Quaternary development of the southern sector of the Greenland Ice Sheet, with particular reference to the Qassimiut lobe: Boreas, v. 33, no. 4, p. 284-299. Doi 10.1080/03009480410001947
Weidick, A., Oerter, H., Reeh, N., Thomsen, H. H., and Thorning, L., 1990, The Recession of the Inland Ice Margin during the Holocene Climatic Optimum in the

Jakobshavn-Isfjord Area of West Greenland: Global and Planetary Change, v. 82, no. 3-4, p. 389-399.
Willemse, N. W., Koster, E. A., Hoogakker, B., and van Tatenhove, F. G. M., 2003, A continuous record of Holocene eolian activity in West Greenland: Quaternary Research, v. 59, no. 3, p. 322-334. Doi 10.1016/S0033-5894(03)00037-1
Young, N. E., Briner, J. P., Stewart, H. A. M., Axford, Y., Csatho, B., Rood, D. H., and Finkel, R. C., 2011, Response of Jakobshavn Isbrae Greenland, to Holocene climate change: Geology, v. 39, no. 2, p. 131-134. Doi 10.1130/G31399.1

APPENDIX I

Table of previously published ^{10}Be data from Greenland

Date	Author	Sample Name	Sample Type	Lat.(°N)	Long. (°E)	Elevation (m asl)	^{10}Be Concentration (atoms/g)	Uncertainty (atoms/g)
2007	Hakansson et al	G.-004	boulder	76.085	-18.642	93	70000	5000
2007	Hakansson et al	G.-001	boulder	76.112	-18.575	630	105000	7000
2007	Hakansson et al	G.-005	boulder	76.176	-18.677	617	128000	8000
2007	Hakansson et al	G.-008	boulder	76.389	-18.856	568	674000	24000
2007	Hakansson et al	G.-011	boulder	76.260	-18.748	652	258000	13000
2007	Hakansson et al	G.-007	bedrock	76.384	-18.952	686	405000	20000
2007	Hakansson et al	G.-010	bedrock	76.254	-18.752	704	1350000	41000
2007	Hakansson et al	KB-1	boulder	70.151	-23.075	230	106000	17000
2007	Hakansson et al	KB-2	boulder	70.151	-23.076	230	99000	13000
2007	Hakansson et al	KB-3	boulder	70.151	-23.078	251	85000	10000
2007	Hakansson et al	KB-4	boulder	70.151	-23.081	239	51000	8000
2008	Kelly et al	MKG-93	boulder	71.510	-24.945	790	8190	408
2008	Kelly et al	MKG-94c	boulder	71.510	-24.944	780	4190	732
2008	Kelly et al	MKG-95c	boulder	71.510	-24.943	780	7050	479
2008	Kelly et al	MKG-97	boulder	71.511	-24.943	778	3180	231
2008	Kelly et al	MKG-32b	boulder	71.554	-24.904	709	103000	2600
2008	Kelly et al	MKG-33	boulder	71.553	-24.905	684	115000	2650
2008	Kelly et al	MKG-35b	boulder	71.540	-24.889	610	118000	2530
2008	Kelly et al	MKG-36	boulder	71.543	-24.887	626	10200	3410
2008	Kelly et al	MKG-89	boulder	71.482	-24.814	375	76800	2230
2008	Kelly et al	MKG-90	boulder	71.481	-24.811	365	94600	2370
2008	Kelly et al	MKG-91	boulder	71.480	-24.808	348	117000	2840
2008	Kelly et al	MKG-92	boulder	71.478	-24.806	330	76100	2050
2008	Kelly et al	MKG-98	boulder	71.512	-24.811	500	94100	3140
2008	Kelly et al	MKG-99	boulder	71.515	-24.821	515	351000	6080
2008	Kelly et al	MKG-100c	boulder	71.513	-24.936	720	108000	4770

2008	Kelly et al	MKG-101	boulder	71.513	-24.936	720	100000	4100
2008	Kelly et al	MKG-102	boulder	71.512	-24.938	740	118000	2830
2008	Kelly et al	MKG-103	boulder	71.511	-24.939	750	107000	2640
2008	Kelly et al	MKG-104c	boulder	71.511	-24.907	603	890000	2180
2008	Kelly et al	MKG-11	boulder	71.423	-24.770	345	85100	2890
2008	Kelly et al	MKG-12	boulder	71.419	-24.773	360	235000	5420
2008	Kelly et al	MKG-13	boulder	71.403	-24.715	129	94100	2810
2008	Kelly et al	MKG-14	boulder	71.421	-24.710	134	101000	2340
2008	Kelly et al	MKG-15	boulder	71.408	-24.707	134	61800	1440
2008	Kelly et al	MKG-20b	boulder	71.431	-24.673	215	75500	1940
2008	Kelly et al	MKG-21	boulder	71.432	-24.670	230	133000	5550
2008	Kelly et al	MKG-22	boulder	71.444	-24.667	317	87100	2020
2008	Kelly et al	MKG-24	boulder	71.443	-24.684	372	138000	4730
2008	Kelly et al	MKG-25	boulder	71.450	-24.684	385	388000	9140
2008	Kelly et al	MKG-26b	boulder	71.450	-24.684	385	158000	3030
2008	Kelly et al	MKG-30	boulder	71.418	-24.678	124	79100	1840
2008	Kelly et al	MKG-07	boulder	71.418	-24.767	360	170000	3910
2008	Kelly et al	MKG-08	boulder	71.418	-24.768	360	251000	5910
2008	Kelly et al	MKG-09	boulder	71.438	-24.776	380	168000	5640
2008	Kelly et al	MKG-16	boulder	71.458	-24.681	478	639000	1370
2008	Kelly et al	MKG-19b	boulder	71.442	-24.651	333	279000	4660
2008	Kelly et al	MKG-27	boulder	71.445	-24.671	375	172000	6300
2008	Kelly et al	MKG-28	boulder	71.442	-24.664	338	235000	5390
2008	Roberts et al	TI1	bedrock	65.746	-38.148	683	99050	5390
2008	Roberts et al	TI2	bedrock	65.749	-38.180	740	120300	6360
2008	Roberts et al	TI3	bedrock	65.749	-38.273	709	119700	6140
2008	Roberts et al	TI5	bedrock	65.757	-38.273	122	61730	4230
2008	Roberts et al	TI7	bedrock	65.756	-38.320	126	76120	6980
2008	Roberts et al	TI9	bedrock	65.755	-38.321	103	71080	4520
2008	Roberts et al	TI11	bedrock	65.701	-38.222	344	71370	5090
2008	Roberts et al	TI14	bedrock	65.696	-38.293	436	88350	6180
2008	Roberts et al	TI15	bedrock	65.705	-38.293	481	87390	5190

2008	Roberts et al	TI17	bedrock	65.703	-38.287	78	60660	4200
2008	Roberts et al	TI19	bedrock	65.725	-38.157	244	64750	3010
2008	Roberts et al	TI20	bedrock	65.725	-38.162	96	56340	2640
2009	Goehring et al	MKG-04	boulder	71.395	-24.900	94	51300	1500
2009	Goehring et al	MKG-05	boulder	71.393	-24.901	92	63700	2200
2009	Goehring et al	MKG-06	boulder	71.385	-24.902	89	51800	2000
2009	Goehring et al	MKG-169	boulder	70.564	-26.038	139	64000	2100
2009	Goehring et al	MKG-170	boulder	70.564	-26.038	139	51400	1100
2009	Goehring et al	MKG-172	boulder	70.562	-26.044	160	51700	1400
2009	Goehring et al	MKG-173	boulder	70.561	-26.047	148	61000	1700
2009	Goehring et al	MKG-140	boulder	70.568	-26.035	181	52600	1500
2009	Goehring et al	MKG-141	boulder	70.567	-26.035	181	52700	1500
2009	Goehring et al	MKG-144	boulder	70.564	-26.038	139	55200	1700
2009	Goehring et al	MKG-145	boulder	70.564	-26.038	139	54100	1400
2009	Goehring et al	MKG-148	boulder	70.562	-26.044	160	53700	1300
2009	Goehring et al	MKG-151	boulder	70.561	-26.047	148	52700	1300
2009	Goehring et al	IC0610	sand/gravel	71.389	-24.892		52800	2800
2009	Goehring et al	IC06125	sand/gravel	71.389	-24.892		44200	1500
2009	Goehring et al	IC06150	sand/gravel	71.389	-24.892		39500	1300
2009	Goehring et al	IC061100	sand/gravel	71.389	-24.892		23100	600
2009	Goehring et al	IC061150	sand/gravel	71.389	-24.892		15100	700
2009	Goehring et al	IC0620	sand/gravel	71.390	-24.890		48900	2100
2009	Goehring et al	IC06225	sand/gravel	71.390	-24.890		42600	1300
2009	Goehring et al	IC06250	sand/gravel	71.390	-24.890		27600	1600
2009	Goehring et al	IC062100	sand/gravel	71.390	-24.890		24300	1000
2009	Goehring et al	IC062150	sand/gravel	71.390	-24.890		16300	700
2009	Goehring et al	IC0630	sand/gravel	71.389	-24.886		57600	2900
2009	Goehring et al	IC06325	sand/gravel	71.389	-24.886		43900	2600
2009	Goehring et al	IC06350	sand/gravel	71.389	-24.886		35200	1100
2009	Goehring et al	IC063100	sand/gravel	71.389	-24.886		23700	900
2009	Goehring et al	IC063150	sand/gravel	71.389	-24.886		15200	600
2009	Goehring et al	MT0610	sand/gravel	70.562	-26.114		47000	2000

2009	Goehring et al	MT06125	sand/gravel	70.562	-26.114		50400	1300
2009	Goehring et al	MT06150	sand/gravel	70.562	-26.114		33900	1200
2009	Goehring et al	MT061100	sand/gravel	70.562	-26.114		25400	700
2009	Goehring et al	MT061155	sand/gravel	70.562	-26.114		20700	500
2009	Goehring et al	MT0620	sand/gravel	70.562	-26.037		50000	1800
2009	Goehring et al	MT0625	sand/gravel	70.562	-26.037		38900	1500
2009	Goehring et al	MT06250	sand/gravel	70.562	-26.037		28800	1200
2009	Goehring et al	MT062100	sand/gravel	70.562	-26.037		23600	1000
2009	Goehring et al	MT062150	sand/gravel	70.562	-26.037		16800	700
2009	Roberts et al	NAG01	bedrock	66.463	-53.432	856	1408000	36550
2009	Roberts et al	NAG02	bedrock	66.463	-53.431	841	1658000	46210
2009	Roberts et al	NAG03	bedrock	66.464	-53.440	755	604700	21170
2009	Roberts et al	NAG04	bedrock	66.463	-53.435	813	1160000	32300
2009	Roberts et al	NAG05	bedrock	66.464	-53.442	734	317900	11180
2009	Roberts et al	NAG06	bedrock	66.463	-53.444	574	194700	6995
2009	Roberts et al	NAG07	bedrock	66.464	-53.454	498	174700	6303
2009	Roberts et al	NAG08	bedrock	66.456	-53.431	449	220900	6414
2009	Roberts et al	NAG09	bedrock	66.453	-53.435	359	138700	5040
2009	Roberts et al	NAG10	bedrock	66.450	-53.444	230	106600	3360
2009	Roberts et al	NAG11	bedrock	66.464	-53.489	431	217000	5857
2009	Roberts et al	NAG12	bedrock	66.464	-53.489	409	144600	4290
2009	Roberts et al	NAG14	bedrock	66.463	-53.503	309	106900	3457
2009	Roberts et al	NAG15	bedrock	66.459	-53.509	150	82480	4721
2009	Roberts et al	NAG16	bedrock	66.454	-53.547	339	73000	2720
2009	Roberts et al	NAG17	bedrock	66.455	-53.531	243	69030	2752
2009	Rinterknecht et al	GRE-1	boulder	66.988	-53.736	385	13500	3600
2009	Rinterknecht et al	GRE-2	boulder	67.162	-53.008	721	18400	3400
2009	Rinterknecht et al	GRE-3	bedrock	67.162	-53.008	721	29100	1300
2009	Rinterknecht et al	GRE-4	bedrock	67.238	-52.174	1118	140800	5300
2009	Rinterknecht et al	GRE-5	boulder	67.323	-51.369	687	8300	3300

2009	Rinterknecht et al	GRE-6	boulder	67.437	-50.171	576	6300	1100
2009	Rinterknecht et al	GRE-7	boulder	67.426	-50.152	682	11900	1500
2009	Rinterknecht et al	GRE-8	boulder	67.426	-50.152	682	11400	1400
2009	Rinterknecht et al	GRE-9	boulder	67.424	-50.205	539	7900	500
2009	Rinterknecht et al	GRE-10	boulder	67.425	-50.201	442	6000	1300
2009	Rinterknecht et al	GRE-11	boulder	67.429	-50.211	439	6400	900
2009	Rinterknecht et al	GRE-12	boulder	67.429	-50.213	437	6700	500
2010	Corbett	GU091	bedrock	72.782	-56.586	24	69800	
2010	Corbett	GU092	boulder	72.782	-56.586	21	61900	
2010	Corbett	GU093	bedrock	72.740	-56.385	91	72900	
2010	Corbett	GU094	boulder	72.740	-56.386	90	51700	
2010	Corbett	GU095	bedrock	72.744	-56.382	20	66300	
2010	Corbett	GU096	bedrock	72.754	-55.873	778	909000	
2010	Corbett	GU097	boulder	72.754	-55.872	774	177000	
2010	Corbett	GU098	bedrock	72.793	-55.932	372	83800	
2010	Corbett	GU099	boulder	72.793	-55.933	366	71100	
2010	Corbett	GU100	bedrock	72.812	-55.826	74	101000	
2010	Corbett	GU101	boulder	72.812	-55.826	71	50300	
2010	Corbett	GU102	boulder	72.718	-55.473	980	490000	
2010	Corbett	GU103	bedrock	72.718	-55.473	998	907000	
2010	Corbett	GU106	bedrock	72.741	-55.552	498	228000	
2010	Corbett	GU107	boulder	72.741	-55.551	500	97900	
2010	Corbett	Gu104	boulder	72.773	-55.503	253	60300	
2010	Corbett	GU105	bedrock	72.774	-55.504	270	23500	
2010	Corbett	GU108	bedrock	72.781	-55.443	33	85500	
2010	Corbett	GU109	boulder	72.780	-55.442	27	69800	
2010	Corbett	GU110	bedrock	72.661	-55.122	745	567000	
2010	Corbett	GU111	bedrock	72.682	-55.025	325	426000	
2010	Corbett	GU112	boulder	72.682	-55.025	325	121000	

2010	Corbett	GU113	bedrock	72.660	-54.983	90	237000	
2010	Corbett	GU114	boulder	72.660	-54.983	91	55800	
2010	Corbett	GU001	bedrock	72.536	-53.733	603	103000	
2010	Corbett	GU002	boulder	72.536	-53.733	603	80600	
2010	Corbett	GU006	bedrock	72.539	-53.732	539	118000	
2010	Corbett	GU017	boulder	72.539	-53.732	539	93200	
2010	Corbett	GU041	bedrock	72.615	-53.589	898	783000	
2010	Corbett	GU042	bedrock	72.615	-53.592	895	502000	
2010	Corbett	GU043	bedrock	72.616	-53.596	857	495000	
2010	Corbett	GU044	bedrock	72.617	-53.596	808	579000	
2010	Corbett	GU045	bedrock	72.619	-53.597	776	382000	
2011	Young et al	JAKN08-01	bedrock	69.206	-51.124	112	47576	1168
2011	Young et al	JAKN08-08	bedrock	69.199	-50.967	338	61424	1727
2011	Young et al	JAKN08-21	bedrock	69.243	-50.981	390	63882	3383
2011	Young et al	JAKN08-22	boulder	69.241	-50.961	360	59645	1868
2011	Young et al	09GRO-01	bedrock	69.110	-51.041	204	50246	1254
2011	Young et al	JAKN08-13	bedrock	69.184	-50.906	180	41082	1043
2011	Young et al	FST08-BR	bedrock	69.197	-51.054	65	53768	1337
2011	Young et al	FST08-04	boulder	69.147	-51.054	65	36284	941
2011	Young et al	09GRO-03	bedrock	69.114	-51.064	124	38919	1139
2011	Young et al	09GRO-06	boulder	69.116	-50.991	245	41475	1323
2011	Young et al	09GRO-33	boulder	69.191	-51.007	125	37484	1169
2011	Young et al	JAKN08-28	bedrock	69.241	-49.985	215	39588	1902
2011	Young et al	JAKN08-39	bedrock	69.221	-49.995	206	38695	1262
2011	Young et al	JAKN08-40	bedrock	69.226	-50.057	147	38905	997
2011	Young et al	JAKN08-44	bedrock	69.308	-50.148	347	44534	1676
2011	Young et al	JAKN08-56	bedrock	69.301	-50.329	425	49360	1214

2011	Young et al	JAKS08-33	bedrock	69.147	-50.125	222	40673	1727
2011	Young et al	JAKS08-34	bedrock	69.147	-50.104	180	38013	975
2011	Corbett et al	GL022	bedrock	69.432	-50.289	515	55400	
2011	Corbett et al	GL023	boulder	69.433	-50.289	511	53500	
2011	Corbett et al	GL001	bedrock	69.433	-50.272	434	46200	
2011	Corbett et al	GL002	boulder	69.433	-50.273	432	48600	
2011	Corbett et al	GL003	bedrock	69.434	-50.266	395	47300	
2011	Corbett et al	GL004	boulder	69.434	-50.266	392	49900	
2011	Corbett et al	GL080	bedrock	69.395	-50.416	621	61800	
2011	Corbett et al	GL081	boulder	69.395	-50.416	618	60100	
2011	Corbett et al	GL086	bedrock	69.374	-50.458	304	42800	
2011	Corbett et al	GL087	boulder	69.374	-50.458	303	44500	
2011	Corbett et al	GL088	bedrock	69.344	-50.429	95	34900	
2011	Corbett et al	GL089	boulder	69.344	-50.429	93	36100	
2011	Corbett et al	GL103	bedrock	69.318	-50.640	578	68900	
2011	Corbett et al	GL104	boulder	69.318	-50.640	578	62600	
2011	Corbett et al	GL105	bedrock	69.293	-50.602	300	46500	
2011	Corbett et al	GL106	boulder	69.293	-50.602	300	45800	
2011	Corbett et al	GL090	bedrock	69.269	-50.581	93	40200	
2011	Corbett et al	GL091	boulder	69.269	-50.582	91	36100	
2011	Corbett et al	GL096	bedrock	69.250	-50.823	468	72700	
2011	Corbett et al	GL097	boulder	69.251	-50.822	470	66200	
2011	Corbett et al	GL094	boulder	69.229	-50.810	308	54900	
2011	Corbett et al	GL095	bedrock	69.229	-50.810	308	46100	
2011	Corbett et al	GL098	bedrock	69.199	-50.791	163	49700	
2011	Corbett et al	GL092	boulder	69.230	-50.902	397	65900	
2011	Corbett et al	GL093	bedrock	69.230	-50.902	397	66900	
2011	Corbett et al	GL100	boulder	69.227	-50.930	292	59500	
2011	Corbett et al	GL101	bedrock	69.227	-50.929	295	56200	
2011	Corbett et al	GL107	bedrock	69.180	-50.891	53	36600	
2011	Corbett et al	GL108	boulder	69.180	-50.891	53	37300	
2011	Corbett et al	GL102	bedrock	69.207	-51.134	85	47900	

2011	Hakansson et al	06-FE-5	bedrock	70.635	-23.136	495	313000	15000
2011	Hakansson et al	06-FE-56	bedrock	70.639	-23.129	462	429000	16000
2011	Hakansson et al	06-FE-65	bedrock	70.645	-23.109	456	297000	12000
2011	Hakansson et al	06-FE-67	bedrock	70.666	-23.119	490	249000	25000
2011	Hakansson et al	06-FE-55	bedrock	70.634	-23.132	443	263000	18000
2011	Hakansson et al	06-FE-48	bedrock	70.639	-23.136	470	187000	15000
2011	Hakansson et al	06-FE-46	bedrock	70.639	-23.135	524	306000	31000
2011	Hakansson et al	06-FE-50	bedrock	70.639	-23.136	470	228000	23000
2011	Hakansson et al	06-FE-57	bedrock	70.637	-23.133	449	173000	17000
2011	Hakansson et al	06-FE-53	bedrock	70.633	-23.134	430	167000	17000
2011	Hakansson et al	06-FE-51	bedrock	70.636	-23.134	444	147000	15000
2011	Hakansson et al	06-FE-19	bedrock	70.640	-23.212	377	113000	11000
2011	Hakansson et al	06-FE-25	bedrock	70.643	-23.098	500	136000	14000
2011	Hakansson et al	06-FE-24	bedrock	70.653	-23.098	510	152000	15000
2011	Hughes et al	SF-09-01	bedrock	65.634	-37.948	37	55140	1250
2011	Hughes et al	SF-09-62	boulder	65.857	-38.006	112	48620	1680
2011	Hughes et al	SF-09-63	boulder	65.857	-38.006	110	49830	2560
2011	Hughes et al	SF-09-64	bedrock	65.857	-38.006	116	55960	2610
2011	Hughes et al	SF-09-53	bedrock	66.060	-37.705	110	52130	1450
2011	Hughes et al	SF-09-54	boulder	66.060	-37.705	111	48220	1700
2011	Hughes et al	SF-09-55	boulder	66.060	-37.705	110	50180	1840
2011	Hughes et al	SF-09-29	boulder	66.226	-37.593	76	48220	1320
2011	Hughes et al	SF-09-30	bedrock	66.226	-37.593	77	49610	1520
2011	Hughes et al	SF-10-01	bedrock	66.319	-37.554	191	60560	1550
2011	Hughes et al	SF-09-03	bedrock	66.280	-37.726	40	52660	2180
2011	Hughes et al	SF-09-04	boulder	66.280	-37.726	47	43030	1090
2012	Levy et al	LL0901	boulder	67.105	-50.290	247	34700	817
2012	Levy et al	LL0902	boulder	67.103	-50.282	241	37700	1080
2012	Levy et al	LL0903	boulder	67.101	-50.283	242	37800	1120
2012	Levy et al	LL0904	boulder	67.092	-50.294	224	36500	974
2012	Levy et al	LL0906	boulder	67.159	-50.102	432	44200	973
2012	Levy et al	LL0907	boulder	67.158	-50.104	434	45600	1190

2012	Levy et al	LL0908	boulder	67.158	-50.105	423	47200	1450
2012	Levy et al	LL0909	boulder	67.161	-50.119	449	43200	1350
2012	Levy et al	LL0911	boulder	67.162	-50.116	458	43600	1130

APPENDIX II

Table of *in situ* ^{10}Be concentration data for sediment and relevant field and sample processing information

Sample ID	Latitude (°N)	Longitude (°E)	Elevation (m asl)	Source Category	Quartz (g)	^{9}Be (µg)	^{10}Be/^{9}Be Ratio	^{10}Be/^{9}Be Uncertainty	^{10}Be Conc. (x 10^{3} a g^{-1})	Uncertaint (x 10^{3} a g^{-1}
Kangerlussuaq										
GLX-01	67.019	-50.627	25	Mixed	28.53	253	3.243×10^{-15}	8.196×10^{-16}	1.9	0.5
GLX-01R	67.019	-50.627	25	Mixed	34.60	252	1.093×10^{-14}	1.528×10^{-15}	5.3	0.7
GLX-02	67.039	-50.484	72	Mixed	33.57	257	4.973×10^{-15}	7.834×10^{-16}	2.5	0.4
GLX-02R	67.039	-50.484	72	Mixed	39.12	252	1.500×10^{-14}	2.215×10^{-15}	6.5	1.0
GLX-03	67.065	-50.365	127	Mixed	34.16	253	3.563×10^{-15}	7.855×10^{-16}	1.8	0.4
GLX-03R	67.065	-50.365	127	Mixed	20.30	247	3.952×10^{-15}	1.275×10^{-15}	3.2	1.0
GLX-04	67.073	-50.062	132	Mixed	32.46	255	3.997×10^{-14}	1.367×10^{-15}	2.1	0.7
GLX-04R	67.073	-50.062	132	Mixed	33.77	254	8.054×10^{-15}	1.172×10^{-15}	4.0	0.6
GLX-05	67.079	-50.273	134	Mixed	40.20	242	1.367×10^{-14}	8.931×10^{-16}	5.5	0.4
GLX-05R	67.079	-50.273	134	Mixed	32.08	254	7.523×10^{-15}	1.174×10^{-15}	4.0	0.6
GLX-06	67.157	-50.067	404	Glacial	25.18	253	3.903×10^{-15}	7.498×10^{-16}	2.6	0.5
GLX-07	67.155	-50.071	400	Glacial	29.22	246	7.992×10^{-15}	9.960×10^{-16}	4.5	0.6
GLX-08	67.008	-50.675	24	Terrace	34.27	254	1.755×10^{-14}	1.011×10^{-15}	8.7	0.5

GLX-08R	67.008	-50.675	24	Terrace	40.67	254	1.073×10^{-14}	1.533×10^{-15}	4.5	0.6
GLX-09	67.007	-50.678	12	Mixed	35.05	254	6.282×10^{-15}	1.182×10^{-15}	3.0	0.6
GLX-09R	67.007	-50.678	12	Mixed	32.09	254	1.135×10^{-14}	1.442×10^{-15}	6.0	0.8
GLX-41	67.013	-50.636	14	Mixed	38.21	253	1.189×10^{-14}	7.712×10^{-16}	5.3	0.3
GLX-41R	67.013	-50.636	14	Mixed	34.83	254	9.616×10^{-15}	1.227×10^{-15}	4.7	0.6
GLX-42	66.997	-50.776	7	Mixed	38.78	254	1.141×10^{-14}	7.101×10^{-16}	5.0	0.3
GLX-42R	66.997	-50.776	3	Mixed	36.27	254	1.202×10^{-14}	1.414×10^{-15}	5.6	0.7
GLX-80	66.992	-50.403	90	Mixed	40.93	245	1.547×10^{-14}	1.560×10^{-15}	6.2	0.6
GLX-81	67.006	-50.213	135	Ice-free	40.06	245	3.168×10^{-14}	2.123×10^{-15}	12.9	0.9
GLX-82	67.022	-50.313	129	Ice-free	41.73	246	4.201×10^{-14}	2.590×10^{-15}	16.6	1.0
GLX-83	66.979	-50.201	95	Mixed	24.00	248	9.895×10^{-15}	1.835×10^{-15}	6.8	1.3
GLX-84	66.965	-49.971	127	Glacial	22.21	248	1.207×10^{-14}	2.949×10^{-15}	9.0	2.2
GLX-85	66.970	-50.051	91	Glacial	19.90	249	6.212×10^{-15}	1.554×10^{-15}	5.2	1.3
GLX-86	67.063	-50.178	290	Glacial	37.84	248	1.319×10^{-14}	3.004×10^{-15}	5.8	1.3
GLX-87	67.069	-50.218	219	Mixed	33.96	249	1.291×10^{-14}	2.558×10^{-15}	6.3	1.3
GLX-88	67.069	-50.218	219	Aeolian	36.19	248	1.927×10^{-14}	2.337×10^{-15}	8.8	1.1
GLX-89	67.109	-50.192	291	Mixed	40.25	252	1.720×10^{-14}	1.726×10^{-15}	7.2	0.7
GLX-90	67.156	-50.067	446	Glacial	36.12	248	9.225×10^{-15}	1.460×10^{-15}	4.2	0.7
GLX-91	67.181	-50.345	85	Glacial	30.23	250	9.588×10^{-15}	1.406×10^{-15}	5.3	0.8
GLX-92	67.227	-50.441	117	Mixed	40.80	251	2.610×10^{-14}	2.231×10^{-15}	10.7	0.9

GLX-93	67.190	-50.744	90	Mixed	35.30	252	1.252×10^{-14}	1.838×10^{-15}	6.0	0.9
Narsarsuaq										
GLX-10	67.187	-45.388	12	Mixed	20.39	247	2.002×10^{-15}	5.922×10^{-16}	1.6	0.5
GLX-11	61.221	-45.504	2	Ice-free	15.01	253	1.207×10^{-14}	8.409×10^{-16}	13.6	0.9
GLX-12	61.265	-45.509	20	Ice-free	15.21	256	7.008×10^{-15}	8.204×10^{-16}	7.9	0.9
GLX-13	61.300	-45.567	272	Ice-free	31.38	256	4.511×10^{-14}	1.597×10^{-15}	24.5	0.9
GLX-18	61.336	-45.410	432	Ice-free	19.71	256	3.938×10^{-14}	1.838×10^{-15}	34.1	1.6
GLX-19	61.420	-45.122	578	Glacial	21.46	257	2.338×10^{-14}	9.186×10^{-16}	18.7	0.7
GLX-20	61.429	-45.034	720	Glacial	30.55	255	2.199×10^{-14}	9.543×10^{-16}	12.3	0.5
GLX-21	61.084	-45.034	148	Glacial	22.81	256	5.764×10^{-15}	7.186×10^{-16}	4.3	0.5
GLX-22	61.086	-45.133	95	Mixed	17.42	248	4.789×10^{-15}	6.523×10^{-16}	4.6	0.6
GLX-23	61.087	-45.250	14	Mixed	24.04	256	8.354×10^{-15}	6.675×10^{-16}	5.9	0.5
GLX-34	61.174	-45.407	18	Terrace	37.45	255	7.088×10^{-15}	6.346×10^{-16}	3.2	0.3
GLX-35	61.174	-45.400	11	Mixed	37.69	256	7.988×10^{-15}	7.105×10^{-16}	3.6	0.3
GLX-37	61.198	-45.337	17	Mixed	38.01	256	4.233×10^{-15}	5.719×10^{-16}	1.9	0.3
GLX-39	61.195	-45.502	30	Ice-free	18.55	253	4.936×10^{-15}	5.730×10^{-16}	4.5	0.5
GLX-40	61.205	-45.513	11	Ice-free	35.17	253	2.051×10^{-14}	9.503×10^{-16}	9.9	0.5
GLX-94	61.089	-45.261	5	Terrace	30.48	255	7.607×10^{-15}	1.250×10^{-15}	4.2	0.7

Tasiilaq

GLX-63	65.611	-38.671	100	Glacial	37.37	242	7.551×10^{-15}	1.596×10^{-15}	3.3	0.7
GLX-64	65.611	-38.671	100	Glacial	35.05	246	8.639×10^{-15}	1.285×10^{-15}	4.1	0.6
GLX-65	65.612	-38.691	82	Glacial	38.01	246	5.180×10^{-15}	1.154×10^{-15}	2.2	0.5
GLX-66	65.721	-38.563	78	Glacial	16.22	252	5.933×10^{-15}	1.323×10^{-15}	6.2	1.4
GLX-67	65.715	-38.460	109	Glacial	36.40	244	1.121×10^{-14}	1.731×10^{-15}	5.0	0.8
GLX-68	65.768	-38.307	189	Glacial	24.52	250	5.710×10^{-15}	1.817×10^{-15}	3.9	1.2
GLX-69	65.991	-38.279	250	Glacial	21.41	249	4.399×10^{-15}	1.311×10^{-15}	3.4	1.0
GLX-71	66.020	-37.563	271	Glacial	35.13	245	2.005×10^{-14}	1.918×10^{-15}	9.3	0.9
GLX-72	65.974	-37.588	217	Glacial	35.91	243	2.256×10^{-14}	2.007×10^{-15}	10.2	0.9
GLX-73	65.935	-37.658	7	Mixed	30.07	249	1.640×10^{-14}	2.285×10^{-15}	9.1	1.3
GLX-74	65.879	-37.652	6	Ice-free	36.47	243	2.544×10^{-14}	2.174×10^{-15}	11.3	1.0
GLX-75	65.814	-37.486	15	Ice-free	33.26	245	2.694×10^{-14}	2.473×10^{-15}	13.3	1.2

APPENDIX III

GLX-01

Field Area: Kangerlussuaq
Collection Date: 5/19/11, 6/8/12
Latitude: 67.019 **Longitude:** -50.627
Site Description: Watson River sediment sample from a cobble bar just past the golf course. This is the most down stream of the Watson River samples in a transect spanning the Russell Glacier ice margin to the fjord mouth.
Category: Mixed

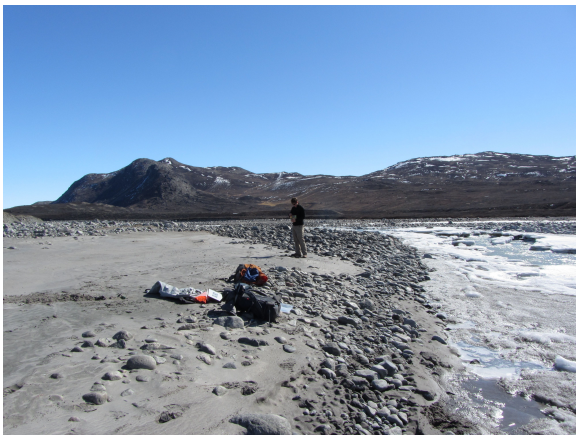

GLX-02

Field Area: Kangerlussuaq
Collection Date: 5/19/11, 6/8/12
Latitude: 67.039 **Longitude: -**50.484
Site Description: Watson River sediment sample from close to the waterfall turnoff. The sampling area was mostly gravel and there was evidence for lots of wind erosion so there was some worry in 2011 that the sampled material could be aeolian.
Category: Mixed

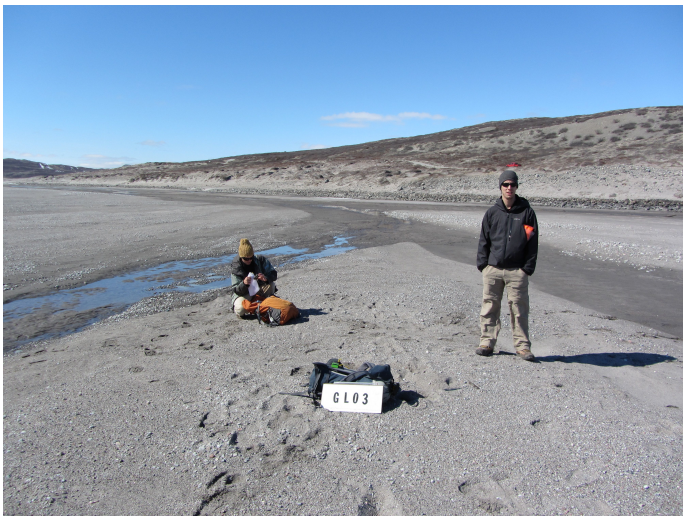

GLX-03

Field Area: Kangerlussuaq
Collection Date: 5/19/11, 6/8/12
Latitude: 67.065 **Longitude:** -50.365
Site Description: Watson River sediment sample from a wide sand plain containing few cobbles. The sample location is near the 90º junction close to the road.
Category: Mixed

GLX-04

GLX-04R

Field Area: Kangerlussuaq
Collection Date: 5/19/11, 6/8/12
Latitude: 67.073 **Longitude:** -50.062
Site Description: Watson River sediment sample from close to the headwaters. The sample location is ~2 km from the Russell Glacier ice margin. The sample was from a broad outwash plain. In 2011, we sampled from the bar where there was no water and the nearby water was not flowing. In 2012, there was much more flowing water at this site.
Category: Mixed

GLX-05

GLX-05R

Field Area: Kangerlussuaq
Collection Date: 5/19/11, 6/8/12
Latitude: 67.079 **Longitude:** -50.273
Site Description: Watson River sediment sample from close to the headwaters. This sample site is close to GLX-04 and is also ~2 km from the ice margin. The sample came from within the channel and the sediment was in transit – the stream was flowing from the Russell Glacier.
Category: Mixed

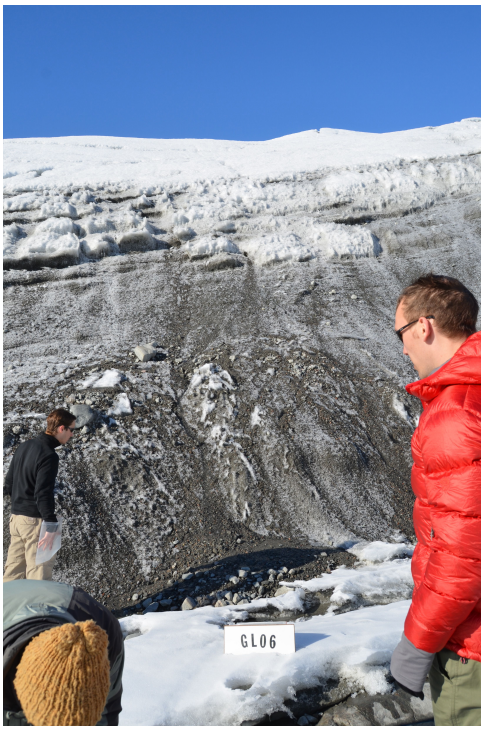

GLX-06

Field Area: Kangerlussuaq
Collection Date: 5/19/11
Latitude: 67.157 **Longitude:** -50.067
Site Description: The sample was melting out of basal ice at the ice sheet margin. The sample site is north of the Russell Glacier lobe of the ice sheet.
Category: Glacially sourced

GLX-07

Field Area: Kangerlussuaq
Collection Date: 5/19/11
Latitude: 67.155 **Longitude:** -50.071
Site Description: This mixed-grain size sample came from the lobe of a fan. The fan is by a lake that is fed by a glacier outwash tunnel that is located near GLX-06.
Category: Glacially sourced

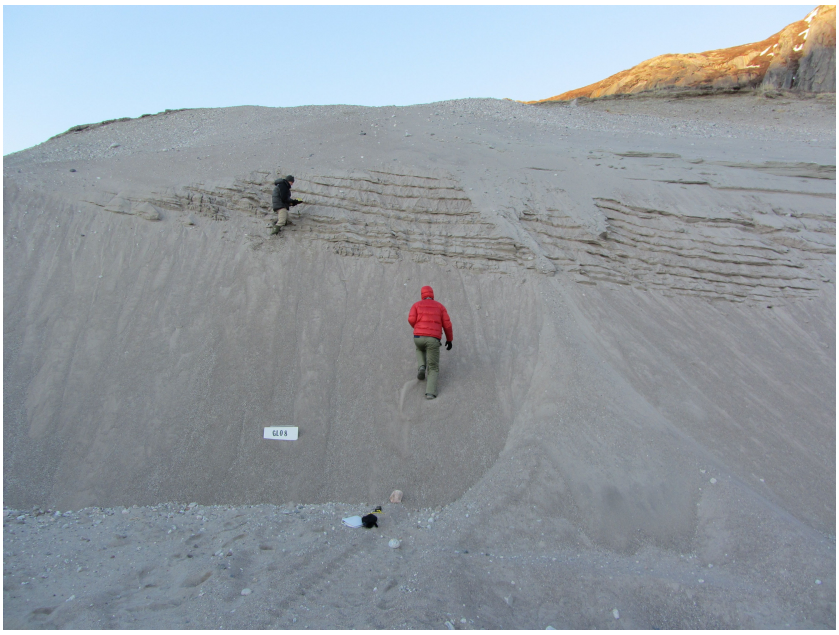

GLX-08

GLX-08R

Field Area: Kangerlussuaq
Collection Date: 5/19/11, 6/8/12
Latitude: 67.008 **Longitude:** -50.675
Site Description: This sample is from the foreset beds in a gravel pit at the bottom of an 8 ky terrace. The terrace is situated close to the fjord mouth, just past the confluence of the Watson River and the southern drainage.
Category: Early Holocene terrace

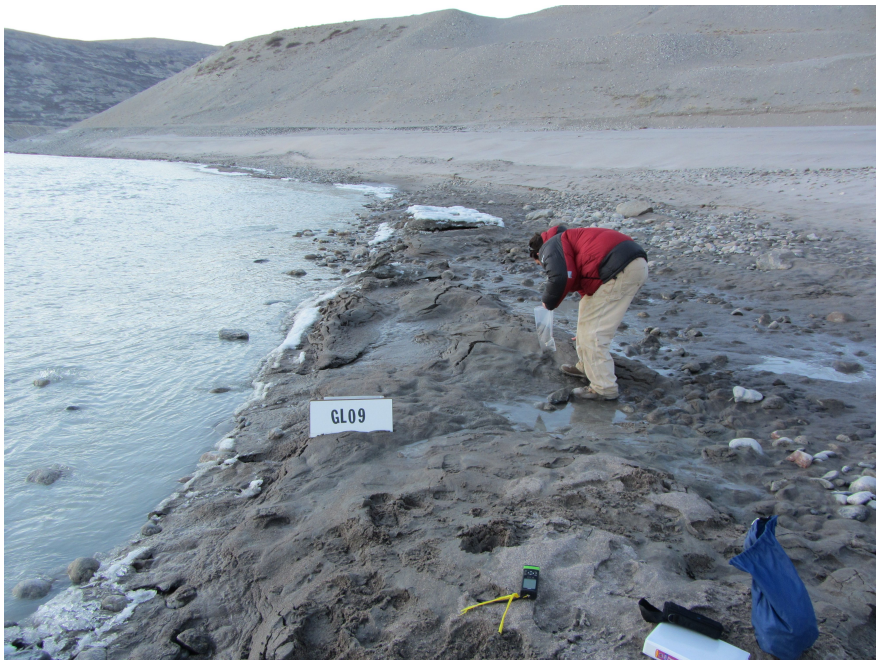

GLX-09

GLX-09R

Field Area: Kangerlussuaq
Collection Date: 5/19/11, 6/8/12
Latitude: 67.007 **Longitude:** -50.678
Site Description: We sampled active sand from the channel at a location just upstream of the bridge. This sample site is downstream of the confluence of the Watson River and the southern drainage.
Category: Mixed

GLX-10

Field Area: Narsarsuaq
Collection Date: 5/20/11
Latitude: 67.187 **Longitude:** -45.388
Site Description: This sample is from a small sand bar in a channel draining the northern of the two valley constrained lobes of the ice sheet. This particular sample is midway down the drainage, it is the middle sample in a three sample transect.
Category: Mixed

GLX-11

Field Area: Narsarsuaq
Collection Date: 5/20/11
Latitude: 61.221 **Longitude:** -45.504
Site Description: This sample is from a bouldery fan with debris lobes that is on the northeastern side of the fjord. The drainage that feeds this fan is presently ice free, though ice may have occupied this steeply sided valley earlier in the Holocene.
Category: Ice-free drainage

GLX-12

Field Area: Narsarsuaq
Collection Date: 5/20/11
Latitude: 61.265 **Longitude:** -45.509
Site Description: The sample is from a bar complex in a channel, ~1km upstream of the fjord. This sample is the farthest downstream in a group of samples that are in a presently ice-free basin. This basin is currently separated from the ice by topographic highs, and by a lake, which is a sediment trap for subglacially sourced sediment from northern lobes of the ice sheet.
Category: Ice-free drainage

GLX-13

Field Area: Narsarsuaq
Collection Date: 5/20/11
Latitude: 61.300 **Longitude:** -45.567
Site Description: This is a mid-stream sediment sample from a flat, just beyond the bridge and above waterfalls. The sample site is ~5 km upstream of GLX-12 and is in the same ice-free drainage basin. Directly west of this sample site is a U-shaped valley that was likely occupied by ice in the past.
Category: Ice-free drainage

GLX-18

Field Area: Narsarsuaq
Collection Date: 5/21/11
Latitude: 61.336 **Longitude:** -45.410
Site Description: The sample is from a delta into a small lake where there were very large marginal fans. Upstream of this lake is a much larger lake that acts as a sediment trap for upstream subglacially sourced sediment.
Category: Ice-free drainage

GLX-19
(view down valley)

Field Area: Narsarsuaq
Collection Date: 5/21/11
Latitude: 61.420 **Longitude:** -45.122
Site Description: The sample site is within 1 km of the ice margin where there were large (>1m) outwash boulders. There are three ice sheet lobes that converge in this area. Glacially produced sediment is likely trapped in a downstream lake and so may not be reaching the fjord.
Category: Glacially sourced (high-elevation)

GLX-20

Field Area: Narsarsuaq
Collection Date: 5/21/11
Latitude: 61.429 **Longitude:** -45.034
Site Description: The sample site is ~500 m from the icefront and there has been minimal LIA advance here. This sample is from a similar location to GLX-19, the ice-lobe here is just northeast of the ice margin sampled for GLX-19. Similarly, glacially produced sediment is likely trapped in a downstream lake.
Category: Glacially sourced (high-elevation)

GLX-21

Field Area: Narsarsuaq
Collection Date: 5/21/11
Latitude: 61.084 **Longitude:** -45.034
Site Description: The sample site is 200 m from ice margin. There are small low gradient extended LIA moraines that dam the adjacent lake. This sample is the first in a transect that spans the ice margin to the fjord mouth. This is the southern of the two low elevation, valley-constrained tongues of the ice-sheet.
Category: Glacially sourced

GLX-22

Field Area: Narsarsuaq
Collection Date: 5/21/11
Latitude: 61.086 **Longitude:** -45.133
Site Description: This is a channel sample that is downstream of GLX-21. This is the middle sample in a transect that spans the ice margin to the fjord mouth. The channel is in a very steeply walled valley and there are large fans on the sides of the valley. In the area that we sampled, there were massive cobble bars.
Category: Mixed

GLX-23

Field Area: Narsarsuaq
Collection Date: 5/21/11
Latitude: 61.087 **Longitude:** -45.250
Site Description: This sample is downstream of GLX-22, this is the lowest sample in a transect that spans the ice margin to the fjord mouth. The location is ~800 m from fjord. There was a lot of sand in this area and a stream cutting at the base of a delta.
Category: Mixed

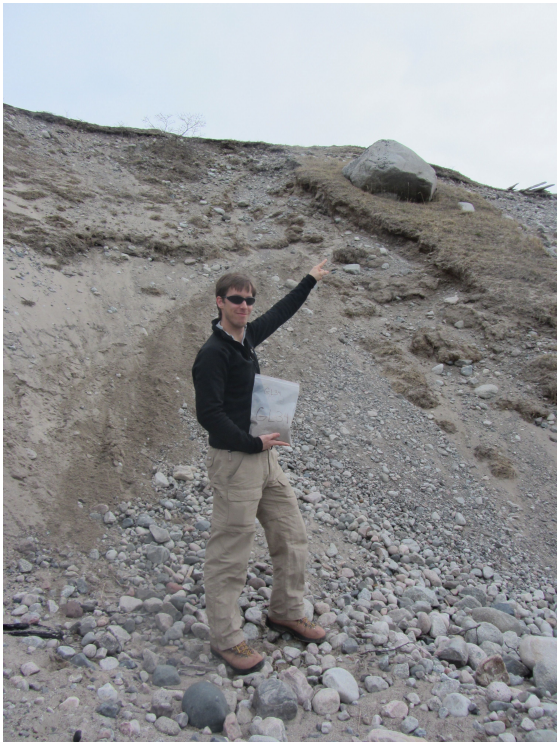

GLX-34

Field Area: Narsarsuaq
Collection Date: 5/23/11
Latitude: 61.174 **Longitude:** -45.407
Site Description: This sample is from a terrace below the airport where there were gravel and cobbles over sand. The terrace location is close to the GLX-35 sampling site. Material in the terrace probably came from the upstream lobe of the ice sheet in the past (present day marginal sample is GLX-37).
Category: Early Holocene terrace

GLX-35

Field Area: Narsarsuaq
Collection Date: 5/23/11
Latitude: 61.174 **Longitude:** -45.400
Site Description: This sample is the lowest in a transect spanning the ice margin to the fjord mouth. This is the northern of the two valley constrained lobes of the ice sheet. We sampled from the last sandbar before cobble/incised reach and the material was well sorted.
Category: Mixed

GLX-37

Field Area: Narsarsuaq
Collection Date: 5/23/11
Latitude: 61.198 **Longitude:** -45.337
Site Description: The sample site is 1-2 km from the ice margin and this is the first sample in a transect that reaches the fjord mouth. We sampled in a channel on the far side of the river, near a bedrock outcrop.
Category: Mixed

GLX-39

Field Area: Narsarsuaq
Collection Date: 5/23/11
Latitude: 61.195 **Longitude:** -45.502
Site Description: This sample is from a meteoric creek that drains into the western side of the fjord. The creek has an angular boulder bed and we sampled from the sand bar by the road.
Category: Ice-free drainage

GLX-40

Field Area: Narsarsuaq
Collection Date: 5/23/11
Latitude: 61.205 **Longitude:** -45.513
Site Description: This sample is from an active fan delta that is fed by a meteoric creek. This site is also on the ice-free western side of the fjord, just north of GLX-39.
Category: Ice-free drainage

GLX-41

GLX-41R

Field Area: Kangerlussuaq
Collection Date: 5/24/11, 6/8/12
Latitude: 67.013 **Longitude:** -50.636
Site Description: This sample is the lowest in a transect that spans from the southern lobe of the ice sheet to the fjord mouth. The sample site is just upstream of the confluence with the Watson River. In 2011, we sampled from a bouldery area where there were a few sand bars that was three meters above and 15 meters from the main channel. In 2012, the water level was higher.
Category: Mixed

GLX-42

GLX-42R

Field Area: Kangerlussuaq
Collection Date: 5/24/11, 6/8/12
Latitude: 66.997 **Longitude:** -50.776
Site Description: The sample is from the large delta beyond the Kanger airport. This is the closest sample to the fjord mouth.
Category: Mixed

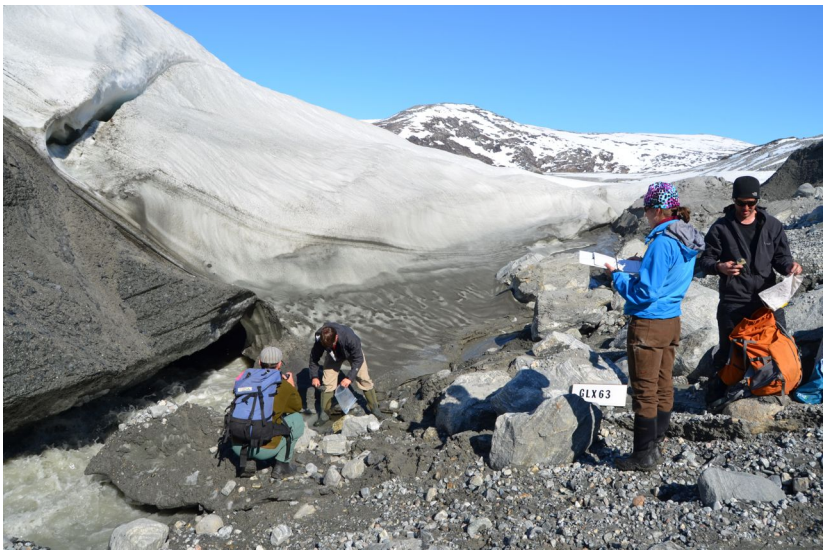

GLX-63

GLX-63 came from the outwash stream, near the people (middle of the photo)
GLX-64 is from the moraine to the viewer's left
GLX-65 is from the outwash plain behind the viewer

Field Area: Tasiilaq
Collection Date: 6/4/12
Latitude: 65.611 **Longitude:** -38.671
Site Description: This sample is from the margin of an ice sheet lobe that is southwest of Sermilik fjord. We sampled from the marginal drainage stream (GLX-63), from the nearby moraine (GLX-64), and from the flat outwash plain (GLX-65).
Category: Glacially sourced

GLX-64

Field Area: Tasiilaq
Collection Date: 6/4/12
Latitude: 65.611 **Longitude:** -38.671
Site Description: The sample is from a moraine (possibly LIA) and the location is very close to the ice margin and GLX-63 (viewer's left). The moraine is in the foreground of the picture and the outwash plain where we took sample GLX-65 is by the helicopter.
Category: Glacially sourced

GLX-65

GLX-65
(view from GLX-64)

Field Area: Tasiilaq
Collection Date: 6/4/12
Latitude: 65.612 **Longitude:** -38.691
Site Description: The sample is from a flat outwash plain in front of the glacier, this is the same area as GLX-63 and GLX-64.
Category: Glacially sourced

GLX-66

Field Area: Tasiilaq
Collection Date: 6/4/12
Latitude: 65.721 **Longitude:** -38.563
Site Description: This sample is from an ice marginal drainage and we sampled ~100 m from the ice. The sediment was sourced from a valley-constrained lobe of the Greenland Ice Sheet that is west of the Sermilik Fjord outlet.
Category: Glacially sourced

GLX-67

Field Area: Tasiilaq
Collection Date: 6/4/12
Latitude: 65.715 **Longitude:** -38.460
Site Description: This sample site is ~2 km east of GLX-66. We collected sediment close to the outwash tunnel of a glacier tongue that is constrained between two ridges. The setting is similar to GLX-66, the sediment is sourced from a valley-constrained tongue of the Greenland Ice Sheet, just west of the Sermilik Fjord outlet.
Category: Glacially sourced

GLX-68

Field Area: Tasiilaq
Collection Date: 6/4/12
Latitude: 65.768 **Longitude:** -38.307
Site Description: The sample site is by the margin of a glacier tongue that is in between two ridges. We sampled in the ice marginal outwash. Sediment sourced here will eventually be deposited in the outer portion of Sermilik Fjord.
Category: Glacially sourced

GLX-69

Field Area: Tasiilaq
Collection Date: 6/4/12
Latitude: 65.991 **Longitude:** -38.279
Site Description: The sample is from an ice marginal drainage, though the ice is possibly not connected to the big ice sheet. The ice that feeds this drainage is a small ice cap that is connected to the larger ice sheet by a narrow strip of glacier, though the connection was probably greater in the past.
Category: Glacially sourced

GLX-70

Field Area: Tasiilaq
Collection Date: 6/4/12
Latitude: 65.046 **Longitude:** -37.626
Site Description: This sample is from an ice-free drainage on the eastern side of Sermilik fjord. We sampled from a wide channel containing a lot of silt, big boulders, and cobbles.
Category: Ice-free drainage

GLX-71

Field Area: Tasiilaq
Collection Date: 6/4/12
Latitude: 66.020 **Longitude:** -37.563
Site Description: The sample is from an outwash stream draining a glacier on an island east of the fjord and so the ice here is not connected to the big ice sheet. There were two streams coming from the margin and we sampled from both.
Category: Glacially sourced (not the mainland ice sheet)

GLX-72

Field Area: Tasiilaq
Collection Date: 6/4/12
Latitude: 65.947 **Longitude:** -37.588
Site Description: The sample is from a fast moving outwash stream and we sampled less than 10 m from the ice margin. This glacier is on the eastern side of the fjord and is not connected to the mainland ice sheet.
Category: Glacially sourced (not the mainland ice sheet)

GLX-73

Field Area: Tasiilaq
Collection Date: 6/4/12
Latitude: 65.935 **Longitude:** -37.658
Site Description: GLX-73 is ~3 km downstream of GLX-72 and the sample is from a braided outwash stream containing mixed meteoric and glacial sediment. The glacial contribution is sourced from a glacier not connected to the large ice sheet.
Category: Mixed

GLX-74

Field Area: Tasiilaq
Collection Date: 6/4/12
Latitude: 65.879 **Longitude:** -37.652
Site Description: This sample is from an ice-free drainage on the eastern side of Sermilik Fjord.
Category: Ice-free drainage

GLX-75

Field Area: Tasiilaq
Collection Date: 6/4/12
Latitude: 65.814 **Longitude:** -37.486
Site Description: The sample is from an ice-free drainage, the drainage flows into a smaller fjord that is east of Sermilik Fjord.
Category: Ice-free drainage

GLX-80

Field Area: Kangerlussuaq
Collection Date: 6/8/12
Latitude: 66.992 **Longitude:** -50.403
Site Description: This is a mid-transect sample from the bank of the river that drains the southern lobe of the ice sheet. This is the drainage that is immediately south of the Watson River and the Russell Glacier ice sheet lobe.
Category: Mixed

GLX-81

Field Area: Kangerlussuaq
Collection Date: 6/8/12
Latitude: 67.006 **Longitude:** -50.213
Site Description: Drainage coming into the main channel, lots of rock flour suspended in the water. This sample is classified as an ice-free drainage because sand-sized sediment sourced from the glacier to the north is trapped in a lake.
Category: Ice-free drainage

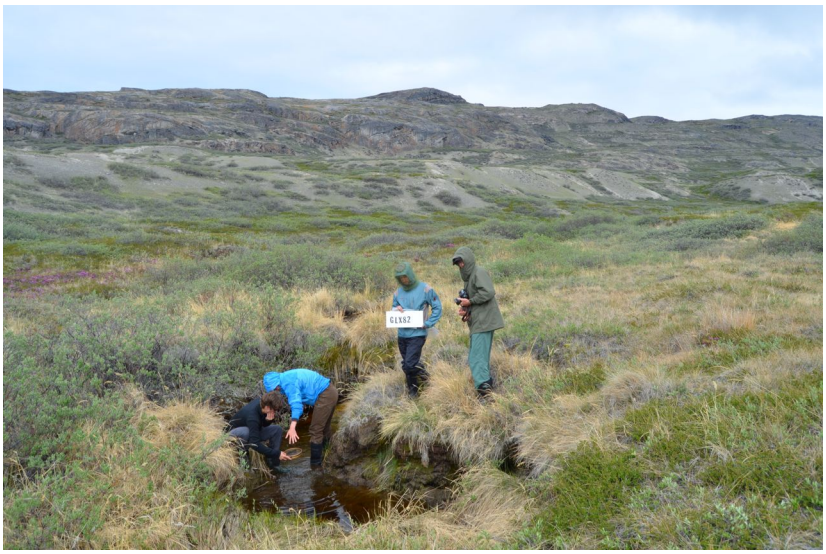

GLX-82
(view upstream)

GLX-82
(view downstream towards main drainage)

Field Area: Kangerlussuaq
Collection Date: 6/8/12
Latitude: 67.022 **Longitude:** -50.313
Site Description: This sample is from an ice-free drainage (very buggy), and when we sampled, there was not very much water moving in the narrow stream. The surrounding area was well vegetated and sediment here is sourced from the ice-free uplands that separate the two fluvial valleys.
Category: Ice-free drainage

GLX-83

GLX-83

(view from the helicopter, looking upstream towards GLX-84 and 85)

Field Area: Kangerlussuaq
Collection Date: 6/8/12
Latitude: 66.979 **Longitude:** -50.201
Site Description: The sample is from a sand bar in the middle of the southern drainage. There was a lot of sand and many rounded cobbles. This sample is from one of the two intermediate locations along the southern drainage transect.
Category: Mixed

GLX-84

Field Area: Kangerlussuaq
Collection Date: 6/8/12
Latitude: 66.965 **Longitude:** -49.971
Site Description: The sample is from an ice-dominated channel, the location is very close to a sub-ice tunnel. This is the lobe of the ice sheet that is just south of Russell Glacier and at this location, two lobes of the ice sheet come together and there is a small ice-free knoll to the east.
Category: Glacially sourced

GLX-85

Field Area: Kangerlussuaq
Collection Date: 6/8/12
Latitude: 66.970 **Longitude:** -50.051
Site Description: The sample is from a braided portion of the channel and the location is more distal from the ice margin than GLX-84 (pictured in the background), though the sediment source is still ice dominated. The channel is fed by two converging lobes of the ice sheet.
Category: Glacially sourced

GLX-86
(view upstream towards ice)

GLX-86
(view downstream towards fjord)

Field Area: Kangerlussuaq
Collection Date: 6/8/12
Latitude: 67.063 **Longitude:** -50.178
Site Description: The sample is from an ice marginal outwash channel, ~400 m from the Russell Glacier lobe of the ice margin (pictured in the background).
Category: Glacially sourced

GLX-87

GLX-87
(close up photo showing the incised bedrock channel)

Field Area: Kangerlussuaq
Collection Date: 6/8/12
Latitude: 67.069 **Longitude:** -50.218
Site Description: This sample is from river outwash that flows through an incised bedrock channel. The location is downstream of GLX-86 and is ~2 km from the ice margin.
Category: Mixed

GLX-88
(Dylan is pointing at the aeolian sand)

GLX-87 and GLX-88
(The aeolian sand is on the left side of the photo)

Field Area: Kangerlussuaq
Collection Date: 6/8/12
Latitude: 67.069 **Longitude:** -50.218
Site Description: This sample is aeolian sand from the same location as GLX-87
Category: Aeolian sand

GLX-89

Field Area: Kangerlussuaq
Collection Date: 6/8/12
Latitude: 67.109 **Longitude:** -50.192
Site Description: This is a river outwash sample and the location is ~1 km downstream of the Russell Glacier margin (pictured in the background).
Category: Mixed

GLX-90

Field Area: Kangerlussuaq
Collection Date: 6/8/12
Latitude: 67.156 **Longitude:** -50.067
Site Description: This glacially sourced sample is from the 660 (glacier margin) outwash tunnel. This sample site is located in between GLX-6 and GLX-7. All three samples are essentially the same site.
Category: Glacially sourced

GLX-91

Field Area: Kangerlussuaq
Collection Date: 6/8/12
Latitude: 67.181 **Longitude:** -50.345
Site Description: This sample is proximal to the northern most of the three ice sheet lobes in the study area.
Category: Glacially sourced

GLX-92

Field Area: Kangerlussuaq
Collection Date: 6/8/12
Latitude: 67.227 **Longitude:** -50.441
Site Description: This sample is from a side drainage that feeds into the northern drainage. This channel flows through a long ice-free valley (>10 km), however the water source is a more northern portion of the ice sheet.
Category: Mixed

GLX-93

Field Area: Kangerlussuaq
Collection Date: 6/8/12
Latitude: 67.190 **Longitude:** -50.744
Site Description: This sample is from a sandbar in the middle of a big channel. This channel drains the northern ice sheet lobe and the sample location is downstream of GLX-92 and GLX-91.
Category: Mixed

GLX-94

Field Area: Narsarsuaq
Collection Date: Fall 2012
Latitude: 61.089 **Longitude:** -45.261
Site Description: Terrace
Category: Terrace